



UNIVERSITY OF MALTA

MASTER OF SCIENCE IN ENGINEERING DISSERTATION

Localisation of Brain Activity for SSVEP-based BCIs: An fMRI and EEG Study

Cheryl GILFORD

Supervised by:

Prof. Ing. Kenneth P. CAMILLERI

Co-supervised by:

Dr Tracey CAMILLERI and Dr Claude BAJADA

A dissertation submitted in partial fulfilment of the requirements
for the degree of Master of Science in Engineering

by the

Faculty of Engineering

October 2023



L-Università
ta' Malta

University of Malta Library – Electronic Thesis & Dissertations (ETD) Repository

The copyright of this thesis/dissertation belongs to the author. The author's rights in respect of this work are as defined by the Copyright Act (Chapter 415) of the Laws of Malta or as modified by any successive legislation.

Users may access this full-text thesis/dissertation and can make use of the information contained in accordance with the Copyright Act provided that the author must be properly acknowledged. Further distribution or reproduction in any format is prohibited without the prior permission of the copyright holder.



**L-Università
ta' Malta**

FACULTY/INSTITUTE/CENTRE/SCHOOL Faculty of Engineering

DECLARATIONS BY POSTGRADUATE STUDENTS

(a) Authenticity of Dissertation

I hereby declare that I am the legitimate author of this Dissertation and that it is my original work.

No portion of this work has been submitted in support of an application for another degree or qualification of this or any other university or institution of higher education.

I hold the University of Malta harmless against any third party claims with regard to copyright violation, breach of confidentiality, defamation and any other third party right infringement.

(b) Research Code of Practice and Ethics Review Procedures

I declare that I have abided by the University's Research Ethics Review Procedures. Research Ethics & Data Protection form code ENG-2022-00108.

As a Master's student, as per Regulation 77 of the General Regulations for University Postgraduate Awards 2021, I accept that should my dissertation be awarded a Grade A, it will be made publicly available on the University of Malta Institutional Repository.

Abstract

Brain-computer interface (BCI) systems provide an alternative neural pathway for individuals with neuromuscular disorders, enabling them to control external devices when conventional muscle movements are not feasible. These systems capture the brain's electrical activity, typically using electroencephalography (EEG), and translate it into commands for external devices. Among various control signal types in BCIs, steady-state visually evoked potentials (SSVEPs) have shown remarkable performance. These are electrical signals generated in the brain in response to repetitive visual stimuli (RVS), showing rhythmic neural oscillations matching the stimulus frequency. To interact with the BCI, the user selects a command by focusing on the corresponding visual stimulus. When the BCI detects the SSVEP response, it executes the corresponding command, enabling device control.

Current SSVEP-based BCIs use a single-graphic black-white flickering stimulus to generate the SSVEP response, which is typically recorded from the occipital region of the brain. However, the literature suggests that altering stimulus characteristics such as colour, shape, and texture at different flickering frequencies can enhance the SSVEP response in both occipital and non-occipital brain areas. This study uses functional magnetic resonance imaging (fMRI) and EEG recordings to localise the SSVEP activity and investigate how this varies with different stimulus parameters and flicker frequencies. Additionally, identifying robust SSVEP-related brain activity beyond the occipital region would allow a more practical placement of electrodes, in particular on non-occipital areas.

Seven different stimuli parameters were presented to the subjects during separate fMRI and EEG data recording sessions. The recorded data was analysed using the general linear model (GLM), signal-to-noise ratio (SNR) and z-score. As expected, it was found that the highest SSVEP response in the brain is located at the occipital region, however temporal and parietal regions still exhibited significant SSVEP amplitudes when using the random dot stimulus in the low frequency range (7.5 Hz and 10 Hz), and the blue-green stimulus in mid and high frequencies ranges (15 Hz, 20 Hz, 24 Hz). Furthermore, this study concluded that flickering frequencies greater than 24 Hz should be avoided as these do not elicit robust SSVEP signals. These findings aid in developing more comfortable, accurate and stable BCIs through the suitable choice of stimuli frequencies, characteristics and electrode placement.

Acknowledgements

First and foremost, I would like to express my deepest appreciation to my supervisor, Prof. Kenneth P. Camilleri, for his unrelenting support, dedication and motivation throughout these last months. His expertise in the field of biomedical engineering gave thoughtful discussions and allowed me to overcome any challenges that I experienced during the course of this dissertation.

I am deeply grateful and wish to extend my sincere appreciation to my esteemed co-supervisors, Dr Tracey Camilleri for her constructive feedback, knowledge, and guidance throughout this study, and Dr Claude Bajada, whose expertise in magnetic resonance imaging (MRI) played a pivotal role in the successful completion of this study.

I would like to thank the University of Malta Magnetic Resonance Imaging Platform (UMRI) for access to scanning equipment and services, use of its infrastructure, and resources such as documentation and preprocessing scripts.

Lastly, I wish to express my warmest gratitude to my family and friends for their continuous encouragement and moral support. Your understanding of the demands of academic research and your encouragement have been a constant source of motivation. I would also like to thank the people who took the time to contribute to this project.

Contents

| | |
|---|------------|
| Abstract | i |
| Acknowledgements | ii |
| Contents | iii |
| List of Figures | vii |
| List of Tables | x |
| List of Acronyms | xi |
| 1 Introduction | 1 |
| 1.1 Background | 1 |
| 1.2 Objectives of the Dissertation | 2 |
| 1.3 Layout of the Dissertation | 3 |
| 2 Theoretical Background | 5 |
| 2.1 Introduction | 5 |
| 2.2 The Anatomy of the Human Brain | 5 |
| 2.2.1 The Neuron | 5 |
| 2.2.2 Regions and Lobes of the Brain | 7 |
| 2.2.3 The Occipital Lobe | 8 |
| 2.2.4 General Structure and Cellular Organisation | 9 |
| 2.2.5 Neural Signal Characteristics | 10 |
| 2.3 Brain-Computer Interfaces | 12 |
| 2.3.1 Types of BCI Systems | 13 |
| 2.3.2 Control Signal Types in BCIs | 14 |
| 2.4 Signal Acquisition Methods | 15 |
| 2.4.1 Instrumentation to Analyse Brain Activity | 15 |
| 2.4.2 Electroencephalography | 16 |
| 2.4.3 Electrodes and Electrode Placement | 16 |
| 2.4.4 Magnetic Resonance Imaging | 18 |
| 2.4.4.1 Working Principles of MRI | 18 |

| | | |
|----------|--|-----------|
| 2.4.4.2 | MRI Images | 20 |
| 2.4.4.3 | Functional Magnetic Resonance Imaging | 21 |
| 2.5 | Chapter Summary | 22 |
| 3 | Literature Review | 24 |
| 3.1 | Introduction | 24 |
| 3.2 | Overview of SSVEP-based BCIs | 24 |
| 3.3 | Practical Issues of SSVEP-based BCIs | 25 |
| 3.4 | EEG Alternative Electrode Placement | 27 |
| 3.4.1 | Source Localisation of the SSVEP | 27 |
| 3.4.1.1 | The Visual Pathway | 28 |
| 3.4.1.2 | SSVEP Source Investigated Using EEG and fMRI Modalities | 29 |
| 3.4.2 | Behind the Ear SSVEP-based BCIs | 31 |
| 3.5 | The SSVEP Response and Stimuli Properties | 33 |
| 3.5.1 | Stimulus Frequency | 33 |
| 3.5.2 | Stimulus Colour | 35 |
| 3.5.3 | Stimulus Shape | 37 |
| 3.5.4 | Stimulus Texture | 40 |
| 3.5.5 | Rendering Device, Stimulus Size and Duty-cycle | 41 |
| 3.6 | Chapter Summary | 43 |
| 3.6.1 | Localisation of SSVEPs in the Brain | 43 |
| 3.6.2 | Stimuli Properties | 43 |
| 3.6.2.1 | Stimulus Frequency | 44 |
| 3.6.2.2 | Stimulus Colour | 44 |
| 3.6.2.3 | Stimulus Shape | 44 |
| 3.6.2.4 | Stimulus Type | 45 |
| 3.7 | Conclusion | 45 |
| 4 | fMRI Experiment Design and Setup | 47 |
| 4.1 | Introduction | 47 |
| 4.2 | Objectives of fMRI Analysis | 47 |
| 4.3 | Task-Based and Resting-State fMRI | 48 |
| 4.4 | Design of Variable Parameters | 49 |
| 4.4.1 | Control Condition | 49 |
| 4.4.2 | Tested Stimuli Properties | 50 |
| 4.4.2.1 | Colour, Shape and Texture | 50 |
| 4.4.2.2 | Frequency | 52 |
| 4.5 | System Architecture | 52 |
| 4.5.1 | Hardware Description | 53 |
| 4.5.1.1 | MRI Data Acquisition Parameters | 55 |
| 4.5.2 | Software Description | 56 |
| 4.6 | Subjects and Experimental Setup | 57 |
| 4.6.1 | Experimental Protocol | 58 |

| | | |
|----------|--|-----------|
| 4.7 | Data Organisation and Preprocessing | 61 |
| 4.8 | Chapter Summary | 62 |
| 5 | fMRI Analysis | 64 |
| 5.1 | Introduction | 64 |
| 5.2 | Data Analysis | 64 |
| 5.2.1 | General Linear Model | 65 |
| 5.2.2 | Applying the General Linear Model | 69 |
| 5.3 | Results | 73 |
| 5.3.1 | The Activated Cortical Brain Regions | 74 |
| 5.3.2 | Number of Activated Voxels in Different Regions | 77 |
| 5.3.3 | Z-Statistic Variation Across Brain Regions and Frequencies | 82 |
| 5.4 | Chapter Summary | 85 |
| 6 | EEG Setup and Analysis | 86 |
| 6.1 | Introduction | 86 |
| 6.2 | Objectives of the EEG Analysis | 86 |
| 6.3 | System Architecture | 87 |
| 6.3.1 | Hardware Description | 87 |
| 6.3.2 | Software Description | 88 |
| 6.4 | Subjects and Experimental Setup | 89 |
| 6.4.1 | Data Acquisition | 89 |
| 6.4.2 | Experimental Paradigm | 90 |
| 6.5 | Data Analysis | 91 |
| 6.5.1 | Preprocessing | 92 |
| 6.5.2 | Feature Extraction | 92 |
| 6.5.2.1 | Fast Fourier Transform | 93 |
| 6.5.2.2 | Power Spectral Density | 93 |
| 6.5.2.3 | Signal-to-noise Ratio | 94 |
| 6.5.2.4 | Z-score | 95 |
| 6.5.3 | Statistical Analysis | 96 |
| 6.5.3.1 | Permutation-based Statistics | 96 |
| 6.5.3.2 | Correction for Multiple Comparisons | 97 |
| 6.5.3.3 | Stationary Signals | 98 |
| 6.6 | Results | 100 |
| 6.6.1 | Single Trial Analysis | 100 |
| 6.6.2 | Permutation-based Statistics | 102 |
| 6.6.2.1 | Results from Permutation-based Statistics | 104 |
| 6.6.3 | SNR Topographic Maps | 107 |
| 6.6.4 | Z-score Analysis | 110 |
| 6.6.4.1 | Analysis of the SNR Topographic Maps Using Z-score | 111 |
| 6.6.4.2 | Analysis of Stimuli Properties Using Z-score | 114 |
| 6.7 | Chapter Summary | 117 |

| | | |
|----------|--|------------|
| 7 | Discussion | 119 |
| 7.1 | Introduction | 119 |
| 7.2 | Project Main Aims | 119 |
| 7.3 | fMRI Study | 120 |
| 7.4 | EEG Study | 125 |
| 7.5 | Combining the fMRI and EEG Results | 128 |
| 7.6 | Overall Conclusions | 129 |
| 7.7 | Limitations and Further Improvements | 131 |
| 8 | Conclusions | 133 |
| A | fMRI Data Recording Session Procedures | 137 |
| B | fMRIPrep Processing Workflow | 139 |
| C | Brain Activations Visual Maps | 142 |
| | Bibliography | 145 |

List of Figures

| | | |
|-----|---|----|
| 2.1 | The structure of the neuron. | 6 |
| 2.2 | The four lobes of the brain and the location of the main Brodmann areas labelled as numbers. | 8 |
| 2.3 | Gyri, sulci and fissures of the brain. | 9 |
| 2.4 | The 10-20 electrode system set up. | 18 |
| 2.5 | The process of magnetisation of the hydrogen protons in the body. | 19 |
| 2.6 | BOLD hemodynamic response function (HRF) following a single brief stimulus. | 22 |
| 3.1 | An example of a laboratory SSVEP-based BCI setup. | 27 |
| 3.2 | The visual pathway explained in terms of the three pathways. Green, orange and yellow arrows represent the M, P and K pathways respectively. | 29 |
| 3.3 | Standard single-graphic black-white stimulus that is used in SSVEP-based BCIs. | 36 |
| 3.4 | Highlighted cortical brain areas mentioned in Section 3.5. | 38 |
| 3.5 | Different shaped stimuli used by the studies discussed in this section: (a) The different circular stimuli used by Cavina-Pratesi et al. (b) The two different shapes used by Stylianos-Korsnes et al. (c) A clock image stimulus that has been broken down into randomly rearranged squares used by Freud et al. (d) An apple image stimulus randomly rearranged into small squares used by Denys et al. (e) A non-object line drawing image stimulus used by Kraut et al. | 39 |
| 3.6 | Different stimuli types used by the studies discussed in this section: (a) Different graded texture stimuli used by Cavina-Pratesi et al. (b) Different graded texture stimuli used by Stylianos-Korsnes et al. (c) Stimuli used by Beason-Held et al. Figures on the first row show the ‘random’ textured stimulus and the bottom row figures show the ‘correlated’ textured stimulus. | 42 |
| 4.1 | Black-white stimulus. | 49 |
| 4.2 | The two different colour stimuli tested in this study. | 50 |
| 4.3 | The two different shape stimuli tested. | 51 |
| 4.4 | The two different texture stimuli tested. | 51 |
| 4.5 | The magnet and control room of the University’s MRI scanner located at Mater Dei Hospital. | 53 |

| | | |
|------|--|-----|
| 4.6 | The Siemens 64-channel head coil and Siemens head mirror used in the fMRI experiments. | 54 |
| 4.7 | The MRI system layout. | 55 |
| 4.8 | Timing paradigm of one trial. | 59 |
| 4.9 | Flowchart describing the fMRI experimental protocol for each subject. | 60 |
| 4.10 | Preprocessing steps. | 61 |
| 5.1 | Illustration of the HRF for one trial generated by a boxcar stimulus. | 66 |
| 5.2 | Application of the GLM on an imaginary voxel with time series Y | 68 |
| 5.3 | The design matrix in FEAT showing the six essential regressors in the first six columns and the six nuisance regressors in the last six columns. Columns 1-6 regressors describe the six trials during which the stimulus flickered at 7.5 Hz, 10 Hz, 15 Hz, 20 Hz, 25 Hz, 30 Hz respectively. | 71 |
| 5.4 | Results generated by FEAT for Subject 1, black-white stimulus, first contrast. | 72 |
| 5.5 | The FEATQuery output when applying an occipital lobe mask to the second-level analysis result of Subject 6, black-white stimulus, first contrast. | 74 |
| 5.6 | The brain cortical regions in Table 5.1 visualised on the MNI atlas brain image with the corresponding labels. (a) 2D axial and sagittal views of the MNI atlas template image having the coloured brain cortical regions (b) 3D-view of the MNI atlas image having the coloured brain cortical regions. | 75 |
| 5.7 | The three most frequently activated locations of the maximum z -value voxels for Subject 1, showing the results for each stimulus evaluated across the six frequencies. Red label shows the most frequented area, followed by the green and yellow labels. | 76 |
| 5.8 | Pie chart for each stimulus showing the average number of voxels activated in each brain mask evaluated across all subjects and frequencies. | 79 |
| 5.9 | Pie charts showing the number of activated voxels in each brain mask evaluated for each subject across all frequencies. | 81 |
| 5.10 | Bar graphs for each stimulus showing the mean value of the maximum z -statistic across all subjects obtained in each brain mask and frequency. | 83 |
| 6.1 | EEG data acquisition setup showing the subject focusing on the RVS displayed on an LCD monitor screen. | 89 |
| 6.2 | The 64-channel BioSemi head cap with the corresponding 10-20 system and MCN layout labels, and the CMS and DRL electrodes. | 90 |
| 6.3 | Protocol of trial structuring: (a) Two 22.8 s trials for each stimulus-frequency condition (b) Discarding the first 2.8 s (c) Dividing the 20 s trials into 10 four-second trials. | 100 |
| 6.4 | The time-domain EEG signal for one 22.8 s trial for the 7.5 Hz black-white stimulus period of Subject 2 at the Oz channel. | 101 |

| | | |
|------|--|-----|
| 6.5 | The SNR averaged across the 6 subjects for one 4 s trial when presenting the 10 Hz black-white stimulus at the Oz channel. | 102 |
| 6.6 | Permutation-based statistic results for the frequency that obtained the most statistically significant activations for each stimulus. Yellow labels represent that the SNR values at the tested stimulus condition (condition 2) are statistically significantly greater than the SNR values at the black-white stimulus condition (condition 1). Blue labels indicate that the SNR values at the black-white condition (condition 1) are statistically significantly greater than the SNR values at the tested stimulus condition (condition 2). f_1 , f_2 and f_3 indicate the SNR value at the first, second and third harmonic respectively. | 105 |
| 6.7 | EEG topographic maps showing the SNR power for the different stimuli at each of the six frequencies. | 108 |
| 6.8 | Z-score evaluated at the Oz, T7, Cpz and Fpz channels for the 15 Hz black-white stimulus. | 111 |
| 6.9 | Z-score plots for the frontal electrodes that obtained the highest SNR values for each stimulus. | 113 |
| 6.10 | Z-score plots for the Fpz channel from the random dot stimulus for the 10 Hz, 24 Hz and 30 Hz frequencies. | 114 |
| 6.11 | Z-score generated by the 20 Hz blue-green stimulus compared with the 20 Hz black-white stimulus at the Oz, CPz, P7 and P10 channels. The blue and orange plots show the result from the blue-green stimulus and the black-white stimulus, respectively. The threshold of 2 is marked by a green dotted line. | 115 |
| 7.1 | Average SNR across the six subjects at the 64 channels located across the whole scalp. | 124 |
| 7.2 | Average z-score across the six subjects at the Fpz, F3 and F4 electrodes for the 10 Hz black-white stimulus. | 125 |
| B.1 | fMRIprep workflow. | 141 |
| C.1 | Subject 2. | 142 |
| C.2 | Subject 3. | 143 |
| C.3 | Subject 4. | 143 |
| C.4 | Subject 5. | 144 |
| C.5 | Subject 6. | 144 |

List of Tables

| | | |
|-----|--|----|
| 5.1 | The most frequently activated locations of the z-max voxels for all subjects and stimuli, analysed across all frequencies. | 75 |
| 5.2 | The average activated number of voxels across the six subjects. . . . | 78 |

List of Acronyms

BCI

brain-computer interface. i, 1–5, 12–16, 22–27, 29, 31–34, 36, 40–43, 45, 48, 50, 86, 93, 110, 119, 120, 126, 127, 130, 132–136

EEG

electroencephalography. i, iv, viii, ix, 1–5, 10, 13–18, 22–36, 40–45, 49, 85–96, 98–101, 107, 108, 117–120, 123, 125–135

SSVEP

steady-state visually evoked potential. i, 1–4, 14–16, 22–38, 40–45, 47–51, 59, 64, 74, 85–87, 91, 92, 94–96, 98–102, 107, 110–112, 114–120, 122–136

RVS

repetitive visual stimuli. i, 2, 15, 24, 45, 47, 49, 50, 85, 87–89, 91, 92, 95, 119, 120, 122, 125, 127, 128, 131, 134, 135

fMRI

functional magnetic resonance imaging. i, iv, viii, 2–5, 13, 15, 20–23, 27, 29–31, 34–36, 38, 40, 41, 43–50, 52, 54–60, 62–67, 69–71, 73, 87–91, 98, 118–120, 122, 125, 128–135, 137, 139, 140

GLM

general linear model. i, 64, 65, 67–71, 73, 85, 120, 135

SNR

signal-to-noise ratio. i, ix, 14, 17, 25, 26, 31, 32, 36, 37, 40, 50, 70, 94–96, 100–114, 116–118, 123–128, 130, 134, 135

MRI

magnetic resonance imaging. ii, 3, 5, 10, 16, 18, 20–22, 47, 52–55, 57, 59, 61–63, 86, 120, 134, 137, 139, 140

UMRI

University of Malta Magnetic Resonance Imaging Platform. ii, 52, 57

GUI

graphical user interface. 2, 35

MNI

Montreal Neurological Institute. 10, 62, 73–76, 139, 141, 142

ICBM

International Consortium for Brain Mapping. 10

3D

three-dimensional. 10, 18–20, 75, 139

NREM

non-rapid eye movement. 11

SWS

slow wave sleep. 11

BMI

brain machine interface. 12

ALS

amyotrophic lateral sclerosis. 12, 32

FES

functional electrical stimulation. 12

MEG

magneto-encephalography. 13, 16

fNIRS

functional near-infrared spectroscopy. 13

CBF

cerebral blood flow. 13, 21

oxyHb

oxygenated hemoglobin. 13, 15, 21

deoxyHb

deoxygenated hemoglobin. 13, 15, 20, 21

SMR

sensorimotor rhythm. 14

VEP

visual-evoked potential. 14, 29

SCP

slow cortical potential. 14

ERP

event-related potential. 14, 88

TVEP

transient visually evoked potential. 14, 15

ITR

information transfer rate. 15, 25, 26, 31, 33, 36, 40, 42, 51, 132, 135

BOLD

blood oxygenation level dependent. 15, 21, 22, 30, 34, 35, 40, 41, 45, 47, 48, 57, 59, 62, 64–66, 68, 77, 84, 85, 120–122, 125, 130, 131, 134, 135, 140, 141

PET

positron emission tomography. 16, 29, 35

MCN

modified combinatorial nomenclature. 18, 87, 90

2D

two-dimensional. 18–20, 75, 107

CT

computed tomography. 18

RF

radio frequency. 19, 20, 53, 54

TR

repetition time. 20, 21

TE

time to echo. 20, 21

dMRI

diffusion magnetic resonance imaging. 21

HRF

hemodynamic response function. 21, 22, 59, 66, 68, 70, 120

TRCA

task-related component analysis classification algorithm. 25, 32, 33

DS

dynamic stopping. 25

TACCA

temporal alignments enhanced canonical correlation analysis. 25

VET

vision-based eye gaze tracker. 25

EOG

electroocoulogram. 25, 92

sEMG

surface electromyography. 25

FPGA

field programmable gate array. 26

EMG

electromyography. 28

LGN

lateral geniculate nucleus. 28, 35

CRT

cathode ray tube. 31, 41

CCA

canonical correlation analysis. 31, 32

LM

linked mastoids. 32

LED

light-emitting diode. 34–36, 41, 42, 44, 120

sLORETA

low-resolution brain electromagnetic tomography. 34

rCBF

regional cerebral blood flow. 35

LCD

liquid crystal display. 41, 42, 44, 50, 52, 54–56, 87, 89, 91, 120, 137

RGB

red, green and blue. 50

MR

magnetic resonance. 53, 55, 56, 59, 140

NMR

nuclear magnetic resonance. 54

EPI

echo planar imaging. 55, 140

VBL

vertical blank. 56

UREC

University Research Ethics Committee. 57, 89

DICOM

digital imaging and communications in medicine. 61

BIDS

brain imaging data structure. 61, 63

MRIQC

magnetic resonance imaging quality control. 61, 63

NIFTI

neuroimaging informatics technology initiative. 61, 139

JSON

JavaScript object notation. 61

IQM

image quality metric. 61, 62

HTML

hypertext markup language. 62

SPM

statistical parametric map. 64, 70

OLS

ordinary least squares. 67

iid

independent and identically distributed. 67

FWHM

full width half maximum. 69

COPE

contrast of parameter estimate. 71

DC

direct current. 87, 88, 90

ECG

electrocardiogram. 87, 92

EMG

electromyography. 87, 92

ADC

analogue-to-digital converter. 88, 90

BDF

BioSemi data format. 88

CMS

common mode sense. 89, 90

DRL

driven right leg. 89, 90

FT

Fourier transform. 93

DFT

discrete Fourier transform. 93

FFT

fast Fourier transform. 93

PSD

power spectral density. 93–95, 101, 102, 110, 117

ADF

Augmented Dickey-Fuller. 98–100

KPSS

Kwiatkowski-Phillips-Schmidt-Shin. 98–100

INU

intensity non-uniformity. 139

RAS

right, anterior and superior. 139

AAL

automatic anatomic labelling. 140

SDC

susceptibility distortion correction. 141

Chapter 1

Introduction

1.1 Background

Brain-computer interfaces (BCIs) represent an expanding field of research offering an innovative approach to operate computers and external devices. Such systems enhance computer interaction by harnessing human neural activity as a control signal, enabling direct control over electronic devices like personal computers and tablets [1]. Numerous studies in recent years have demonstrated that non-invasive neural activity can effectively replace traditional methods of human-computer interaction, eliminating the need for muscular activity. The primary objective of BCI research is to provide individuals with restricted mobility or suffering from motor neuron degenerative diseases, an alternative means of communication. Such interfaces hold the potential to enhance the quality of life for these individuals and an increased level of independence. Brain-computer interface (BCI) technology has generated significant interest even among healthy users, particularly in the fields of computer gaming and virtual reality. Moreover, this technology holds promise in various other domains, including applications aimed at assessing fatigue in demanding occupations like air traffic controllers or truck drivers [2].

Brain-computer interfaces (BCIs) typically rely on the continuous monitoring of an individual's brain activity, often employing electroencephalography (EEG). Among the different neurophysiological phenomena suitable for driving BCI systems, one of the most reliable approaches relies on steady-state visually evoked potentials (SSVEPs) [3]. Steady-state visually evoked potentials (SSVEPs) are changes in the brain's neural activity in response to a visual stimulus flickering at a specific

frequency [4]. This neural response appears as an oscillatory pattern in brain signals, synchronising with the frequency of the visual stimulation. An SSVEP-based BCI is comprised of diverse stimuli, each flickering at a distinct frequency and associated to a specific command. These stimuli are presented to the user via a graphical user interface (GUI). The user selects a particular command by directing his/her attention towards the target stimulus. The BCI then analyzes the SSVEP signals to identify the user's intent, subsequently translating it into the corresponding command to operate a software application or an external device.

The nature of the repetitive visual stimuli (RVS), including its shape, colour, design and flickering frequency, are known to have an effect on the SSVEP response induced in the subject's brain. Thus, finding the ideal stimuli properties that evoke the strongest SSVEP is crucial for efficient SSVEP-based BCI systems. The placement of EEG electrodes for SSVEP detection across the scalp is an important factor in the utilization of such systems. Identifying the most practical and comfortable electrode locations is essential to enhance the accuracy and user comfort of BCI systems.

1.2 Objectives of the Dissertation

The aim of this dissertation was to use functional magnetic resonance imaging (fMRI) and EEG brain signal recording modalities to help localise the brain cortical areas where steady-state neural activity is modulated and obtain information about the changes in the SSVEP when subjects are presented with different stimuli parameters, namely, colour, shape and texture. To the best of our knowledge, no fMRI study has analysed the SSVEP response with different shaped and coloured stimuli, while only one study evaluated the SSVEP with a textured stimulus. Thus this research will provide new insights into the cortical regions activated by the brain when using different stimuli parameters. Furthermore, the analysis conducted in this research will contribute to developing more efficient SSVEP-based BCIs. To gather separate fMRI and EEG data to analyse the effects of varying the stimuli characteristics typical of an SSVEP-based BCI system, this study involves conducting experimental sessions on several subjects. Signal processing and statistical techniques are used to examine and compare the generated SSVEP

response from each of the stimuli parameters. Considering these aims, the specific objectives of this work can be outlined as follows:

1. To set up the fMRI modality for the University of Malta's MRI scanner and attain mastery in the execution of fMRI experiments, achieving a significant milestone by pioneering the first-of-its-kind study in the country.
2. To design an experimental protocol for presenting a range of stimulus characteristics to participants, from whom both fMRI and EEG data is collected during two separate experiments.
3. To identify the brain regions where SSVEPs are localized in the brain through findings from the EEG and fMRI modalities. This investigation aims to shed light on the neural mechanisms underpinning SSVEP responses and contribute to our understanding of individual differences in these cortical patterns, while answering the following questions:
 - What is the influence of different colour, shape and texture stimuli on SSVEPs from different areas of the brain?
 - Which of the different stimuli parameters brings about the strongest SSVEP response and in which area of the brain is this located?
 - Is the SSVEP response in non-occipital areas of the brain strong enough to be used to control an SSVEP-based BCI system?
 - How does the SSVEP response evoked by these stimuli vary in different frequency bands?

1.3 Layout of the Dissertation

Chapter 2 gives an introduction to SSVEP-based BCIs. An overview of the anatomy of the human brain focusing on the neurons, regions and lobes of the brain is given. The neural signal characteristics are highlighted, and the control signal types used in BCIs are explained focusing on the SSVEP. A discussion on EEG and fMRI is then given describing how brain signals are recorded using such techniques.

Chapter 3 is a literature review on SSVEP-based BCIs and their practical issues. A literature review on the current research that there is on the generation and localisation of SSVEPs in the brain is presented. Various stimuli properties namely,

colour, shape and texture, that affect the performance of SSVEP-based BCIs and how these may lead to more practical BCI setups are then discussed.

Chapter 4 starts with a description of the variable parameters to be investigated in this study. A description of the fMRI data recording setup is given by outlining the system architecture and the designed experimental protocol used to collect data from subjects. The preprocessing steps used to analyse the recorded data are presented.

Chapter 5 starts with an explanation of the algorithm used to analyse the fMRI data and how this was applied to the fMRI data recorded in this study while subjects were presented with different flickering stimuli. The results obtained are analysed, and the stimuli parameters that lead to strong SSVEPs at different frequencies and areas of the brain are identified.

Chapter 6 describes the setup used to conduct an EEG recording session to investigate the different stimuli parameters. The signal processing techniques used to preprocess and extract features from the EEG data are presented. The SSVEP response across the scalp is then analysed using these techniques, highlighting how this varies with different stimuli characteristics.

Chapter 7 discusses the main findings and provides a detailed analysis of the results from both the fMRI and EEG studies whilst pointing out any interesting observations that were identified. The findings from the two recording modalities were then compared to each other. Any limitations faced throughout this study and suggestions for possible future work are presented.

Chapter 8 provides an overview of the project's accomplishments and the primary findings derived from it.

Chapter 2

Theoretical Background

2.1 Introduction

The process of understanding how a brain-computer interface (BCI) operates requires an understanding of the characteristics and functionality of the brain. A thorough comprehension of how scalp electroencephalography (EEG) and functional magnetic resonance imaging (fMRI) are recorded is also essential since these were the two modalities employed in this study to analyse brain signals. This chapter gives a theoretical background on the building blocks of the brain, including the function of the neuron, the brain regions and structures, and the different neurophysiological frequency bands present in the EEG signals. It also describes how BCI systems operate and the data acquisition methods used to record brain signals, focusing on EEG and MRI.

2.2 The Anatomy of the Human Brain

The brain is the human body's most complex organ. This section introduces the neuron, which is the brain's basic building block. This is followed by a discussion about the different areas of the brain and their functions whilst delving into more detail on the occipital region and the surrounding areas. Finally, some standard brain atlases which are relevant to this study are described.

2.2.1 The Neuron

The brain is responsible for operating all bodily processes, interpreting data from the outside environment and generating all thoughts and memories. The neuron or

the nerve cell is one of the most essential components of the nervous system and is the primary component of the brain [5, 6].

Three crucial components make up the neuron; the axon, cell body, and dendrites [5–7]. Information from sensory receptors or from another neuron is received through the dendrites of the neurons which extend from the neuron’s cell body [8, 9]. This information is then transported to the cell body and to the axon where it is converted to an electrical signal [7, 10]. The axon is a long, tail-like structure which carries the electrical signal that is known as the action potential along the entire length of the neuron [7–9]. The action potentials are transferred from one neuron to another by means of neurotransmitters through the synapse [11].

Neurons can regulate their chemical environment by moving ions and molecules across their cell membranes [12]. This transfer of ions creates a voltage difference, known as the membrane potential, between the cell’s interior and exterior [11–13]. Neurons maintain a negative internal potential compared to the external environment when at rest. The action potential temporarily reverses this polarity, making the transmembrane potential briefly positive [9]. This resting potential and action potential generation are explained by the neuron’s selective ion permeability and the distribution of ions across the cell membrane [11, 13]. Figure 2.1 presents a visual representation of the neuron structure and how electrical signals propagate along axons via synapses.

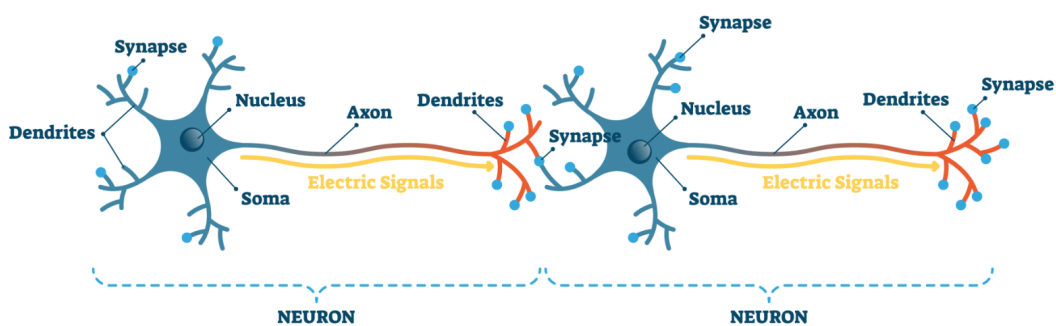


FIGURE 2.1: The structure of the neuron. Adapted from [11].

2.2.2 Regions and Lobes of the Brain

The cerebrum, brainstem, and cerebellum are the three main parts of the brain [6]. The cerebrum and cerebellum are connected to the spinal cord by the brainstem which controls automatic processes like breathing, pulse and heart rate, wake and sleep cycles, digesting, and swallowing [14, 15]. There are two hemispheres in the cerebellum and cerebrum. The purpose of the inner area of the cerebellum is to communicate with the cerebral cortex, which is a component of the cerebrum, and the outer portion of the cerebellum is made up of neurons [14, 15]. Higher-order processes including preserving posture, balance, equilibrium, and synchronising voluntary muscle movements are handled by the cerebellum [14, 15].

The cerebrum is the biggest and uppermost part of the human brain [15]. The cerebrum consists of grey matter (commonly referred to as the cerebral cortex) and white matter. The cerebrum is linked to higher brain activities like conscious thought and sensory processing [14, 15]. The protective myelin-coated axons make up the majority of the white matter, while the neuron's cell body makes up the majority of the grey matter [9]. In addition, the cerebral cortex is split into four sections known as lobes. These are the occipital, frontal, temporal, and parietal lobes [16].

The largest lobe in the forepart of the head is the frontal lobe [5, 17]. It is responsible for reasoning, expressive language, higher-order cognition, motor movement, and fine muscle control [15, 17]. The middle section of the brain contains the parietal lobe, which helps to notice the surroundings and comprehend spatial relationships [17]. The parietal lobe also handles touch and pain experienced by the body [17]. The temporal lobe, which is found towards the base of the centre of the cortex behind the temples, interprets sensory input to derive meanings through language, emotional connections, and visual memories [17]. In the rear part of the brain lies the occipital lobe, which houses the visual cortex that interprets visual stimuli [17]. The location of these four lobes in the brain is highlighted in Figure 2.2.

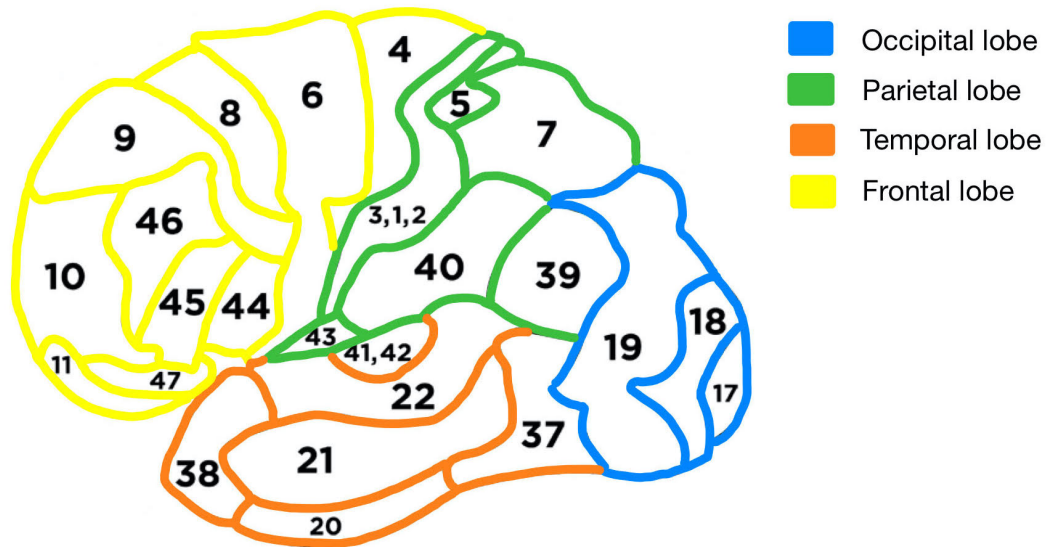
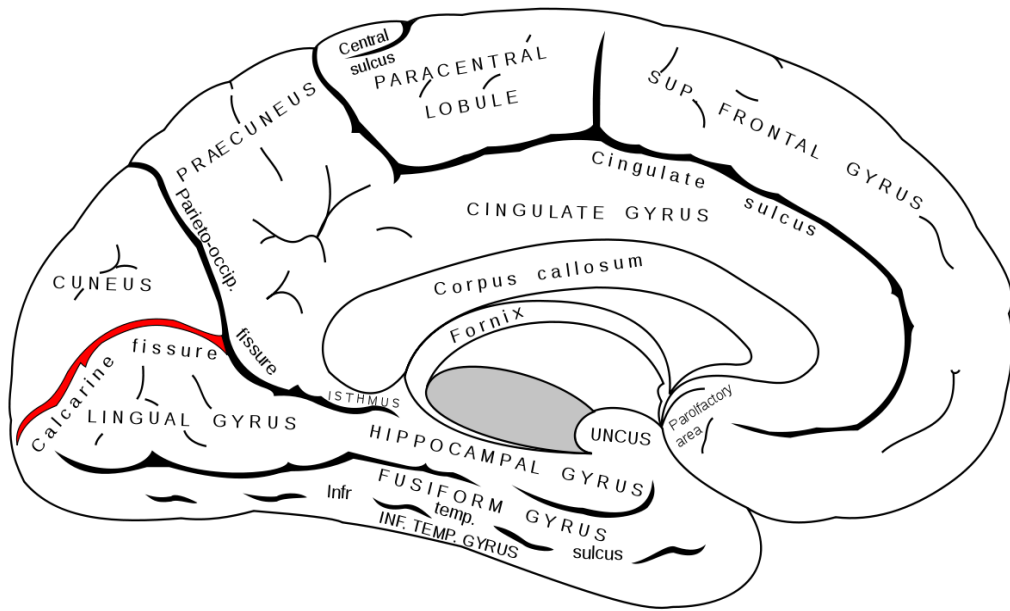


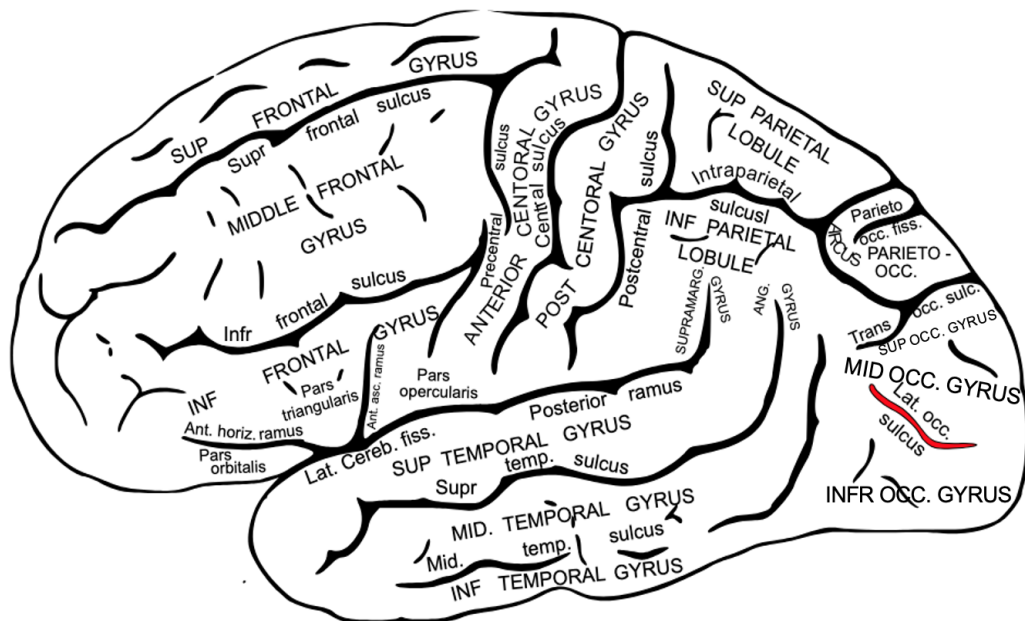
FIGURE 2.2: The four lobes of the brain and the location of the main Brodmann areas labelled as numbers.

2.2.3 The Occipital Lobe

The visual cortex, which is located in the occipital lobe, is divided into two main areas: the primary and secondary visual cortices [5, 6, 15, 18–20]. The primary visual cortex collects information from the retina and is located in and around the calcarine fissure shown in red in Figure 2.3(a) [18–20]. The calcarine fissure in turn separates the medial occipital lobe into the cuneus and lingual gyrus also shown in Figure 2.3(a) [21]. The middle occipital gyrus is located laterally between the superior and inferior occipital gyrus and its location is shown in Figure 2.3(b). The primary visual cortex is surrounded by the secondary visual cortex. Located below the lingual gyrus and extending from the temporal lobe is the fusiform gyrus, or lateral occipitotemporal gyrus. To the side of the fusiform gyrus is the hippocampal gyrus, or medial occipitotemporal gyrus, which runs along the medial sides of the occipital and temporal lobes [22]. The location of the fusiform and hippocampal gyri can be seen in Figure 2.3(a). Figure 2.3(b) also shows the gyri and sulci of the frontal, temporal and parietal lobes which will be referenced in the next chapters.



(a) Medial surface of the left cerebral hemisphere.



(b) Lateral surface of the left cerebral hemisphere.

FIGURE 2.3: Gyri, sulci and fissures of the brain. Adapted from [21, 23].

2.2.4 General Structure and Cellular Organisation

Anatomical location-based navigation, characterization, and information processing are made possible by the use of brain atlases which are used as spatial reference systems in neuroscience [24]. Anatomical, genetic, or functional characteristics may be included in brain atlases, which provide results of visual brain mapping [24].

The most popular brain atlas used and which was used in this study is the Montreal Neurological Institute (MNI) structural atlas [25, 26]. The MNI atlas, which is defined by unbiased averages of 152 T1-weighted MRI scans from 152 young adults from the International Consortium for Brain Mapping (ICBM) study, is a three-dimensional (3D) rendering of the human brain that can be used to map the locations of different brain structures without regard to individual variations in the brain's size and general form [25, 26]. Another brain atlas that was used in this study to reference cortical structures in the brain is the Harvard-Oxford Cortical Structural Atlas. This encompasses 21 subcortical and 48 cortical brain regions that have been obtained from MRI structural images given by the Harvard Center for Morphometric Analysis [27].

The Brodmann area is a numbered map of the brain cortical areas in humans dividing the brain into 43 differing parts (numbered sequentially from 1 to 43), which have been originally defined by Korbinian Brodmann based on the organisation of neurons analysed using the Nissl method of cell staining [28, 29]. For nearly a century this numbered map has been discussed and refined and remained the most frequently cited cytoarchitectural organization of the human cortex. This project will reference the Brodmann area when mentioning different regions of the cerebral cortex in the brain [28, 29]. Figure 2.2 shows a selection of Brodmann areas (labelled as numbers) and their corresponding location in the brain.

2.2.5 Neural Signal Characteristics

Rhythmic or repetitive electrical signals that are generated spontaneously or in reaction to stimuli by neural tissue in the central nervous system are commonly known as “neural signal oscillations” [30]. Electroencephalography (EEG) is a technique that is able to measure large-scale neuronal activity. The neurons in the cerebral cortex, which are positioned perpendicular to the surface of the brain, are assumed to be the main source of EEG [31]. Particularly, the neural signals captured by the EEG represent the combined electrical activity resulting from the excitatory and inhibitory postsynaptic potentials of clusters of neurons firing in synchrony [31]. These various neuron signals are correlated with particular states of consciousness, attention, or emotion [6, 12]. Since these frequencies can vary from person to person as well as depending on the stimulus characteristics and

internal states, five different frequency bands are defined: the delta band (0.5 Hz - 3 Hz), theta band (4 Hz - 7 Hz), alpha band (8 Hz - 12 Hz), beta band (13 Hz - 30 Hz), and gamma band (> 30 Hz) [17].

Delta band (0.5 Hz – 3 Hz): Delta band waves have been located in the frontal areas of the brain in adults and posteriorly in children [17]. These have been observed during continuous-attention tasks and during deep non-rapid eye movement (NREM) sleep, also referred to as slow wave sleep (SWS) [12, 17].

Theta band (4 Hz – 7 Hz): Theta band frequencies are primarily present in young children, adults, and adolescents who are drowsy or daydreaming [17]. Theta activity, mostly found in the frontal parts of the brain, is associated with difficult mental tasks like concentrating and memory recall [32].

Alpha band (8 Hz – 12Hz): Alpha band activity is centred over the occipital region in the brain, and it is associated with sensory, motor, and memory processes [17]. High amplitude alpha band activity is described as occurring during relaxed wakefulness when the eyes are closed during mental and physical relaxation [32]. However, it attenuates during mental or bodily tasks when the eyes are open.

Beta band (13 Hz – 30 Hz): Low-amplitude beta band activity is most visible in the frontal and posterior regions of the brain [17, 33]. Beta waves are linked to normal waking consciousness activity, that is generally associated with active thinking, focusness, alertness and anxiousness [17, 32].

Gamma band (> 30 Hz): Gamma waves correspond to large-scale brain network activity and are therefore related to certain perceptions or motor tasks that combine two different senses, such as hearing and sight [17, 33]. Studies have demonstrated a connection between motor activity and the generation of gamma waves during muscle contraction [33]. Gamma waves have also been linked to short-term memory, the recognition of sounds, objects, or tactile experiences [32].

2.3 Brain-Computer Interfaces

A brain-computer interface (BCI) or brain machine interface (BMI) acquires, identifies and evaluates brain signals' features that indicate the user's intent, converting these features in real-time into the corresponding output [33]. As a result, BCIs enable interaction between the brain and external hardware or software without the need for any physical movement. A BCI consists of four main elements: signal acquisition, feature extraction, feature translation and device output [34]. Signal acquisition is the measuring and recording of brain signals using a specific sensor technology followed by amplification, filtering and digitizing of the acquired signals [1, 34]. The signals are then transferred to a computer for further analysis to enable feature extraction, which extracts properties of interest from the digital signals. The feature translation method subsequently processes the obtained signal features and transforms them into the pertinent commands for the application [1, 34]. The control loop is closed once the output device is operated by giving the user feedback.

Originally BCIs were created to assist people with locked-in syndrome to communicate with the environment and people around them [35]. Locked-in syndrome can be the result of long-term neurodegenerative diseases like amyotrophic lateral sclerosis (ALS). However, BCIs can also assist individuals having a wide range of physical disabilities [36]. Such devices are now being used as a means to operate prosthetic limbs, control electric power wheelchairs, as a way to assist people with neuro-regenerative therapies using functional electrical stimulation (FES), and to communicate with technologies such as personal computers and televisions [36]. In the last 10 years, BCI research has expanded to be used by healthy individuals [36]. Such applications include creating improved immersive experiences for video games and virtual reality and to develop smart environments including transportation, workplaces, and smart houses [1, 37].

This section explains and compares different types of BCIs and the signal acquisition techniques used to record the brain signals. This is followed by a discussion on the different control signals used in the literature to control BCIs.

2.3.1 Types of BCI Systems

In general, there exist three types of BCIs. These are invasive, partially or semi-invasive, and non-invasive BCIs [38]. Invasive BCIs consist of implanting electrodes directly into the cerebral cortex of the human brain during the process of neurosurgery such that the firings of hundreds of neurons can be measured [38]. These BCIs have the advantage that they can interpret the highest-quality signals making them very accurate. Despite this, the procedure of implanting electrodes into the brain can cause significant problems as scar tissues may form in the brain and the implanted electrodes may be rejected by the human body [38, 39]. Partially invasive BCIs still require neurosurgery to implant electrodes in the brain, however these differ from invasive BCIs as the electrodes record brain electrical activity by being positioned on the outer surface of the cerebral cortex. [38]. The advantages of such systems include the high spatial resolution, signal fidelity and good signal-to-noise ratio [38, 39]. Apart from this, these systems are robust over long periods and offer lower clinical risk than invasive BCIs since the electrodes do not penetrate into the cortex.

When it comes to non-invasive BCIs, there are several non-invasive techniques to record brain signals including electroencephalography (EEG), functional magnetic resonance imaging (fMRI), magneto-encephalography (MEG) and functional near-infrared spectroscopy (fNIRS).

Electromagnetic fields are used in fMRI to measure the amount of oxygen present during neuronal activity by tracking variations in cerebral blood flow (CBF) [40]. Although this approach provides an excellent spatial resolution, it suffers from an acceptable time resolution making such equipment difficult to use for fast and practical BCI systems [40]. Magneto-encephalography (MEG) measures the magnetic fields caused by the electrical impulses of the neurons that capture the brain signals whilst providing a high spatial and temporal resolution [41]. However, due to their immobility, size, and high cost, MEG scanners require ongoing technical upkeep and training resources making them impractical to use for BCI systems. Near-infrared light is used by fNIRS to measure the cortical oxygenated hemoglobin (oxyHb) and deoxygenated hemoglobin (deoxyHb) changes which occur in response to neural activity [42]. Such method provides a high spatial resolution, though it

is limited by its poor temporal resolution [42].

Non-invasive EEG-based BCIs depend on the placement of electrodes at specific scalp locations to capture brain activity without needing to penetrate the skull, making them easy to wear and safe to use [36]. Nonetheless, when compared to invasive and partially invasive BCIs, these systems have the drawback that they have limited spatial resolution and lower signal-to-noise ratios (SNRs) due to the signal attenuation brought about by the skull and the artefacts in the recorded signals [36]. However, they have an excellent time resolution and out of the non-invasive BCI modalities discussed in the previous paragraph, EEG is the most commonly used due to its low cost and portability [36, 38]. This study focuses on EEG SSVEP-based BCIs.

2.3.2 Control Signal Types in BCIs

Numerous studies have found various brain phenomena that can act as control signals in BCI systems. Four categories of current non-invasive BCIs are separated based on the electrophysiological signals they record. These BCIs employ sensorimotor rhythms (SMRs), P300-evoked potentials, visual-evoked potentials (VEPs), and slow cortical potentials (SCPs).

The SMR paradigm works by imagining the movement of different parts of the body, which generates specific event-related potentials (ERPs), to control the output device [39, 43]. The P300 signal is usually recorded from centroparietal regions 300 ms after displaying an oddball visual, auditory or somatosensory stimulus among a series of routine stimuli [39, 44]. Slow cortical potentials (SCPs) appear in EEG as slow voltage shifts oscillating at a frequency below 1 Hz, where positive SCPs are frequently associated to diminished cortical functions while negative SCPs are related to tasks that require cortical activation and movement [1, 33].

When a subject is exposed to visual stimuli, brain potentials called VEPs [1, 4, 33] are generated. The shape of the visual stimuli, the frequency of visual stimulation, and the area of the exhibited stimulant are the three visual stimulus characteristics that typically influence VEPs. Visual-evoked potentials (VEPs) are produced by simple, single-colour stimulation or by using patterns like a checkerboard [4]. The classification of VEPs as transient visually evoked potentials (TVEPs) and

steady-state visually evoked potentials (SSVEPs) depends on the frequency of the visual stimulus [1]. A visual stimulus flickering at frequencies under 6 Hz produces TVEPs, while SSVEPs arise from higher frequencies [1].

This project focuses on SSVEP-based BCIs due to the advantages that they require no training making them fast to set up, the SSVEPs are induced when subjects are exposed to frequencies up to 100 Hz allowing the BCI to have multiple commands, and current SSVEP-based BCI systems provide very high accuracies and information transfer rates (ITRs) when using electrodes placed on the visual cortex [45–49].

2.4 Signal Acquisition Methods

As mentioned in Section 2.3.1, there are several methods how to acquire brain signals in a non-invasive way. In this section, focus is given to EEG and fMRI since these technologies were used in this study to record and analyse the brain response.

2.4.1 Instrumentation to Analyse Brain Activity

Functional magnetic resonance imaging (fMRI) and EEG are two common modalities used to measure cerebral activity in the brain. While EEG measures electrical potentials on the scalp caused by coherent activity in vast populations of cortical neurons, fMRI measures changes in blood volume and the ratio of oxyHb to deoxyHb, known as the blood oxygenation level dependent (BOLD) response [50].

The fundamental premise of many investigations is that attentional modulations of early sensory responses evaluated with fMRI and EEG represent the same changes in brain activity at various spatial and temporal resolutions, thus findings from fMRI and EEG complement each other [51].

In this study, both modalities were used to analyse the SSVEP response to make use of the advantage of the fine-grained spatial resolution that the fMRI provides and the high temporal resolution of EEG for fast SSVEP-based BCIs in real-time applications. The integration of both modalities allows for a more holistic understanding of the neural processes underlying the response to RVS. It is worth noting

that this is the first study carried out at the University of Malta to implement and carry out a functional MRI study, thus a data collection protocol and experimental paradigm were designed from scratch. A high-channel EEG was also used to locate the SSVEPs providing a good spatial resolution.

2.4.2 Electroencephalography

Electroencephalography (EEG) uses small metal contacts or electrodes placed on the scalp's surface to measure the electrical activity or voltage fluctuations produced by synchronised neurons in the brain [12, 52]. The collected data is digitized and transmitted to an amplifier which is then shown as a series of voltage readings [12, 52, 53]. To make sure that the EEG data is gathered from identical scalp positions across all users and to allow for quicker administration of the electrodes, these are fixed in EEG elastic caps [52]. Mainly this recording modality has the advantage that it is non-invasive providing safety to the participants [52, 53]. Electroencephalography (EEG) has a number of benefits over other non-invasive signal acquisition methods. Alternative neuroimaging techniques, including MEG, MRI, and positron emission tomography (PET), are expensive to maintain and involve bringing participants into a hospital or lab setting in order to conduct the investigations [53]. Other advantages include that it is affordable, portable, has a high temporal resolution, is relatively tolerant to motion artefacts, is silent and it is not claustrophobic [52, 53]. Given these advantages, EEG-based BCIs are the most popular type of BCIs to be researched and developed.

2.4.3 Electrodes and Electrode Placement

Wet and dry electrodes, which can both be passive or active electrodes, are the two types of electrodes that an EEG system can use [54–56]. Wet electrodes are coated with materials such as silver or silver chloride (Ag/AgCl), and to improve conduction, lower the impedance of the skin-electrode interface and reduce motion artefacts, they use an electrolytic gel containing chloride ions that serves as a conductor between the electrode and the scalp [54–56]. These types of electrodes provide high-quality EEG signals however, the skin is abraded and each electrode is separately filled with gel and fitted to the EEG cap which takes time to set up [54, 55]. Dry EEG electrodes are made up of an inert conductive material that mechanically couples to the skin for signal transmission, removing the need for an

electrolytic gel and skin preparation [54, 55, 57]. Dry electrodes can be made of a variety of materials and shapes, including silicone conductive rubber, bristle-type electrodes, comb-like electrodes, multi-pin electrodes, and gold-plated electrodes [58]. Nonetheless, these electrodes are more susceptible to movement artefacts and higher impedances [54].

Conventional passive electrodes use a conductive wire to transmit voltage fluctuations from the conductive material to the amplifier [55, 56, 59, 60]. Active electrodes position a pre-amplification module near the conductive material between the scalp and the electrode [55, 56, 59, 60]. This module amplifies the weak EEG signal directly at the electrode, improving the SNR and reducing vulnerability to electromagnetic interference [59, 60]. Wet electrodes may need skin preparation or electrolytic gel, but a high input impedance pre-amplifier can eliminate these steps by reducing skin impedance [59].

The international standard method known as the 10-20 electrode system, is used to identify and locate the scalp electrodes of an EEG [17, 61]. The numbers “10” and “20” stand for the 10% and 20% of the skull’s total front-back or right-left distance that are used to determine the spacing between neighbouring electrodes as shown in Figure 2.4 [17, 61]. The right-left distance of the skull refers to the distance from the preauricular, a small pit in front of each ear, while the front-back distance refers to the distance from the nasion, the midline bony depression between the eyes at the top of the nose, to the inion [17, 61]. A letter is assigned to each electrode placement which designates the region of the brain from which it is collecting data. Pre-frontal (Fp), frontal (F), temporal (T), parietal (P), occipital (O), and central (C) are the letters that make up this group [61]. A number or additional letter that indicates the separation from the midline follows this letter. The electrode is shown to be located on the right hemisphere when the number is even, and on the left hemisphere when the number is odd. The number increases the farther the electrodes are positioned from the midline [17, 61]. A ‘z’ for zero is used to identify electrodes that are positioned exactly on the midline [17, 61]. The 10-20 system additionally employs two additional electrodes known as the ground electrode and the reference electrode, which usually are the Cz and Fz electrodes [12, 61]. Figure 2.4 shows the 10-20 electrodes for a 21-channel EEG setup, however the 10-20 system can be further expanded to high-density EEG

setups using up to 256 electrodes. This has been done by expanding the existing 10-20 system to the modified combinatorial nomenclature (MCN) [25]. The MCN incorporates additional electrodes at intermediate locations of the existing 10-20 electrodes with extra electrodes using 10% or 5% divisions by introducing extra numbers and letter codes to name the intermediate electrode sites [25].

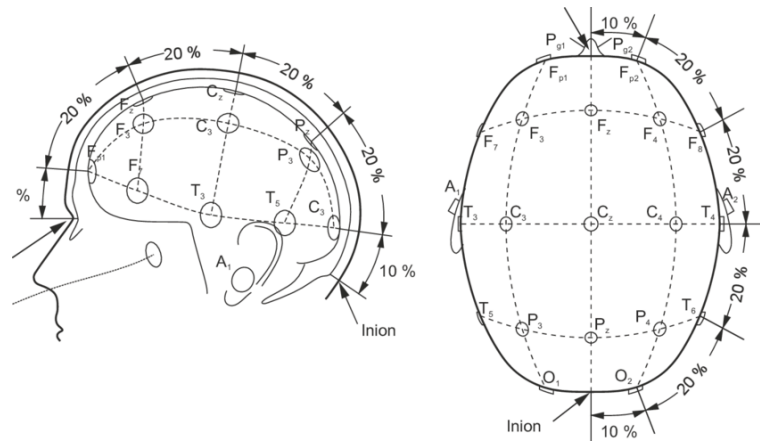


FIGURE 2.4: The 10-20 electrode system set up. Adapted from [62].

2.4.4 Magnetic Resonance Imaging

As the EEG electrodes detect electrical potential at the brain's surface, distinguishing whether the signal originates near the surface (in the cortex) or from deeper brain regions poses a challenge, suggesting that EEG suffers from poor spatial resolution [63]. In contrast, MRI provides high spatial resolution images producing high-quality two-dimensional (2D) or 3D images of the brain. Magnetic resonance imaging (MRI) is a non-invasive, safe procedure for people of all ages including children and pregnant women [63, 64]. It does not use ionizing radiation, as in computed tomography (CT) scans, which could cause tissue and skin damage [63, 64]. Furthermore, contrast agent injections, which can be risky for some individuals with kidney issues or allergies, are not required during an MRI [63, 64].

2.4.4.1 Working Principles of MRI

Magnetic resonance imaging (MRI) relies on the magnetic properties of atomic nuclei as its foundation [65–68]. The hydrogen protons in our cells which make up between 70% and 80% of the typical human brain, are arranged into alignment using a powerful, external, uniform magnetic field [65]. The external disturbance

to this alignment, known as magnetisation, is induced by applying an external radio frequency (RF) pulse within the magnetic field [67, 68]. The RF energy is then turned off, and the nuclei return to their resting alignment through a number of relaxation processes, where they are aligned to the magnetic field releasing RF energy in the process [67, 68]. The signals emitted are detected after a specified time interval following the initial RF pulse [67]. The process of the magnetisation of the hydrogen protons is simplified in Figure 2.5.

Three types of relaxation processes occur, known as the T1, T2 and T2* relaxation times [66, 69, 70]. The T1 relaxation time relates to the speed of the hydrogen protons and how fast they return to equilibrium and realign back to the magnetic field [66]. The T2 relaxation time measures the duration for which hydrogen protons that are spinning perpendicular to the main magnetic field, lose their phase coherence, resulting in the loss of resonance among the spinning protons [66, 69]. These different relaxation times enable the distinction of various tissues like fat, muscle, and water [66]. The data is then processed by a computer to create 2D and 3D tissue maps in the scanned area, generating images of body tissues [66].

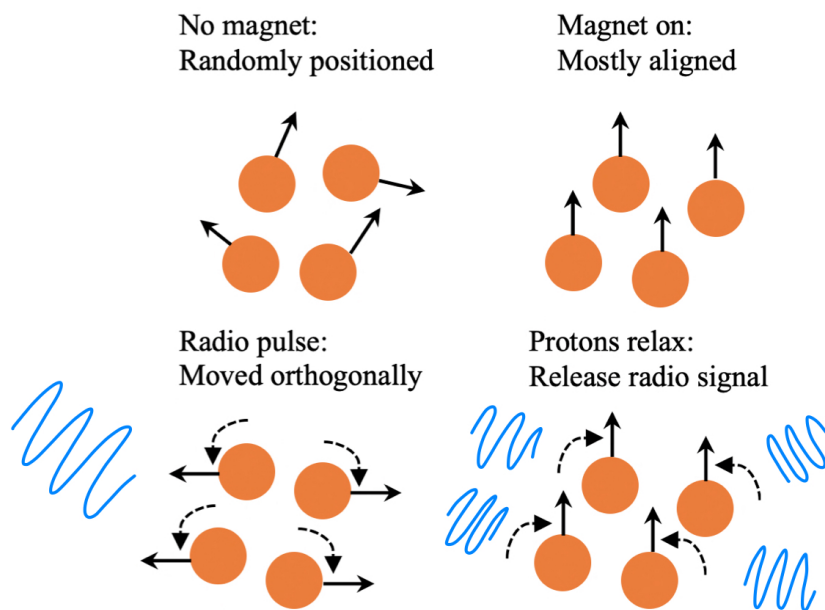


FIGURE 2.5: The process of magnetisation of the hydrogen protons in the body.

T2* relaxation forms the basis of functional magnetic resonance imaging (fMRI) as it quantifies the effect of transverse magnetisation from both magnetic field inhomogeneities and spin-spin relaxation. When there is an abundance of deoxyHb in the blood, the MRI signal decreases, indicating lower neuronal activity [71]. Conversely, increased neuronal activity results in a rise in the MRI signal detected locally. Detecting these signal alterations requires the use of an MRI sequence that is sensitive to T2* relaxation [71]. Hence, the majority of functional imaging relies on rapid gradient-echo sequences that are finely tuned to maximize sensitivity to T2* [71].

A single 3D MRI image or scan is known as a volume that is composed of voxels [71, 72]. Voxels are the 3D equivalent of the 2D pixels that make up digital photos [71, 72]. A structural image usually has high resolution having a standard voxel size of 1 mm x 1 mm x 1 mm while functional images have lower resolutions with a voxel size of 3 mm x 3 mm x 3 mm since they use a faster imaging sequence. Each volume of the brain is recorded in a succession of slices in the fMRI sequences [72]. Because of this, each slice is obtained at a separate time inside the repetition time (TR) [72]. For some preprocessing stages, knowing the slice acquisition order (ascending, descending, or interleaved) can be crucial [72]. Although a slice's thickness can vary, the voxel dimensions within a slice are nearly always the same [71].

During an MRI recording session, the participant is positioned inside a large magnet and must maintain absolute stillness to prevent image blurring [68]. Various types of images can be generated by modifying the order of RF pulses transmitted and received [66, 68]. The time interval between successive RF pulse sequences applied to the same slice is referred to as the TR [66]. The TR can be also described as the time it takes to record one volume of fMRI data. Additionally, the time elapsed between the delivery of the RF pulse and the reception of the echo RF signal is referred to as the time to echo (TE) [66].

2.4.4.2 MRI Images

The T1 and T2 weighted images are the most commonly utilised contrast images in MRI sequences [66, 70]. T1-weighted MRI suppresses the water signal and magnifies the signal of the fatty tissue. Short TE and TR timings are used to

create T1-weighted images [70]. On the other hand, T2-weighted images enhance the water signal by using longer TE and TR periods [70].

Magnetic resonance imaging (MRI) research commonly employs three imaging modalities: structural, diffusion, and functional imaging [40, 71]. The first, known as structural or anatomical imaging, provides details about the broad anatomical divisions of the brain, such as the cerebral cortex's boundaries and those of other structures like the hippocampus [71]. The second modality, diffusion-weighted imaging, or diffusion magnetic resonance imaging (dMRI), offers details on the anatomical connections and microscopic structure of the brain and spinal cord [71]. The third method, functional imaging or fMRI, provides data on the neural activity of the brain, in relation to the participant's neurons' spontaneous activity (resting state fMRI) or their response to particular stimuli or tasks applied by the experimenter [71].

2.4.4.3 Functional Magnetic Resonance Imaging

Functional magnetic resonance imaging (fMRI) is a neuroimaging method used to detect image dynamic changes occurring in the brain tissue as a result of changing neuronal metabolism. The typical method employed in fMRI research is BOLD imaging, which relies on changes in cerebral blood flow (CBF) to detect regional activity [40, 50, 71, 73]. Blood flow within the brain is regulated locally in response to the levels of oxygen and carbon dioxide in the cortical tissue [40, 71]. When a specific cortical region becomes more active during a task, it initially experiences a drop in oxyHb and an increase in local carbon dioxide and deoxyHb [73]. Following a delay of two to six seconds, CBF in the brain increases, carrying large amounts of oxyHb that flushes out the deoxyHb [73]. This large amount of introduced oxyHb that is able to be distinguished from deoxyHb due to the differences in paramagnetic properties is what the fMRI image shows [40, 50].

The hemodynamic response function (HRF) describes the temporal changes in the BOLD signal, usually reaching its peak approximately three to seven seconds after the presentation of a stimulus [71, 74, 75]. This measurement represents the ideal scenario in a noise-free MRI scanner when a subject is exposed to a brief, distinct stimulus, and the brain's response is solely attributed to it, disregarding any other neuronal or physiological variations [71, 75]. The shape of the HRF signal shown in

Figure 2.6 resembles a Gamma Distribution, having a peak close to the beginning of the time axis (the x-axis) and a long tail to the right [75].

The generation of SSVEPs in the brain when a subject is exposed to flashing stimuli is correlated to an increase in neuronal activity [76]. As the neural activity in the visual processing areas intensifies, there is an increased demand for oxygenated blood, and in response the brain's vascular system dilates the blood vessels in the active regions [76–79]. Although any frequency content cannot be extracted from the fMRI BOLD signal, an increase in the HRF response in the brain when a subject is exposed to visual stimuli flickering at a frequency above 6 Hz can be associated with SSVEPs present in brain [76].

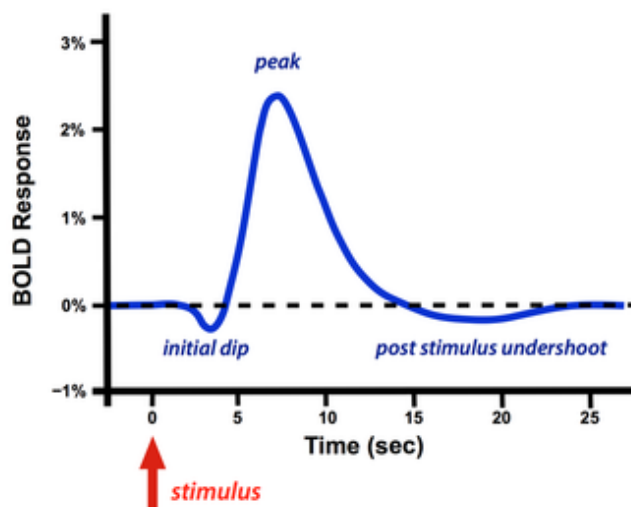


FIGURE 2.6: BOLD hemodynamic response function (HRF) following a single brief stimulus. Adapted from [74].

2.5 Chapter Summary

This chapter presented an overview of the anatomy of the human brain, discussing the neuron and the different lobes and structures of the brain. The neural signals were divided into five frequency ranges, and a description of the state that each frequency band reflects was also provided. A description of BCIs was given, including the different type of BCIs and the various control signals typically used in such systems. Finally, a detailed description of the two brain signal recording methods of EEG and MRI was given.

This project focuses on analysing the brain activity as recorded by both EEG and fMRI during visual stimulation typical of SSVEP-based BCIs. This will provide insight on the brain's response to such stimuli across the whole scalp and how this varies when stimuli parameters are changed. Subsequently, any brain activity related to SSVEPs that can be captured robustly from non-occipital regions of the brain provide a practical way forward to BCIs.

The next chapter presents a literature review on the practical issues of SSVEP-based BCIs and the current literature investigating the generation and location of SSVEPs in the brain. This is followed by a discussion on how the strength of the SSVEP response is affected by varying the visual stimuli properties across different regions of the brain.

Chapter 3

Literature Review

3.1 Introduction

This chapter introduces the general architecture of SSVEP-based BCIs and how these systems have practical issues when used outside of clinical and laboratory environments. This is followed by a discussion on the generation of the SSVEPs from different locations in the brain and how this can vary by changing the stimuli properties that evoke SSVEPs. The review is then utilised to determine the proposed approach to be followed in this study and its primary contributions.

3.2 Overview of SSVEP-based BCIs

An SSVEP-based BCI consists of a number of RVS flickering at particular frequencies [76, 78, 80, 81], which the user needs to attend to in order to activate the corresponding command to control an external device or a computer application. More specifically, to generate a control action the user fixates on the chosen command evoking an SSVEP that is predominantly generated in the primary visual cortex of the brain [76, 78, 80, 81]. This SSVEP appears as an increase in the amplitude of the EEG signal at the stimulus frequency and its harmonics [82]. The BCI is then able to classify this signal to predict at which stimulus the user was looking at and the corresponding command is then executed [82, 83].

3.3 Practical Issues of SSVEP-based BCIs

Steady-state visually evoked potential (SSVEP)-based BCIs using EEG gained a lot of popularity in the last few decades in the areas of neurotechnology and neural engineering. This is due to the advantages of having a high performance and signal-to-noise ratios (SNRs) [82]. Additionally, these systems do not necessarily require any training or calibration, are easy to use and to set up [45, 82, 84].

Steady-state visually evoked potential (SSVEP)-based BCIs still have their own limitations. In recent years a lot of research has been done to address the challenges of EEG measurement. To do this, a considerable amount of studies focus on improving the performance and the speed of such systems by using different encoding techniques and classification algorithms [85–91]. Recently, the original task-related component analysis classification algorithm (TRCA) which has shown to give good results in previous studies [92] has been modified by Tang et al. [85] to obtain a significantly higher performance in the offline analysis. In the same study, the information transfer rate (ITR) for online systems was also improved by incorporating the dynamic stopping (DS) algorithm that is based on Bayesian posterior probability when classifying the EEG signals, reaching a maximum of 420.2 bpm which based on our knowledge, is one of the highest online ITR for SSVEP-based BCIs [85]. In another study, Phyo Wai et al. [86] aimed to decrease the user's response time (i.e. the time required by the user to fixate at the flickering stimulus) for the SSVEP-based BCI while maintaining a high accuracy [86]. This was done by proposing the method of temporal alignments enhanced canonical correlation analysis (TACCA) which managed to increase the accuracy by 10 - 30% for short time responses of 0.5 s and 1 s when compared to other standard algorithms used in literature [86].

Some researchers opted to introduce other signal acquisition techniques with SSVEP-based BCIs to create hybrid systems that can potentially increase the speed and accuracy of the pure SSVEP-based systems [93–99]. Saravankumar and Reddy [93] combined vision-based eye gaze tracker (VET) and electrooculogram (EOG) with SSVEP reaching an average classification accuracy rate of 98.33% and an ITR of 69.21 bpm [93]. Steady-state visually evoked potential (SSVEP) has also been combined with surface electromyography (sEMG) activity. Rezeika et al. [94] developed this system to control a spelling application obtaining faster

accuracies and ITRs when compared to a standard SSVEP-based BCI system, reaching 92.37% accuracy and a 31.02 bpm ITR [94].

Transitioning BCIs to use dry electrodes instead of the traditional wet electrodes has also been one of the main research areas in the past few years [77, 84, 100–103]. Dry electrodes do not require any conductive gel to be placed over the hair-covered areas to obtain the EEG signals. This has the advantage that it reduces the preparation time to set up the EEG system and it will not require the user to clean his/her hair after using the equipment. The BCI designed by Xing et al. [100] which consisted of eight dry electrodes having a claw-like structure located at the occipital region of the brain obtained an ITR of 92.35 bpm and a high average classification accuracy of 93.2% [100]. Lin et al. [84] designed a field programmable gate array (FPGA)-based BCI with SSVEP enhancement having one active dry electrode located at the occipital region of the brain reaching an ITR of 47.91 bpm and a high accuracy of 91% [84]. However, despite the advantages of such systems, the absence of the conductive gel reduces the SNR of the recorded signals, and the performance of dry electrodes is not consistent considering that every individual has different hair length and thickness, thus their performance still remains low and variable when compared to systems using wet electrodes [104, 105].

Overcoming the disadvantage of visual discomfort experienced by the users when using SSVEP-based BCIs has been another goal to improve the practicality of such systems. This is because the flickering stimuli that the user needs to fixate upon to execute the necessary commands can cause tiredness, loss of attention and concentration difficulties when looked at for long periods of time [106, 107]. Furthermore, the flickering light sources can also induce photo epileptic seizures in susceptible individuals [107]. To tackle such an issue, studies have focused on changing the properties of the flickering stimulus such as the frequency, colour, size, duty-cycle, shape and modulation depth, to make the stimuli more comfortable to fixate upon [108–114].

The BCI setup of the studies discussed consists of laboratory-grade EEG systems consisting of an electrode cap having wired electrodes attached to the occipital region of the brain, similar to the one shown in Figure 3.1. This setup makes current SSVEP-based BCIs uncomfortable to wear whilst being socially inappropriate in

non-clinical and laboratory conditions due to the bulkiness of such setup. Although the transition from using wet to dry electrodes increased the practicality of BCI systems, having electrodes at the occipital region at the lower back part of the brain may be an issue when users are lying face up [115]. The help of another individual is also required to place electrodes at the occipital region as this area is unreachable by the user. Thus, finding other areas in the brain where the SSVEP signal can be reliably acquired is crucial to make these systems more practical.

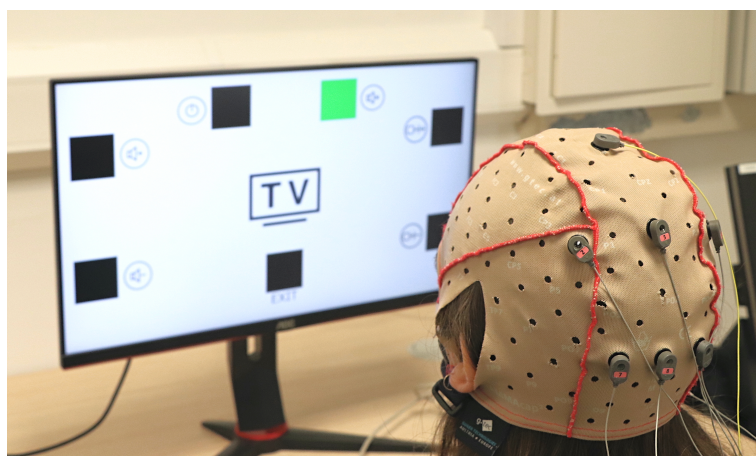


FIGURE 3.1: An example of a laboratory SSVEP-based BCI setup.

3.4 EEG Alternative Electrode Placement

This section delves into the origin of SSVEPs by looking at the visual pathway that describes how light is converted into electrochemical signals that can be interpreted by the brain, and by reviewing EEG and fMRI studies that aimed to locate SSVEPs in our brain. Finally, developed SSVEP-based BCIs that use SSVEPs acquired from non-occipital areas of the brain are discussed.

3.4.1 Source Localisation of the SSVEP

Locating the SSVEPs is an important step in understanding areas in the brain that respond to visual stimulation. These areas have the potential to be used as EEG electrode positions that can reliably capture the SSVEP response. In particular, areas away from the occipital region can improve the practicality of these systems.

3.4.1.1 The Visual Pathway

Steady-state visually evoked potentials (SSVEPs) are natural fluctuations of electrical activity in our brain that occur in response to visual stimulation [116]. The frequency of SSVEPs is directly correlated to the frequency of the visual stimulation in the range of 6 Hz to 90 Hz and such signals are typically recorded using EEG and electromyography (EMG) devices [91]. Understanding the visual pathway, that is, what happens to the visual sensation experienced by the retina as it reaches the brain when the user focuses on a visual stimulus, is thus essential to explain where SSVEPs are likely to be localised in the brain.

The visual pathway includes the retina, optic nerve, the lateral geniculate nucleus (LGN) and the primary visual area of the cerebral cortex known as cortex V1, Brodmann area 17, or striate cortex that are shown in Figure 3.2 [117]. The cortex is made up of six horizontal layers that are numbered from the outermost layer I to the innermost layer VI located near the underlying white matter [117, 118]. The visual information from the lateral geniculate nucleus (LGN) arrives at layer IV in the magnocellular cells, parvocellular cells and koniocellular cells which are found in extrastriate cortices that surround the primary visual cortex V1 [118, 119]. The extrastriate cortices are known as V2, V3, V4 and V5.

The visual system has parallel pathways corresponding to different properties of the stimuli, such as distinct pathways for conveying brightness and contrast. This is usually divided into the parvocellular (or P-pathway), magnocellular (or M-pathway) and koniocellular (or K-pathway) pathways [118, 119]. The M-pathway is associated with carrying information about moving stimuli, shapes, and depth while the P-pathway transmits information about spatial contrasts and the red and green colour [118, 119]. The K-pathway reacts to the blue and yellow colour and responds to spectral stimuli [119]. The information by the P and K pathways is then transmitted to the temporal lobe by the ventral stream and the information by the M-pathway is transferred to the parietal lobe by the dorsal stream as depicted in Figure 3.2 [120].

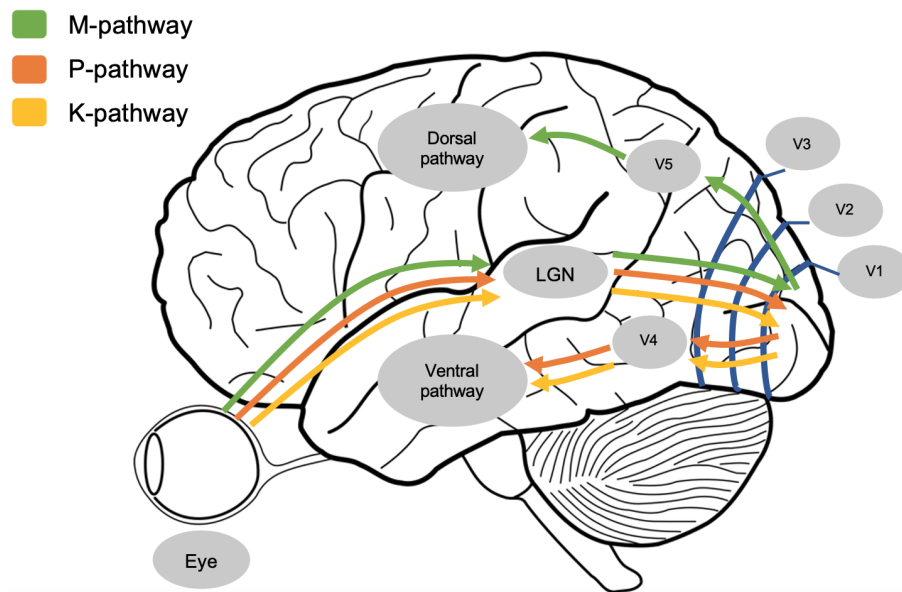


FIGURE 3.2: The visual pathway explained in terms of the three pathways. Green, orange and yellow arrows represent the M, P and K pathways respectively.

The visual pathway suggests that other areas of the brain apart from the primary visual cortex, such as the parietal and temporal regions are associated with processing the visual information. Thus, the development of VEPs at the cortical level is significantly influenced by the three pathways. It is therefore vital to understand if the origin of SSVEPs and different stimuli properties including shape, colour and contrast are related to these three pathways, and if SSVEPs are also generated in the parietal and temporal regions.

3.4.1.2 SSVEP Source Investigated Using EEG and fMRI Modalities

Research throughout the years has focused on trying to identify the cortical and sub-cortical locations of SSVEP signals in the brain by using brain signal acquisition techniques, including EEG, fMRI and PET modalities. Understanding this could help in identifying EEG electrode positions where high quality SSVEP signals can be recorded other than the occipital region of the brain, to make BCIs more practical and accessible.

Hillyard et al. [76] have investigated the localisation of SSVEPs using both EEG and fMRI modalities in separate sessions by allowing subjects to fixate their attention on black character stimuli superimposed on a black-white flickering square at 8.6 Hz and 12 Hz. The SSVEP activations were first acquired using a 30-channel

EEG where dipole modelling was then executed to find the regions of the SSVEP generators modulated by attention. In a separate session, fMRI scanning was done using a gradient echo sequence to collect functional images while the users attended to the stimuli.

The fMRI images show significant activations at the inferior occipital gyri and medial occipital temporal gyri (which are located at the borders between the occipital lobe and the posterior and temporal lobes respectively) and occipital areas V2 - V5. EEG results showed that the mean SSVEP amplitude is increased over posterior scalp sites. Analysing the results from the two modalities together, the study concludes that attending to visual stimulations increases the activations in extrastriate cortical areas (V2 - V5) found in the occipital lobe which are regions surrounding the primary visual cortex V1.

Similar results were reported by Di Russo et al. [78] where one Gabor grating black-white stimulus having a frequency of 6 Hz was shown to the subjects. In this case the 64-channel EEG data, which were also evaluated by dipole modelling, resulted in an SSVEP localised in the medial occipital and mid-temporal regions of the contralateral hemisphere. The fMRI results from Di Russo et al. [78] indicate that the two major sources of activation when the subjects are presented with flashing stimuli are the primary visual cortex (V1) and the motion-sensitive areas (V5) although minor activations were also found in mid-occipital (V3) and ventral occipital (V4) areas which are extrastriate cortical areas [78].

Sammer et al. [121], Itthipuripat et al. [51] and Ji et al. [122] also localised SSVEP activations through their studies. According to Sammer et al. who investigated the SSVEP and other EEG waveforms using fMRI, clusters of voxel activations were identified in the occipital lobe, particularly in the primary visual cortex V1 and the left and right occipital gyri. Itthipuripat et al. observed BOLD activations in the regions of V1 - V4 and Ji et al. observed these responses from the EEG and fMRI data in the visual cortical areas (cuneus, calcarine fissure, fusiform gyrus, and occipital gyrus). From the study by Ji. et al., other areas where SSVEP activations from the EEG and simultaneous BOLD activations were obtained included the postcentral cortex, rolandic operculum (located between the precentral and postcentral gyri) and superior temporal gyrus.

The literature discussed in this section shows that the main cortical locations where SSVEPs are localised is the occipital lobe. However, the visual pathway, fMRI and EEG studies conducted by the literature highlight that areas in the parietal and temporal lobe are also modulated by the SSVEP suggesting that these areas can be used as EEG electrode locations.

3.4.2 Behind the Ear SSVEP-based BCIs

Throughout the past years, research was carried out to determine whether SSVEPs can be recorded from regions other than the occipital lobe with the aim of developing a truly practical SSVEP-based BCI system to be used outside well-controlled laboratory settings. In particular, non-hair bearing areas have been given a lot of attention since dense hairy areas of the scalp like the occipital area may have poor contact with the scalp requiring an electrode gel to increase the conductivity between the electrode and the scalp. Thus using electrodes at non-hair bearing areas may remove the need for using an electrode gel. This will reduce the time to set up the EEG equipment, the risk of having the electrode gel drying up after a few hours and the user having to clean his/her hair after using the equipment.

Studies mainly focus on three regions of non-hair bearing areas, these are: the face (forehead and sides of face), the neck and behind the ear regions. The performance of the three regions has been compared with electrodes placed at the occipital lobe. To do this, Wang et al. [115] used a black-white flickering stimulus which was displayed on a cathode ray tube (CRT) monitor having frequencies in the range of 9 Hz - 13 Hz. Results suggest that the consequent SNRs and classification accuracy from high to low were from the occipital lobe, behind the ear, neck and face. Furthermore, an online 12-target identification task was developed acquiring data from four electrodes placed on both sides of the ear and an average accuracy and ITR of 84.08% and 30.21 bpm was obtained.

The performance obtained by behind the ear electrodes by Wang et al. [115] is good however occipital SSVEP-based BCIs still achieve a higher performance. One way of increasing the performance of non-hair SSVEP-based BCIs is to improve the algorithm to classify the recorded SSVEPs. This has been done with occipital SSVEP-based BCIs, where algorithms such as template-based canonical correlation

analysis (CCA) and TRCA have shown a significant improvement in performance [123]. Chan et al. [124] compared these algorithms to each other when using non-hair SSVEP-based BCIs concluding that the TRCA is superior to CCA when using short data lengths, however, CCA performs better when the available number of trials is limited [124]. These results could be used to design non-hair SSVEP-based BCIs depending on the data length and number of trials. Chan et al. also determined that the average accuracy of 81.36% when utilising 4 s length data at non-hair behind the ear regions was similar to or better than using 1 s or 1.5 s data obtained from occipital areas.

The performance of SSVEP-based BCIs also depends on the age of the users and if they suffer from a condition or not. The EEG study by Hsu et al. [105] was performed on three different groups: young subjects, elders and ALS patients, and the performance from each group was compared. Apart from this, Hsu et al. also aimed to compare the performance of a single electrode when placed at the occipital and frontal areas of the brain. Interestingly, the amplitude of the SSVEP collected from the frontal electrode was found to be constant across the three groups, in contrast to the amplitude at the occipital region.

In accordance with the default setup of EEG acquisition devices, the reference electrode of an SSVEP-based BCI is often positioned at the mastoids or Cz electrode. The best reference may, however, differ from occipital SSVEP-based BCIs when employing signals from non-occipital locations. Lan et al. [125] conducted a study where they examined the spectra and topographical aspects of both the linked mastoids (LM) and Cz references. Their aim was to assess the influence of these Cz and LM references. When comparing electrodes from the central and temporal regions of the brain, it was concluded that the LM reference provides better SNRs. However, when the performance is evaluated in terms of accuracy and classification accuracy it was determined that the Cz reference is preferred for temporal region electrodes, while the LM reference is better suited for central region electrodes.

Two studies are known to have developed a prototype SSVEP-based BCI using non-occipital electrodes. Guermandi et al. [104] used eight electrodes placed behind each ear using a flexible board to obtain an average SNR of 5.1 dB for a window length of 1 s. A more sophisticated prototype by Yu-Te Wang et al. [126]

was developed known as EarEEG. This consists of an earpiece having embedded electrodes, that is specifically designed to fit the anatomical shape of the user's ear. Such device provided a very good performance providing an average accuracy of 87.92% and an ITR of 16.6 bpm.

The current SSVEP-based BCI research on systems utilizing non-occipital electrodes, as discussed in this section, demonstrates the potential for achieving good performance, especially when employing classification algorithms like the TRCA. However, it is noteworthy that the performance of SSVEP-based BCIs using occipital electrodes remains superior, emphasizing the necessity for further research aimed at enhancing SSVEP detection in non-occipital regions.

3.5 The SSVEP Response and Stimuli Properties

Varying the properties of the flashing stimuli can affect the SSVEP response in two ways: (i) it may improve the detection of the SSVEP, and (ii) it can evoke the SSVEP in non-occipital areas of the brain. Stimuli properties include the frequency, colour, type and shape of the stimuli, and this section highlights the present literature that investigated the effect of these properties on the SSVEP response. Identifying stimuli properties that can elicit a strong SSVEP response in both the occipital and non-occipital regions is an approach to make these systems faster and more efficient. It should be mentioned that direct comparison of the stimuli properties described in the literature is difficult since (i) there are many different characteristics that might affect how well a BCI performs, and (ii) there are various evaluation metrics available.

3.5.1 Stimulus Frequency

High-frequency stimuli provide the advantage that they are visually more comfortable to look at since the flicker is less visible to the eye. Additionally, using the frequencies of 15 Hz - 25 Hz eliminates the risk of photo epileptic seizures and false positives due to the alpha rhythm [91, 127, 128]. Several EEG studies that have investigated the ideal stimuli frequency for a high SSVEP response concluded that low frequencies (< 20 Hz) produce a stronger response than higher ones [91, 107, 114, 129, 130]. Despite this, some studies still concluded that a good performance was obtained when using high frequencies. This can be seen

by Won et al. [91] who compared low (< 20 Hz) and high (> 25 Hz) frequency visual light-emitting diode (LED) stimuli by implementing a 30 character real-time SSVEP-based BCI QWERTY keyboard. Results show that high frequency stimuli obtained a higher classification accuracy of 80% than the lower frequency stimuli that obtained an accuracy of 70%.

The conflicting conclusions of these EEG studies were based on SSVEP signals recorded from occipital and occipital-parietal electrodes, thus these studies do not give any information if the SSVEP response behaves in the same manner at non-occipital areas of the brain.

The origin and dispersion of SSVEPs all over the scalp in the gamma frequency band (40 Hz - 60 Hz) using LED stimuli has been investigated by Tsoneva et al. [46] and Pan et al. [80]. Tsoneva et al. used a 32-channel EEG setup to produce low-resolution brain electromagnetic tomography (sLORETA) maps which determined that the primary visual cortex V1, the extrastriate cortices (V2 - V5) and some central and frontal sites all contribute to SSVEP origination in that frequency range. Pan et al. investigated the SSVEP when using frequencies in the gamma band (40 Hz - 60 Hz) together with alpha band frequencies (7 Hz - 15 Hz) and beta band (15 Hz - 40 Hz) to determine whether the three frequency bands are spatially distinct from each other. This study was performed by analysing fMRI images to investigate the BOLD response when the subjects were shown a flickering LED stimulus. Pan et al. concluded that for all frequency bands, all subjects have SSVEPs in the visual cortex V1 with some subjects having SSVEPs in the parietal and frontal cortices. Interestingly, this study concludes that no differences were found in the amplitude over the three frequency bands.

These findings contradict Vij et al. [131] who investigated the generation of SSVEP potentials using a flickering black-white stimulus ranging from 1 to 100 Hz. Both the fMRI and EEG modalities were used to investigate this and the results were evaluated both individually and using a proposed EEG-fMRI fusion framework. The results of the EEG activity alone suggest that the power of the SSVEP decreases as the frequency increases, with SSVEP components found only till the 26.67 Hz frequency. Similarly, the fMRI analysis and fused fMRI and EEG results reveal significant activations for frequencies up to 20 Hz. For all frequency bands

except the high-frequency band (>20 Hz), since no BOLD response was observed for such frequency, activations were mainly located in the primary visual cortex (V1). Another study used flickering LED lights up to frequencies of 46 Hz by simultaneously recording EEG and fMRI data to investigate the SSVEP response. After investigating the BOLD responses from the fMRI data, the study by Bayram et al. [79] concluded that SSVEP amplitudes were found in all frequencies tested at the LGN, primary visual cortex V1 and the extrastriate cortices (V2 - V5). Blood oxygenation level dependent (BOLD) activations were also identified in the precuneus and in the hippocampi and dorso-lateral prefrontal cortices (Brodmann areas BA46 and BA47). However, similar to Vij et al. they observe that the level of SSVEP activity decreases with increasing frequency. This was also observed from the EEG results which additionally highlight that the highest SSVEP amplitudes are located in the occipital lobe.

The cerebral activations to 5 Hz - 40 Hz flickering LED stimuli have been investigated with PET where the regional cerebral blood flow (rCBF) is measured. Through this research Pastor et al. [132] confirmed that the primary visual cortex V1 is activated with all stimuli frequencies. The study also concluded that the amplitude of the SSVEP peaks at the 15 Hz stimulus and starts decreasing beyond 15 Hz to reach the lowest amplitude at 40 Hz, similar to the conclusions from Vij et al. and Bayram et al.

3.5.2 Stimulus Colour

In most SSVEP studies, a single-graphic black-white flickering stimulus seen in Figure 3.3 is used to generate the SSVEP signal in the brain. Such stimulus is typically used since it is the easiest and most straightforward to create on GUIs. Furthermore, the high contrast between the black and white colour is known to provide a high SSVEP response [106, 112]. However, it has been found that using other stimuli colours could lead to a better quality SSVEP and improve the visual comfort [107, 108, 110, 133]. Moreover, coloured stimuli could evoke activations in non-occipital regions as is discussed in this section [110, 134–136].

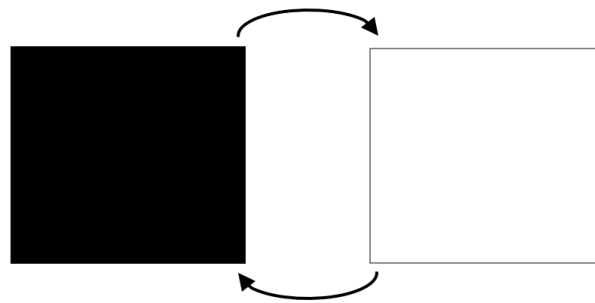


FIGURE 3.3: Standard single-graphic black-white stimulus that is used in SSVEP-based BCIs.

Combinations of black, white, red, green, grey, yellow and blue flickering stimuli have been compared and investigated. Whilst the EEG studies by Bieger et al. [112] and Cao et al. [137] still concluded that using the standard black-white stimulus provides a superior performance, Tello et al. [108] showed that the red-black LED stimuli provide the highest SSVEP amplitude, accuracy rates and ITRs while Li et al. [133] concluded that yellow-red stimuli provide better performance.

The studies discussed up till now all evaluate the SSVEP response from the occipital and parietal-occipital regions of the brain using EEG, thus their results may or may not apply to non-occipital regions. The study by Floriano et al. [110] provides more information about the SSVEP response in non-occipital areas since it evaluated the effect of chromaticity and luminance in low (<12 Hz), medium (12 Hz - 30 Hz) and high frequency (≥ 30 Hz) LED stimuli from both behind the ear and occipital regions. This was done by placing one electrode on the occipital region, and two electrodes behind the ears, one on each side respectively. Three different colour combinations were tested: black-white, blue-green, and red-green stimuli. Results evaluated in terms of SNRs, classification accuracies and ITRs show that the flickering frequency and colour of the stimuli are connected to the SSVEP response. Particularly, the red-green stimulus obtains the highest SSVEP amplitude at the occipital and temporal regions in the low and medium frequency ranges obtaining 90% accuracy values. In the high-frequency range, the flickering blue-green stimulus evoked the highest SSVEP at the occipital and temporal areas, obtaining classification accuracies greater than 80%.

Although to the best of our knowledge no study using fMRI has investigated the SSVEP response and the brain activity with different colour flashing stimuli, fMRI

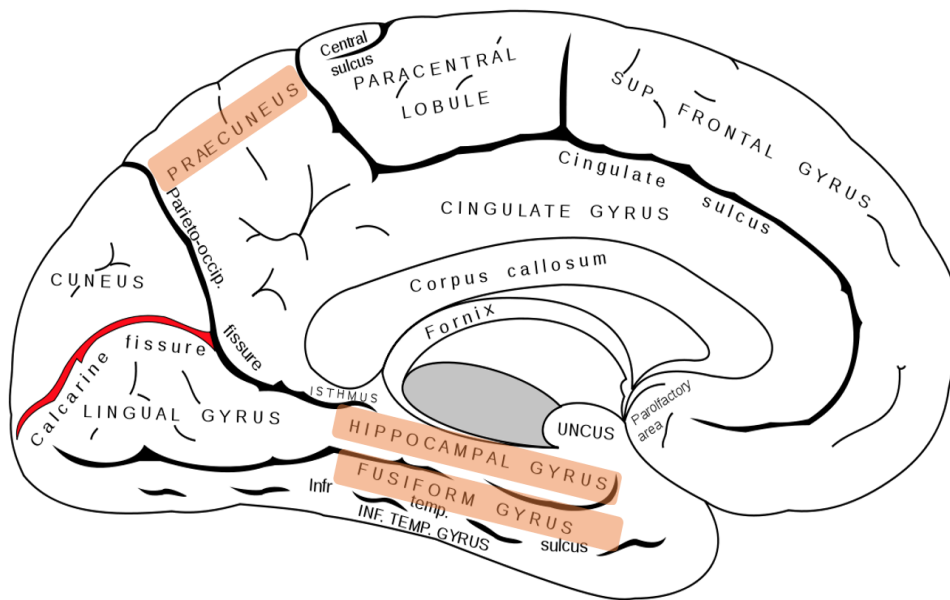
studies have investigated how colour information is depicted by the brain when subjects were exposed to non-flickering shapes and objects having different colours. These studies concluded that colour processing in the brain takes place in temporal and parietal areas due to the visual information that passes through the ventral and dorsal pathways [118, 119]. Bramão et al. [134] determined that the pathway for colour processing is mainly related to the middle temporal gyrus and sulcus but also to parietal regions, the superior frontal gyrus and sulcus, and visual cortex V4. Cavina-Pratesi et al. [135] determined that colour processing is mainly associated with the fusiform gyrus that forms part of the temporal and occipital lobe, and Mullen et al. [136] associated colour processing with the extrastriate cortices (V2 - V5). It is important to note the above studies use stimuli with different shapes and forms, however they all investigated the cortical response of the brain to when the stimuli colours were changed.

Figure 3.4 shown below highlights the cortical brain areas mentioned in this section and the upcoming sections, using the same anatomical brain image that was presented earlier in Figure 2.3.

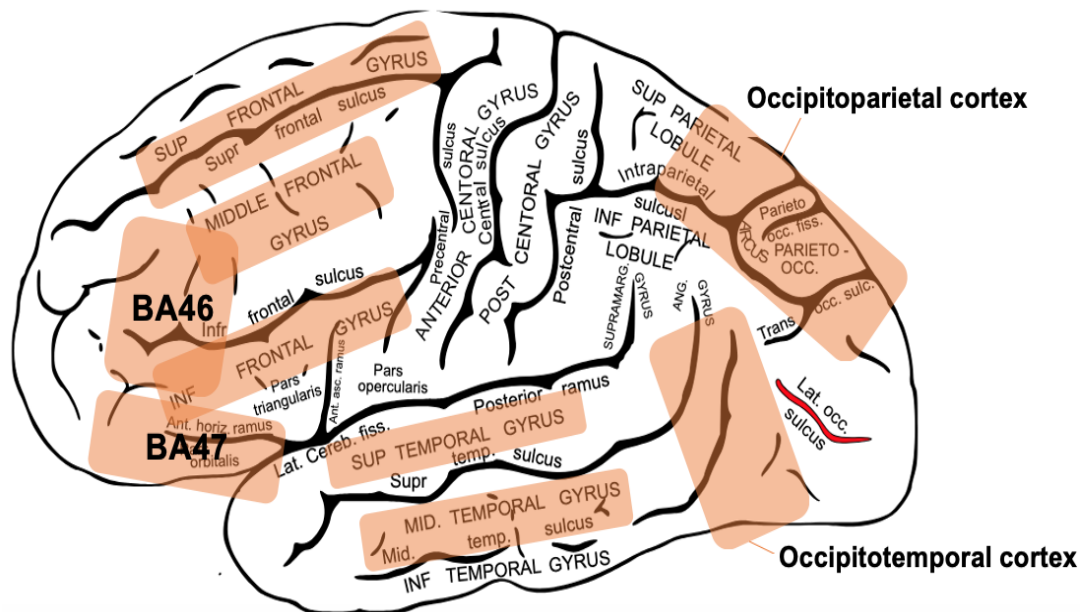
3.5.3 Stimulus Shape

Research is focusing on investigating various stimuli shapes, other than the standard stimulus flickering black box shape, with the aim of identifying how this affects shape processing in our brain and the SSVEP response in occipital and non-occipital areas of the brain.

The SSVEP response to using geometric-shaped stimuli including triangle, square, pentagon, hexagon and circular stimuli was investigated by Embrandiri et al. [138] through an EEG study using electrodes placed on the occipital region of the brain. The colour of these stimuli also varied from black, white, red and green. Results show that single graphic and colour stimuli provide poorer SNR values when compared to shape and colour reversal stimuli (stimuli that change their shape and colour on each flicker). The stimuli with alternating shapes and colours provided the highest SNR although no particular shape and colour pair was observed to provide a consistent superior performance due to the wide inter-subject variability.



(a) Medial surface of the left cerebral hemisphere.



(b) Lateral surface of the left cerebral hemisphere.

FIGURE 3.4: Highlighted cortical brain areas mentioned in Section 3.5.

No fMRI study that investigated the SSVEP response with different flickering shape stimuli has been identified, however fMRI studies that observed how the brain responds to different non-flickering shapes exist. The brain areas involved in shape processing were also investigated using fMRI. Cavina-Pratesi et al. [135] who used circular stimuli with irregular edges as shown in Figure 3.5(a) found activations in the occipitotemporal cortex (which lies on the basal surface of the

temporal and occipital lobes) while Stylianou-Korsnes et al. [139] displayed different abstract shapes (shown in Figure 3.5(b)) to the participants and found activations in the occipital and temporal regions of the brain. Freud et al. [140] and Denys et al. [141] displayed images of objects to the participants which are shown in Figures 3.5(c) and 3.5(d). These images were divided into squares and randomly rearranged. Activations by Freud et al. were found in the extrastriate cortices (V2 - V5) and the posterior regions of the dorsal pathway. Denys et al. found activations in posterior occipital regions, occipitotemporal cortex and occipitoparietal cortex (which lies on the basal surface of the parietal and occipital lobes).

The cortical regions activated during the processing of real and non-real line drawings as shown in Figure 3.5(e) were investigated by Kraut et al. [142]. Most subjects obtained activations in both the occipital and parietal lobe, the occipitotemporal regions, and the posterior superior and middle temporal gyrus which are located at the upper and mid surface of the temporal lobe respectively.

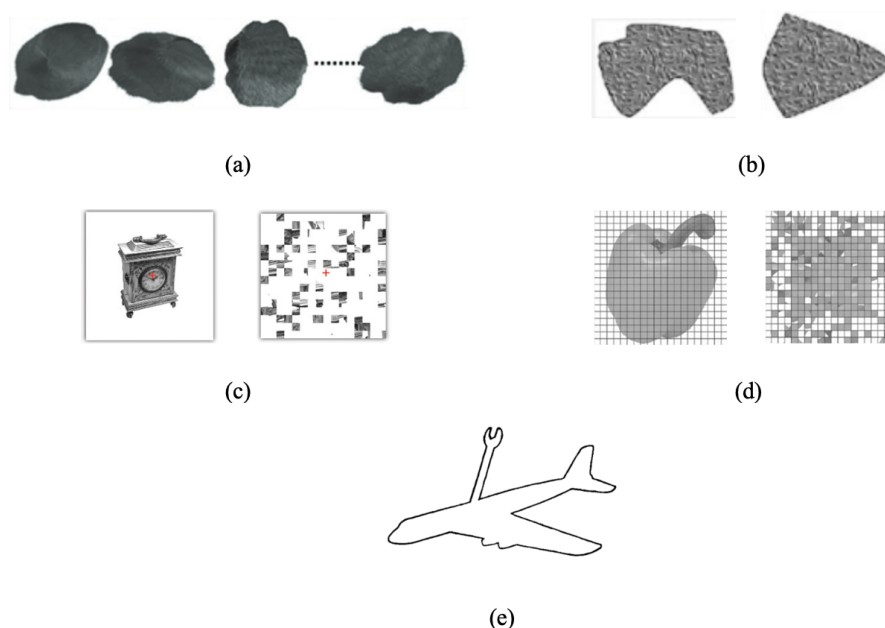


FIGURE 3.5: Different shaped stimuli used by the studies discussed in this section: (a) The different circular stimuli used by Cavina-Pratesi et al. [135] (b) The two different shapes used by Stylianou-Korsnes et al. [139] (c) A clock image stimulus that has been broken down into randomly rearranged squares used by Freud et al. [140] (d) An apple image stimulus randomly rearranged into small squares used by Denys et al. [141] (e) A non-object line drawing image stimulus used by Kraut et al. [142].

3.5.4 Stimulus Texture

The standard stimulus used in SSVEP-based BCIs consists of a single-graphic solid-coloured stimulus. This stimulus is set to flicker at a particular frequency by emerging from and disappearing into the background retaining the same texture. Other stimuli types include, checkerboard stimuli which consist of alternate inverted black and white checkers, random dot stimuli which consist of alternate small random squares and different graded texture stimuli. These stimuli textures may give rise to less visual irritation, an enhancement in the SSVEP response and SSVEP activations in non-occipital areas of the brain [143].

Ming et al. [143], Waytowich et al. [144] and Zerafa et al. [111] involve EEG studies that used occipital and parietal-occipital electrodes to investigate the SSVEP response when the users are displayed with a checkerboard stimulus. Ming et al. compared three checkerboard stimuli with different spatial contrasts, that is, a black-white background, black background and white background, as well as a plain solid-coloured stimulus. The results show that the black background checkerboard stimulus obtained an equivalent SNR to the single graphic stimulus while being less visually irritating for the users to focus on. Waytowich et al. analysed the spatial frequency of checkerboard stimuli when varied from a solid background (0 c/deg) to a single-pixel checkerboard pattern (19.2 c/deg) [144]. By evaluating the classification accuracies and ITRs, the best performance was obtained at the 0 c/deg (solid single graphic stimulus) and at 2.4 c/deg checkerboard conditions. Zerafa et al. however contradict the findings by Ming et al. and Waytowich et al. since this study concluded that the use of a single graphic stimulus exhibits a much higher performance than the checkerboard stimulus for various frequencies tested [111].

The EEG studies discussed are conflicting and no generic conclusion can be made on which stimulus performs better. Furthermore, these studies used electrodes on the occipital and parietal-occipital areas of the brain and thus they do not provide any information about the SSVEP response in non-occipital regions.

To the best of our knowledge only one study evaluated the SSVEP response from fMRI data when subjects were shown flickering checkerboard stimuli. Results from the study of Srinivasan et al. [145] show that all the subjects showed strong BOLD

responses in the occipital lobe together with activations in the medial frontal lobes. Particularly, stimuli flickering in the range of 3.5 Hz - 5 Hz obtained the largest amplitude in the frontal area in all subjects.

Blood oxygenation level dependent (BOLD) signals from fMRI data were also evaluated when subjects were shown different graded texture non-flickering stimuli to analyse where texture processing takes place in the brain. Cavina-Pratesi et al. [135] concluded that different surface features of stimuli (shown in Figure 3.6(a)) are processed in the medial occipitotemporal cortices, while the study of Stylianou-Korsnes et al. [139] found activations in prefrontal regions of the brain at the bilateral inferior frontal gyrus and the left middle frontal gyrus when displaying different textures that are shown in Figure 3.6(b). Two types of random dot stimuli were analysed by Beason-Held et al. [146] who aimed to use fMRI to measure BOLD signals when subjects were presented with ‘random’ textured dot map stimuli and ‘correlated’ textured dot map stimuli as shown in Figure 3.6(c). The ‘correlated’ textured stimulus is an extension of the ‘random’ textured stimulus having extended contours and rectangular blocks at multiple spatial scales. Blood oxygenation level dependent (BOLD) signal activations when subjects were displayed the ‘random’ stimulus were obtained in the occipital lobe and occipitotemporal gyrus. The same areas of the brain were activated with the ‘correlated’ stimulus with additional activations found in the middle temporal region.

3.5.5 Rendering Device, Stimulus Size and Duty-cycle

The rendering device that is used to display the flickering stimuli may also affect the quality of the SSVEP response. Although the EEG studies from Wu et al. [147] and Zhu et al. [148] suggest that LED stimulators provide the highest SSVEP fundamental frequency amplitude when compared to the SSVEP evoked by liquid crystal display (LCD) screens and CRT, LEDs have the disadvantage that they provide a less flexible setup since specialised hardware is required to set different stimuli properties. Since this study aims for a practical BCI setup, it was decided that computer monitor stimulation, using LCD monitors, was to be used as this has the advantage that the stimulation interface can be easily adjusted or changed during BCI development.

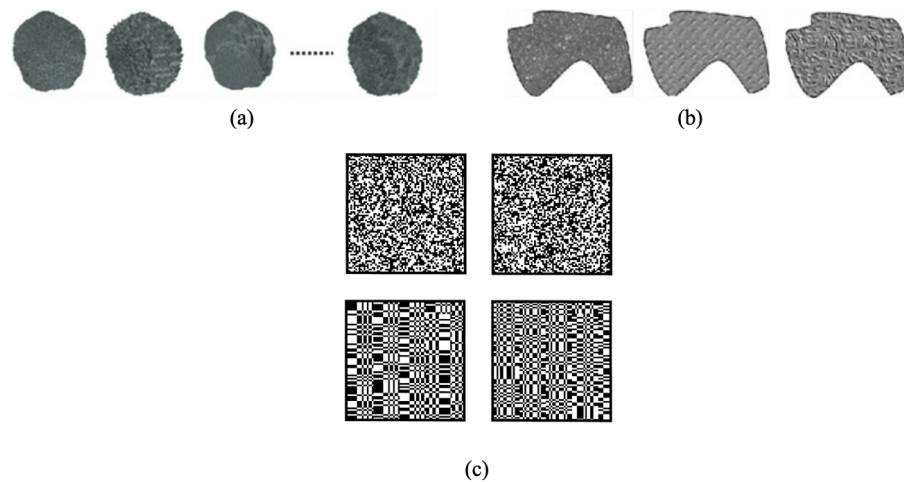


FIGURE 3.6: Different stimuli types used by the studies discussed in this section: (a) Different graded texture stimuli used by Cavina-Pratesi et al. [135] (b) Different graded texture stimuli used by Stylianou-Korsnes et al. [139] (c) Stimuli used by Beason-Held et al. [146]. Figures on the first row show the ‘random’ textured stimulus and the bottom row figures show the ‘correlated’ textured stimulus.

The size of the stimulus determines the amount of light that is transmitted to the user, thus it may also affect the strength of the SSVEP response generated in the brain. Bieger et al. [112] observed the SSVEP response using EEG when the user was shown stimuli with various sizes. The highest ITR of the BCI was obtained when using a 6×6 cm stimulus, thus for this study it was decided to use this stimulus size for the optimal SSVEP.

Another stimulus parameter that may affect the strength of the SSVEP response is the duty-cycle of the flickering stimulus. A clear conclusion on which duty cycle provides the ideal performance was difficult to determine. This is due to the fact that multiple rendering devices were utilised in the literature that evaluated this characteristic, which included Lee et al.’s [109] optimal 89.5% duty cycle for LED stimuli, and Wu [149] and Oralhan and Tokmakci’s [150] 40% duty cycle for LED and LCD rendering devices. In order to achieve a compromise between these findings, a duty cycle of 50% – which is typical in BCI applications [108, 151] – was employed in this research.

3.6 Chapter Summary

3.6.1 Localisation of SSVEPs in the Brain

Analysing the visual pathway, which consists of the M, P and K pathways, gives the first indication that visual processing takes part in other parts of the brain other than the occipital region that consists of the primary visual cortex V1 and the extrastriate cortices V2 - V5. This is because the information that passes through the dorsal and ventral streams are located at the temporal and parietal lobes, respectively. The generation and location of the SSVEP may be related to these areas of the brain, thus the literature review aimed to further analyse what is known about the source localisation of SSVEPs and through this, figure out the ideal EEG electrode placement for SSVEP-based BCIs.

The fMRI and EEG studies performed by Hillyard et al. [76], Di Russo et al. [78], Sammer et al. [121], Itthipuripat et al. [51] and Ji et al. [122] aimed to answer the question of where SSVEPs are located in the brain. Main activations were found at the primary visual cortex V1 and the extrastriate cortices V2 - V5, however, SSVEP activations were also located at temporal and parietal regions by Hillyard et al. [76], Di Russo et al. [78] and Ji et al. [122], which indicates that SSVEPs can be obtained from non-occipital areas. The EEG studies that developed behind the ear SSVEP-based BCIs seem promising with all of the studies obtaining a classification accuracy greater than 80% [88, 104, 105, 124–126]. However, this performance is still less than BCIs using electrodes at occipital regions which obtain accuracies greater than 90% [47–49].

3.6.2 Stimuli Properties

Modifying the stimulus properties from the standard black-white flickering box which has been used in current SSVEP-based BCI setups, has the possibility of increasing the SSVEP response in the occipital region and other areas of the brain. This is one way to improve the performance of BCI setups, and possibly an approach that can make these systems more practical. The fMRI and EEG studies that aimed to localise the SSVEP in the brain, analysed in Section 3.4.1.2, also use one type of stimulus flickering at a single frequency, thus these studies do not reveal any information on whether the SSVEP source changes as the stimulus frequency varies.

3.6.2.1 Stimulus Frequency

The results from the EEG studies that use electrodes at occipital and parietal-occipital regions of the brain which varied the stimulus frequency are conflicting, making it unclear if the SSVEP response is stronger at higher frequencies or lower ones. Similarly, the studies that analysed the SSVEP using fMRI are also conflicting with Tsoneva et al. [46] and Pan et al. [80] concluding that SSVEP activations were found for high frequencies (40 Hz - 60 Hz) while Vij et al. [131] and Bayram et al. [79] concluded that low SSVEP amplitudes or none at all were obtained for high frequencies (> 20 Hz).

3.6.2.2 Stimulus Colour

It is also uncertain whether the SSVEP response is stronger when using coloured stimuli rather than the standard black-white stimulus, based on the results of EEG experiments that used electrodes at the occipital and parietal-occipital areas of the brain who tested various stimuli colours. However, the study by Floriano et al. [110] who looked at the SSVEP at the occipital and behind the ear areas of the brain concluded that coloured stimuli provide a better accuracy than black-white stimuli, suggesting that colour may increase the quality of the SSVEP response. This study however has the disadvantage that the stimuli were rendered on LEDs thus the results cannot be directly applied to stimuli displayed on an LCDs monitor which was used in this study.

Although the fMRI studies by Bramão et al. [134], Cavina-Pratesi et al. [135] and Mullen et al. [136] did not investigate the SSVEP since the stimuli used were not flickering stimuli, such studies provide us with the information that colour processing takes place in parietal, frontal and temporal areas of the brain.

3.6.2.3 Stimulus Shape

To the best of our knowledge, no study used fMRI to analyse the SSVEP response when showing flickering stimuli having different shapes. The studies by Cavina-Pratesi et al. [135], Stylianou-Korsnes et al. [139], Freud et al. [140], Denys et al. [141] and Kruat et al. [142] conclude that shape processing is found at the occipital, temporal and parietal areas of the brain which suggests that SSVEPs might also be generated and located in these areas when different shaped flickering stimuli are shown.

3.6.2.4 Stimulus Type

The checkerboard stimulus has been investigated by various EEG studies that used occipital and parietal-occipital electrodes however the results from these studies are conflicting as it cannot be determined if checkerboard stimuli provide similar performance to a single graphic stimulus. The study by Srinivasan et al. [145] who analysed the SSVEP response using fMRI data determined that frontal areas are activated when using checkerboard stimuli at very low frequencies of 3.5 Hz - 5 Hz. The random dot map stimulus analysed by Beason-Held et al. [146] also found activations at temporal regions of the brain. The studies of Cavina-Pratesi et al. [135] and Korsnes et al. [139] determine that texture processing may be related to temporal and frontal regions, supporting the findings from Srinivasan et al. and Beason-Held et al.

Following this analysis, it was determined that it is not always clear which stimulus frequency, colour, shape and type provides a better SSVEP in different brain regions when compared to the black-white stimulus that has been currently used in SSVEP-based BCIs. Furthermore, the SSVEP response triggered by different flickering RVS has not been investigated using fMRI.

3.7 Conclusion

This review helped to converge a set of stimulus parameters to be used in this work and the main contributions of the study, which are:

1. To design, set up and carry out a BOLD/fMRI and EEG study, and master data collection by recording data from human subjects.
2. To identify the cortical and scalp locations of SSVEPs in the brain and how this varies between subjects using both EEG and fMRI.
3. To determine if different stimuli properties result in a different spatial activity distribution and SSVEP magnitudes in the brain.
4. To identify stimuli properties which may generate strong, reliable SSVEPs that may be captured by electrodes placed on occipital and non-occipital areas.

The next chapter describes in detail the stimuli properties chosen to be tested in this study, while focusing on the setup and procedure used to carry out the fMRI study.

Chapter 4

fMRI Experiment Design and Setup

4.1 Introduction

This chapter starts by highlighting the main aims of conducting an fMRI study. A detailed description of which stimuli parameters were chosen to be analysed in this study was then given. This proceeds with an explanation of the hardware and software of MRI scanners and the procedures taken to conduct an fMRI experiment on human subjects. The experimental protocol designed for this study is described together with the necessary steps to organise and preprocess fMRI data. The details presented in the chapter are being included since this is the first time such an fMRI study is being carried out locally and hence the setting up is of primary importance, both for this and other future studies.

4.2 Objectives of fMRI Analysis

This project involved an fMRI study to analyse the SSVEP signals in the brain, with the following objectives:

- To build and pioneer an fMRI data collection setup.
- To design an experimental protocol and carry out a BOLD/fMRI study by recording data from human subjects.
- To determine the cortical brain-activated areas when displaying RVS with different stimuli parameters.

- To analyse the brain activity in terms of space and amplitude when varying the properties and frequency of the stimuli.
- To understand if varying the stimulus parameters can provide a strong SSVEP response in occipital and non-occipital areas of the brain that is sufficient to control an SSVEP-based BCI system.

4.3 Task-Based and Resting-State fMRI

Functional magnetic resonance imaging (fMRI) uses the technique of blood oxygenation level dependent (BOLD) imaging to detect localised increases in relative blood oxygenation in the brain that is most likely a direct result of neurotransmitter activity, thus reflecting local neural signalling [40, 152]. Neurotransmitter activity is caused by the performance of simple sensory, cognitive, physiological, or motor tasks (such as finger tapping or silent word generation), or more complex, dynamic tasks such as language interpretation [152]. In general, fMRI is recorded during a resting-based experiment or a task-based experiment [40].

In a block design task-based fMRI experiment, the subject lying inside the scanner is instructed to perform a task while avoiding any large body motions that might move the head [40]. The experimental protocol consists of a repetitive pattern where a specific condition is presented for a set duration, with alternating blocks of different conditions over time [152, 153]. In this paradigm, a baseline or resting period is usually added to illustrate specific brain regions that are usually more active in baseline scenarios [152, 153]. In the analyses of a task-based fMRI, the recorded time series data is contrasted to an assumed neural functioning model that is derived from the particular cognitive task and block design experiment being performed. It is important that the timing and synching of the task performed by the user with the simultaneous recording of the fMRI time series data is carefully designed.

Resting-state fMRI is recorded in the absence of a stimulus or task, thus subjects inside the scanner are asked to be in a state of rest [40]. Resting-state fMRI is also recorded during the baseline or resting period in a task-based experiment. Synchronous activations that take place between distinct locations in the brain while a task or stimulus is not present can be investigated using resting-state fMRI

in order to identify resting-state networks [152].

In this project, a task-based fMRI experiment was implemented and shown to the participants. The experiment involved the subjects to focus on specific RVS to trigger a SSVEP response in the brain, while lying inside the scanner. Further detail on the designed experimental paradigm is given in section 4.6.1.

4.4 Design of Variable Parameters

The following section describes the different types of stimuli tested in both the fMRI and EEG analysis performed in this study based on the conclusions drawn from the literature review in Chapter 3.

4.4.1 Control Condition

Studies that do not investigate the effect of stimuli properties on the SSVEP typically use a plain, black-squared stimulus flickering on a white background, similar to the one shown in Figure 4.1. This study will refer to this stimulus as the black-white stimulus.

The black-white stimulus will be considered as the control stimulus, thus the brain activity arising from the other stimuli properties tested throughout this study will be compared and contrasted to the brain activity occurring during the black-white stimulus presentation. This is done to compare if changing the stimuli properties from the standard stimulus, can lead to different brain regions of the brain being activated and an increase in the SSVEP response.

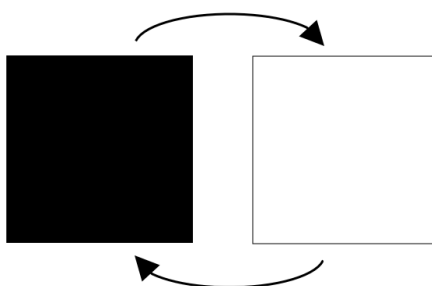


FIGURE 4.1: Black-white stimulus.

4.4.2 Tested Stimuli Properties

4.4.2.1 Colour, Shape and Texture

Following the promising results of Floriano et al. [110], discussed in Section 3.5.2, a blue squared stimulus flickering on a green background (blue-green stimulus) and a red squared stimulus flickering on a green background (red-green stimulus) were chosen as the two coloured stimuli to be tested in this study. These stimuli are shown in Figure 4.2. To render the different stimuli colours on the LCD screen that was used to display the stimuli to the subjects, the red, green and blue (RGB) colour system was applied.

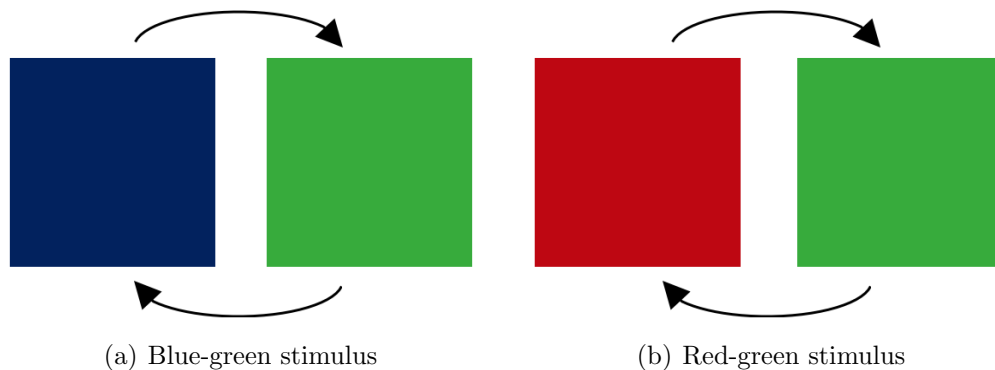


FIGURE 4.2: The two different colour stimuli tested in this study.

Regarding shape, two different shaped stimuli were investigated in this study. The first stimulus is a flickering white ‘power on and off’ symbol superimposed on a black square, as shown in Figure 4.3(a). The second-shaped stimulus consists of a flickering white ‘Turn On’ text icon superimposed on a black square as shown in Figure 4.3(b). These shape stimuli were investigated since according to Embrandiri et al. [138], alternating the shape of the stimulus from a single-graphic stimulus has the potential to increase the SNR of the SSVEP response in the brain. Furthermore, the fMRI studies indicate that these stimuli require cortical processing in the occipital, temporal and parietal areas of the brain. These particular stimuli shapes were chosen as they have not yet been tested in an SSVEP setting and, they are typical RVS that can be employed in SSVEP-based BCI systems to control an external device. These stimuli will be referred to as the symbol and text stimuli, respectively, in this study. To distinguish the boundary between the stimulus and the surrounding white area of the screen, a black 1 mm frame was added to the stimulus.

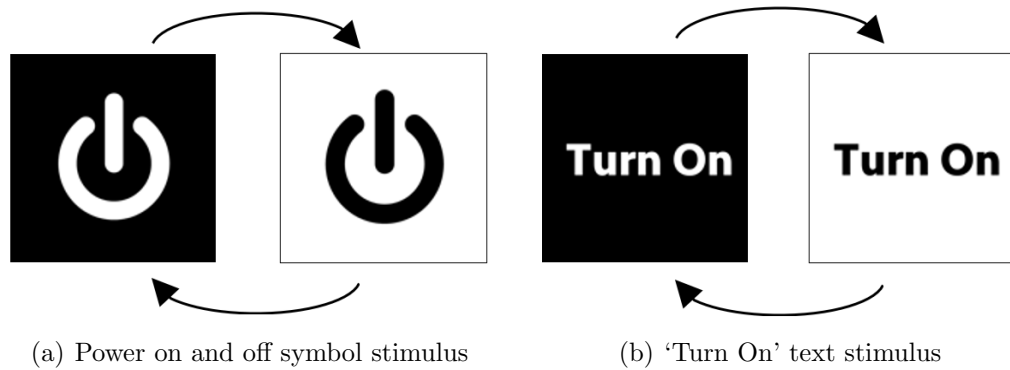


FIGURE 4.3: The two different shape stimuli tested.

The literature review also highlighted conflicting results when analysing the effect of checkerboard stimuli on the SSVEP response. Hence this type of stimulus was investigated in this study. A 32×32 checkerboard stimulus consisting of 0.1 mm squares each subtending a visual angle of 0.6° was used as shown in Figure 4.4(a). Such stimulus size was chosen based on the findings by Waytowich et al. [144] that concluded that a 32×32 checkerboard stimulus obtains a higher information transfer rate (ITR) than the black-white stimulus whilst also decreasing the visual irritation caused by these flickering stimuli.

This study also investigated the random dot patterned stimulus, since, according to the author's knowledge, the SSVEP response to such a stimulus has not been investigated in the literature. The design of this stimulus consisted of 90×90 , 0.05 mm random dots or pixels, each subtending a visual angle of 0.3° flickering against a white background, as shown in Figure 4.4(b). A 1 mm black frame was also added to this stimulus to distinguish the boundary between these stimuli and the surrounding white area of the screen.

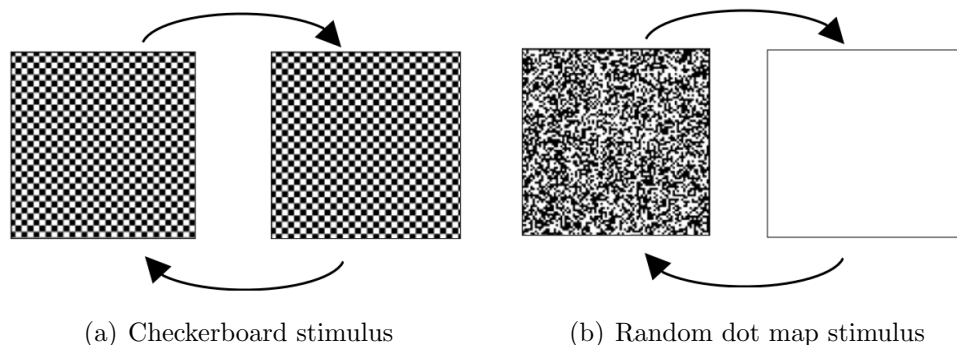


FIGURE 4.4: The two different texture stimuli tested.

4.4.2.2 Frequency

Each of the stimuli described and shown in Section 4.4.2.1, was tested at a range of frequencies to investigate how the brain activity responds to these stimuli at different frequencies. The range of frequencies tested was limited by the refresh rate of the LCD monitor on which these stimuli were displayed. In this study, a 60 Hz refresh rate monitor was used, since this is the most common type of monitor available. For a 60 Hz refresh rate, the maximum stimulation frequency value that can be reached is 30 Hz [112]. The reciprocal of the refresh frequency, or the frame period for a 60 Hz display refresh rate, is 16.667 ms. This shows the shortest possible interval that can exist between images when they are presented on a monitor screen.

To be able to realise any frequency value that is lower or equal to 30 Hz on the monitor, the method proposed by Wang et al. was employed [154]. The presented frame-based method suggests that the stimulus signal at a frequency f can be calculated using Equation 4.1:

$$stim(f, i) = square \left[2\pi f \left(\frac{i}{Refresh\ Rate} \right) \right] \quad (4.1)$$

Here the *RefreshRate* corresponds to the vertical refresh rate of the monitor and i is set to be equal to the frame index. Equation 4.1 generates a 0.5 duty cycle square wave having an amplitude varying from -1 to 1 where -1 represents the amplitude of the background stimulus and 1 represents the amplitude of the foreground stimulus. For this study, six different frequencies within the 7.5 Hz - 30 Hz range were considered specifically 7.5 Hz, 10 Hz, 15 Hz, 20 Hz, 24 Hz and 30 Hz.

4.5 System Architecture

The use of the University's MRI scanner to conduct the fMRI experiments was coordinated with the University of Malta Magnetic Resonance Imaging Platform (UMRI). The 3 Tesla Siemens Magnetom Vida scanner setup found at Mater Dei Hospital (MDH) was used to carry out the task-based fMRI experiment. All of the designed interfaces and the image processing techniques to analyse the MRI images was done using Python, particularly all visual stimuli tested were outlined

and displayed using the open-source PsychoPy Python software package version 2023.2.0 [155].

4.5.1 Hardware Description

At MDH, the complete magnetic resonance (MR) system is made up of components that are found in three adjacent rooms: magnet room, equipment room and control room.



FIGURE 4.5: The magnet and control room of the University's MRI scanner located at Mater Dei Hospital [156].

The magnet room consists of the 3 Tesla Siemens Magnetom Vida scanner that contains the MR magnet, its shell or enclosure, patient table and support footings [157]. The magnet room's walls are constructed with multiple layers, each serving distinct functions. These are, containing the fringe magnetic field through magnetic shielding, preventing noise from escaping into the control room and surroundings through acoustic shielding, and blocking electromagnetic noise from entering or leaving the area using radio-frequency shielding [40, 157]. A window through which the subject inside the scanner can be viewed is present accompanied by an audio system where an individual from the control room can communicate with the subject lying inside the scanner.

To image the brain, the MR scanner comes with a Siemens 64-channel head coil, seen in Figure 4.6(a), that is positioned around the subject's head before they enter the scanner, and is the only coil not integrated into the machine [158]. This specifically designed transmit-receive RF coil provides the same function as the body coil which is built into every MR scanner with the advantage of being more sensitive to receive the weak signals emitted by the hydrogen nuclei within the brain

which the body coil alone is not able to capture [71]. Electrostatic headphones are also worn by the subject while inside the scanner, to provide communication with the control room and sound from any audio stimuli during a task-based experiment [157]. The MRI scanner is fitted with a Push Button Talk-Back Activation system that allows the subject to communicate to the control room while inside the scanner by pressing a button to speak [159].

To perform task-based fMRI experiments, the Nordic Neuro Lab (NNL) 40-inch LCD monitor has been installed in the magnet room to project images or videos to the subject lying inside the scanner [160]. This monitor is able to withstand up to 7 Tesla MRI environments whilst having a 3840×2160 resolution display and a 60 Hz refresh rate [160]. The images or videos on the monitor are presented to the subject via a 45° tilted mirror Siemens head matrix coil that is fixed onto the Siemens 64-channel head coil [161]. This is shown in Figure 4.6(b).

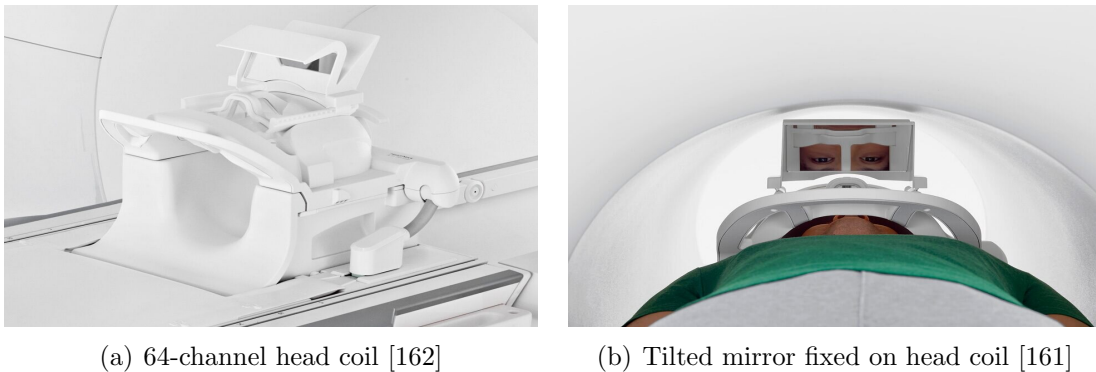


FIGURE 4.6: The Siemens 64-channel head coil and Siemens head mirror used in the fMRI experiments [158, 163].

Adjacent to the magnet room, there is the equipment room that supports all the control systems for the operation of the magnet. This includes a power cabinet that contains all the equipment for electrical distribution and conditioning, the RF cabinet that controls the transmission and reception of RF pulses and nuclear magnetic resonance (NMR) signals respectively, and the gradient cabinet that is responsible for sending currents into the gradients [40, 157].

The control room is situated directly adjacent to the magnet room. It contains all the computer equipment that controls the MR scanner parameters where all MR images are stored. The control room also houses the NNL SyncBox which receives trigger pulses from the MR scanner in the magnet room [164]. This SyncBox is essential for task-based fMRI experiments to appropriately synchronise the stimulus presentation with the MR image acquisition. The process of how proper syncing was performed is described in Section 4.5.2 of this chapter. This room also provides the necessary cables to display the stimuli, images or videos onto the NNL LCD monitor located in the magnet room. Verbal instructions from the control room are delivered to the subject via the audio system communication console using a Push Button Talk-Back Activation System [159]. The main Siemens and NNL components used by the MRI system located both in the magnet room and control room are shown in Figure 4.7.



FIGURE 4.7: The MRI system layout. Adapted from [164].

4.5.1.1 MRI Data Acquisition Parameters

Prior to every MRI data recording session, the MR scanner parameters were set in place by the radiographer, who was present during each data recording session. Setting the appropriate parameters is crucial to obtain high-resolution images. For the task-based fMRI data acquisition session, whole head T2*-weighted gradient-echo planar imaging (EPI) sequence MRI data was acquired using an interleaved slice acquisition sequence having the following parameters for all subjects: TR = 1520 ms, TE = 41 ms, 59° flip angle, 45 axial slices, slice-matrix size = 64 × 64 mm, slice thickness = 2.5 mm with a slice gap = 0.4 mm, field of view = 220 mm,

isotropic voxel-size = $2.5 \times 2.5 \times 2.5$ mm². Prior to starting the task-based fMRI experiment, a T1-weighted high-resolution structural image and gradient-echo field maps were obtained for each subject.

4.5.2 Software Description

The PsychoPy software library written in Python was used to design the visual stimuli explained in Section 4.4 which were presented to the subjects at different time intervals and frequencies [155]. PsychoPy employs a double-buffered rendering approach, where the background stimulus is first rendered onto a virtual screen in the graphics card's memory, known as the back buffer. At the point when the vertical blank (VBL) period or refresh rate occurs that marks the end of one frame and the beginning of the next, the content stored in this back buffer is swapped with the screen buffer holding the foreground stimulus [165]. The flipping of these frames is controlled by PsychoPy which will halt all processing threads until the graphics card notifies the program that a frame flip has taken place [165]. These frame flips are utilised as a very accurate timing mechanism to render the correct frequencies on the screen. The vertical synchronisation prevents the video card from showing a frame until the monitor has completed operating at its current refresh rate [165]. The benefit of this is that screen tearing effects are avoided and only the frames are seen [165].

To ensure that the visual stimuli presented to the user are properly synchronised with the MR image, acquisition was done through PsychoPy. Timing and information must be accurate and verified for the validity of the results. The computer which is loading the PsychoPy software is connected to the NNL LCD monitor (to display the visual stimuli created by PsychoPy) and to the NNL SyncBox. During MR acquisition, the NNL SyncBox sends an 's' key response on every trigger pulse received by the MR scanner. The trigger pulse, in this case, is received on every volume recorded by the scanner. Thus to ensure proper synchronisation with the scanner, each 's' key response received from the scanner is stored and time logged by the PsychoPy software such that in the preprocessing stage of the recorded fMRI data, each volume can be associated to a particular time-point in the experimental paradigm shown to the subject, which is explained in the next section.

4.6 Subjects and Experimental Setup

After obtaining approval from the University Research Ethics Committee (UREC) of the University of Malta, six subjects (three males and three females, age range 22 - 28) having normal or corrected-to-normal vision participated in the MRI data recording sessions. Prior to the data recording session, each participant had to sign a consent form and read an information sheet that included details about the project being held and the handling and storing of data. Both of these forms followed the guidelines given by the UMRI. Participants were asked not to participate if they suffer from claustrophobia, have any medical implants or metal fragments in the body or if they are pregnant. Subjects were also advised to not wear any makeup, talc, cosmetic and prosthetic contact lenses. For more detailed instructions about procedures taken before an fMRI data recording session, refer to Appendix A.

Before starting the fMRI recording session proper communication with the subject was ensured via the audio system, and the radiographer reiterated the experimental protocol to the subject. Each experimental session was divided into four. The first session started by recording structural images for anatomical reference to be used when preprocessing the fMRI data. This was followed by recording gradient-echo field maps. These field maps are recorded to take into consideration the geometrical distortions caused by the field inhomogeneities that are frequently present in echo-planar imaging techniques used for fMRI BOLD acquisitions. Although the fMRI signal affected by these inhomogeneities cannot be restored, the signal that has been shifted can be recovered to its correct position within the image by utilizing the gradient-echo field maps that have been recorded [166]. In the second experimental session, the two colour stimuli shown in Figure 4.2 together with the control condition shown in Figure 4.1 were presented to the user. In the third and fourth sessions, the shape stimuli shown in Figure 4.5 and texture stimuli shown in Figure 4.4 were presented respectively. After each session, the radiographer briefly looked at the collected images to see if any subjects had moved their head throughout the session and affected the results which would have resulted in conducting the MRI recording session again. In this study, all six subjects did not move throughout the recording session and no sessions were repeated.

4.6.1 Experimental Protocol

The experimental protocol started by reminding the participants of the most important instructions to follow during the experiment that is: (i) to remain still throughout the whole experiment (ii) to push the button in hand to communicate with the radiographer (iii) to alert the radiographer in case of an emergency such as claustrophobia. Prior to each recording session, a ‘pre-scanning session’ was performed where five extra volumes were recorded to allow for scanner stabilization which were then discarded during processing. The first session lasted 8 minutes during which structural (anatomical) images of the brain and gradient-echo field maps were recorded. This was directly followed by the second session where the black-white control stimulus, blue-green stimulus and red-green stimulus were shown to the subject at each of the six different frequencies (7.5 Hz, 10 Hz, 15 Hz, 20 Hz, 24 Hz and 30 Hz). A stimulus size of 2.5 cm was set such that every participant who was placed 12 cm away from the head mirror subtended a 12° visual angle.

Prior to every visual stimulus presentation at a particular frequency, a fixation period was shown during which baseline fMRI data was recorded. A rest period was also included after every visual stimulus presentation. The fixation period, stimulation period and rest period, together, made up a trial for every stimulus-frequency condition. The timing paradigm for one trial is shown in Figure 4.8. Each trial started with a fixation period where subjects were instructed to fixate on a black fixation cross positioned at the centre of the screen for 15.2 s (10 volumes). The stimulus was then presented at the centre of the screen for 22.8 s (15 volumes) followed by a 2.04 s rest period (two volumes). A trial for each of the six frequencies per stimulus was performed resulting in six trials per stimulus. Once the six trials per coloured stimulus were performed, these were repeated once again in order to have a total of two runs per coloured stimulus to obtain a total of 12 trials for each stimulus (two trials for each frequency). For this session, a total of 977 volumes were recorded and the recording session lasted 25 minutes. The luminance of the screen during the fixation and rest period was set to be equal to the mean luminance during the stimulation period [145]. This luminance was calculated using the Sefram 9855 lux meter and it was found to be equal to 186.01 lux [167].

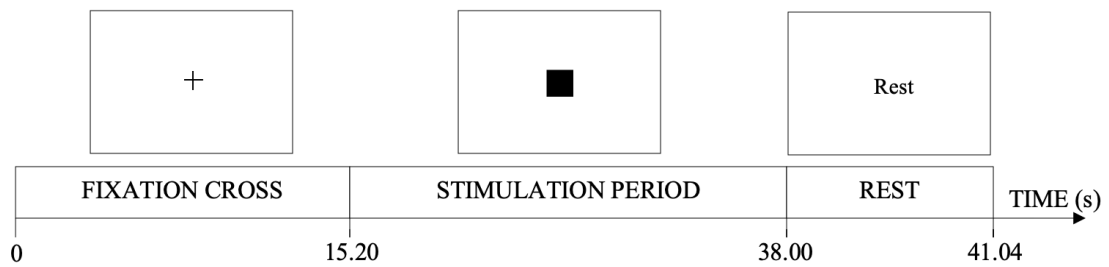


FIGURE 4.8: Timing paradigm of one trial.

The same timing paradigm shown in Figure 4.8 was used in the third session where the power on and off symbol and ‘Turn On’ text stimuli were presented to the subject. Six trials per stimulus were shown to the user (one trial per frequency) and this was repeated twice for a total of two runs to collect a total of 12 trials per stimulus, and hence two trials for each frequency were recorded. For this session, a total of 653 volumes were recorded and the whole recorded session lasted 16 minutes. The fourth session was similar to the third session since a total of 653 volumes were also recorded and this session also lasted for 16 minutes. However, in this case, the checkerboard and random dot stimuli were each displayed for six trials per frequency for a total of two runs. The whole MRI data recording experiment consisting of the four sessions lasted for a total of 65 minutes. The flowchart presented in Figure 4.9, gives an overview of the whole experiment consisting of the four sessions. The experiment was divided into four sessions such that breaks were given in between sessions if requested by the subject. Whenever the participant requested a break between sessions, the ‘pre-scanning session’ and gradient-field maps had to be recorded once again.

The number of volumes chosen for the fixation and stimulation period was set to be long enough for the hemodynamic response function (HRF) that characterizes the BOLD signal recorded during fMRI to be captured and to account for any time delays introduced by the MR scanner [71]. This chosen experimental protocol and the length of the fixation, stimulation and rest period were based on methodologies used in other studies that investigated the SSVEP response using fMRI [79, 80, 121, 131, 145].

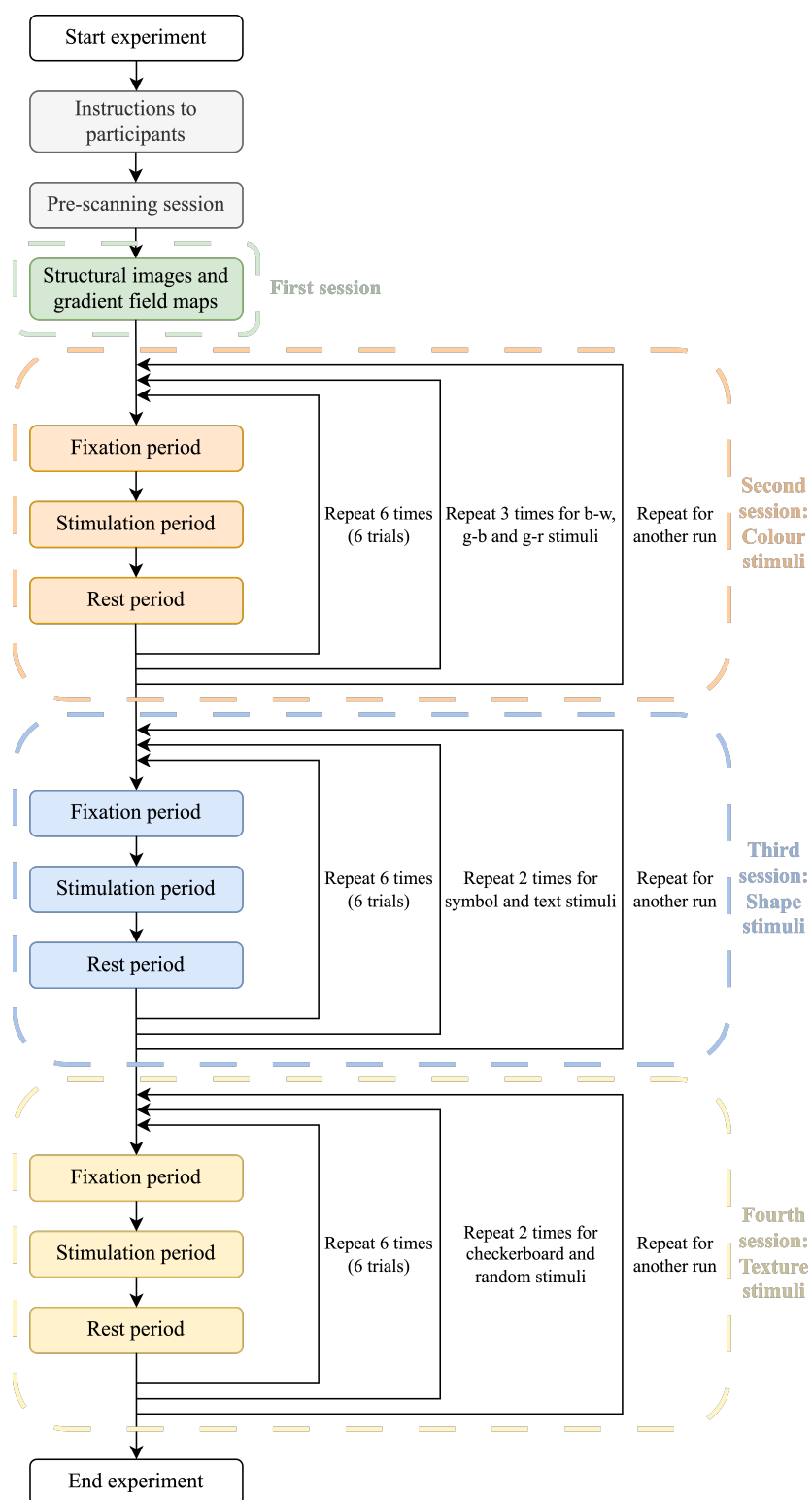


FIGURE 4.9: Flowchart describing the fMRI experimental protocol for each subject.

4.7 Data Organisation and Preprocessing

This section describes all the necessary steps that were taken to organise the MRI data after each recording session, and how preprocessing was done to eliminate noise from the data. Figure 4.10 shows the major steps to do this, which include: storing the raw MRI data in the digital imaging and communications in medicine (DICOM) file format, structuring the data into the brain imaging data structure (BIDS) standard to organise the files in a structured way, quality control using magnetic resonance imaging quality control (MRIQC) and finally preprocessing using the fMRIPrep software [168–172].

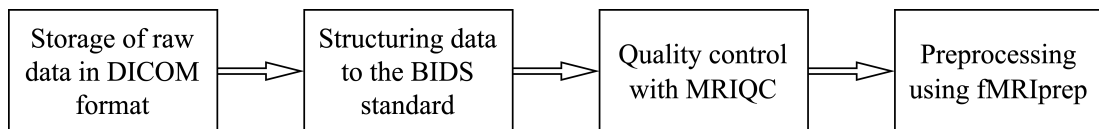


FIGURE 4.10: Preprocessing steps.

Anonymity of each subject was ensured by assigning a PatientID code to each research volunteer. This was inputted into the MRI scanner software by the radiographer present during the data recording session. The MRI data was stored in an encrypted hard drive in DICOM format which is crucial in order to keep a copy of the original metadata [172]. This data was then converted into the BIDS format by transforming the imaging data to the neuroimaging informatics technology initiative (NIfTI)-1 format having JavaScript object notation (JSON) metadata files while populating a directory tree according to the current BIDS specification. The BIDS standard allows preprocessing softwares such as fMRIPrep to easily identify the structure of the input MRI data and collect the metadata files without manual intervention [171, 172]. An online BIDS validator was used to confirm that the dataset fulfils the BIDS specifications [172, 173].

The data was then quality controlled using MRIQC which is a tool used to inspect structural and functional MRI data, and flag subjects, sessions or runs that should be eliminated from the analysis for their insufficient quality before any further preprocessing is performed. Image quality metrics (IQMs) are generated by MRIQC which were visualised using MRIQCEPTION to analyse how the generated image quality metrics (IQMs) compose with those from the MRIQC web API [174]. Before assessing the results, a threshold was set to eliminate the data for which the

IQM value differs from the mean IQM of the API data by more than two standard deviations.

Functional magnetic resonance imaging (fMRI) preprocessing entails a number of procedures to clean and standardise the data prior to statistical analysis [71, 175]. In this study, fMRIPrep, which is a powerful and useful tool has been used to prepare both the task-based and resting-state fMRI data for analysis [171, 172]. For more detail about the algorithms used by fMRIPrep to process the anatomical and functional MRI data, refer to Appendix B.

Together with the preprocessed structural and functional data, fMRIPrep generates one hypertext markup language (HTML) report per subject. These visual reports were screened prior to moving to the data analysis step to ensure that the T1-weighted anatomical reference brain was correctly generated, an adequate brain mask was extracted from the BOLD series, susceptibility distortion correction was accurately applied and the BOLD data was accurately aligned to the T1-weighted anatomical data and MNI space [172].

The FSL software was then used to divide the preprocessed fMRI data into separate folders according to the stimulus (black-white, blue-green, red-green, power on and off symbol, ‘Turn On’ text, checkerboard, random dot stimuli) and trials during the first and second run, whilst making sure to discard the first five volumes of the data since these were not part of the experimental protocol and were added to allow for scanner stabilisation.

4.8 Chapter Summary

This chapter presents the specific objectives of the fMRI study and describes the colour, shape and texture stimuli tested in this project, which include: black-white stimulus, blue-green stimulus and red-green stimulus (colour stimuli), power on and off symbol stimulus and ‘Turn On’ text stimulus (shape stimuli), checkerboard stimulus and random dot stimulus (texture stimuli). A detailed description of the main hardware that is involved in collecting fMRI images is also given. Such information was important to describe how proper synchronisation was attained between the recorded fMRI images and the task-based experiment shown to the

subject.

The experimental protocol used to display the different stimuli properties at six different frequencies was explained. Finally, details on how the collected raw MRI data was converted to the BIDS standard, quality controlled using MRIQC and preprocessed using fMRIPrep is given. The next chapter focuses on describing the algorithm used to process the fMRI data and how this was applied to the data recorded in this study. Furthermore, the gathered results are presented.

Chapter 5

fMRI Analysis

5.1 Introduction

The recorded fMRI data from human subjects was processed and analysed to understand the strength of the BOLD response and to localise the SSVEP in different cortical regions of the brain. This chapter describes the algorithm that was used to do this and it explains how this was applied to the data recorded in this study. The results obtained for the different stimuli properties displayed at different frequencies are then presented and visualised.

5.2 Data Analysis

To analyse the recorded fMRI data that was collected during the task-based fMRI experiment on each subject, the general linear model (GLM), which is a widely used technique to examine fMRI data, was utilised [79, 80, 131, 145]. The GLM model and its parameters, which indicate the effects of each stimulus condition presented to the subject, is used to model the BOLD signal using particular methods. Statistical inference is then applied to identify the voxels that are statistically significant to the different stimuli conditions. Statistical parametric map (SPM) for each stimulus condition which convey the test statistic of the voxels having significant activity are created. General linear model (GLM) is one of the most extensively used methodologies due to its efficiency, robustness, accessibility and simplicity [176].

5.2.1 General Linear Model

Each voxel within an fMRI dataset has a time series containing the same number of time points as the volumes obtained in each session. Finding which voxels have a time-course that correlates with the stimuli presented during the task experiment is the goal of statistically analysing the recorded fMRI dataset which was done in this study using the general linear model (GLM) approach.

The GLM was used to separately analyse the fMRI data of each individual subject; this is commonly known as the first-level analysis [177]. This analysis was separately conducted for each stimulus run, where each run included six trials of the stimulus flickering at one of the six frequencies (7.5 Hz, 10 Hz, 15 Hz, 20 Hz, 24 Hz, 30 Hz) respectively. The GLM models the time course of each voxel as a weighted sum of one or more predefined experimental design variables with the aim of calculating how much each design variable contributes to the observed variability seen in the voxel's time course [178]. Thus, for an experiment where the BOLD signal y is sampled for n times (or volumes), the calculated BOLD response from a single voxel as a function of time y_i can be modelled as the sum of one or more experimental design variables $x_1 \dots x_p$ that are each scaled by a weighting factor β plus a random error ϵ [177]. This is represented by the following equations [177, 179]:

$$\begin{aligned}
 y_1 &= x_{1,1}\beta_1 + x_{1,2}\beta_2 + \dots + x_{1,p}\beta_p + \epsilon_1 \\
 y_2 &= x_{2,1}\beta_1 + x_{2,2}\beta_2 + \dots + x_{2,p}\beta_p + \epsilon_2 \\
 &\dots \\
 y_n &= x_{n,1}\beta_1 + x_{n,2}\beta_2 + \dots + x_{n,p}\beta_p + \epsilon_n
 \end{aligned}
 \tag{5.1}$$

Where the β real values are also called β weights or β estimates and ϵ is the noise term [178]. Essentially the value of β estimates represents how much each design variable contributes to the BOLD signal y_i [178, 179]. Equation 5.1 can be denoted in matrix notation as [177, 180]:

$$Y = X\beta + \epsilon \tag{5.2}$$

Where Y is an $n \times 1$ column vector depicting the BOLD signal time series related with a single voxel, X is an $n \times p$ design matrix where each column represents an

experimental design variable (or essential regressor) and some additional nuisance regressors to model nuisance variables [177, 178]. β is a vector with $p \times 1$ dimensions that represents the unknown weights (coefficients) which define both the strength and direction of the distinct relationship between individual experimental design variables and the BOLD signal data Y for a particular voxel [177]. ϵ denotes an $n \times 1$ vector which contains the error values linked to each observation [177].

The design matrix contains the experimental design variables or essential regressors which are idealized predictions of what the hemodynamic response function (HRF) should resemble if a voxel of interest got activated as a result of a stimulus presentation [178, 179]. For the block-design experiment, which was implemented in the task-based fMRI experiment in this study, where each trial consisted of a 15.2 s fixation period, 22.8 s stimulation period and 2.04 s rest period as explained in Figure 4.8, this was derived by convoluting a condition box-car time course with the HRF function [179, 181]. Since the time points that correspond to the fixation, stimulation and rest periods were known throughout the experiment in this study, a value of 1 was set to the condition box-car time course at the stimulation period time points and a value of 0 was set at all other time points, since at these points the HRF is not expected to be observed [181]. Figure 5.1 describes the convolution of the HRF with one single trial represented via a boxcar function.

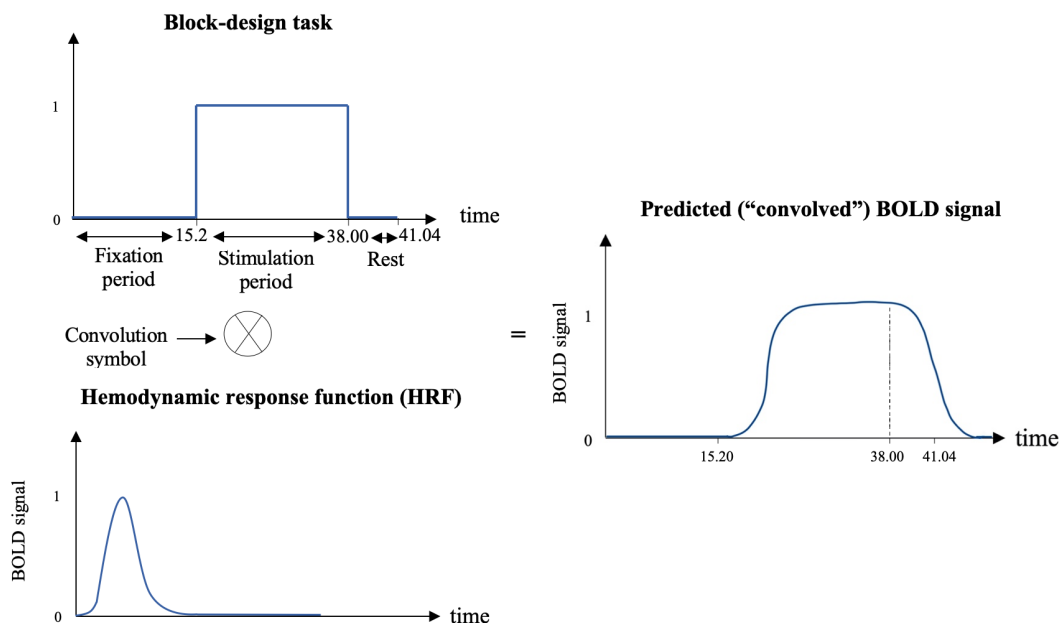


FIGURE 5.1: Illustration of the HRF for one trial generated by a boxcar stimulus.

In this study, the experimental design variables or essential regressors are the six frequencies that correspond to each of the trials shown to the subject per stimulus per run, which will be explained further in the next section. The design matrix also consists of nuisance regressors. The nuisance regressors account for experimental factors that can introduce interference in the analysis, often stemming from head motion and low-frequency drifts [178]. These variables are not inherently of interest on their own. The values in these columns can either be determined through empirical observation or constructed through modelling [177, 178].

To estimate the unknown parameter β and determine if a given regressor significantly describes some portion of the variance observed in a voxel's time-course, the ordinary least squares (OLS) method was used [177]. The OLS finds the optimal β parameter that minimises the sum of squared residuals such that the difference between X multiplied with β , and the true fMRI signal Y is minimized [177]. This is given by:

$$\sum_{i=1}^n (Y_i - X_i \hat{\beta})^2 \quad (5.3)$$

The solution to compute the β parameter and its variance is thus estimated as follows [177, 180]:

$$\hat{\beta} = (X^T X)^{-1} X^T Y \quad (5.4)$$

$$\text{var}(\hat{\beta}) = \sigma^2 (X^T X)^{-1} \quad (5.5)$$

The GLM is a univariate approach, calculating statistics on a voxel-by-voxel basis. According to the Gauss-Markov theorem, the OLS corresponds to finding the optimal β values, provided that the following assumptions are true: (i) the errors are independent and identically distributed (iid) (ii) the regressors of the design matrix X are independent of error, deterministic, and known, following a Gaussian distribution with a mean of zero (iii) none of the regressors can be expressed as a linear combination of one or more of the other regressors. [177, 178].

The GLM is depicted by the example shown in Figure 5.2. This shows the GLM applied on an imaginary voxel where the voxel's time series Y is represented as the linear combination of three essential regressors (describing when a particular stimulus condition was presented to the user during a stimulation period by an

HRF and returning back to baseline when the stimulus was not presented to the user during a baseline period and the instances when other stimuli condition were presented) and several nuisance variables (a linear drift and motion regressors), that were each scaled by a vector of unknown β values, plus an error term ϵ [177]. This model was independently applied to the time series data of each voxel recorded in this study, ignoring any potential spatial variances between adjacent voxels [177].

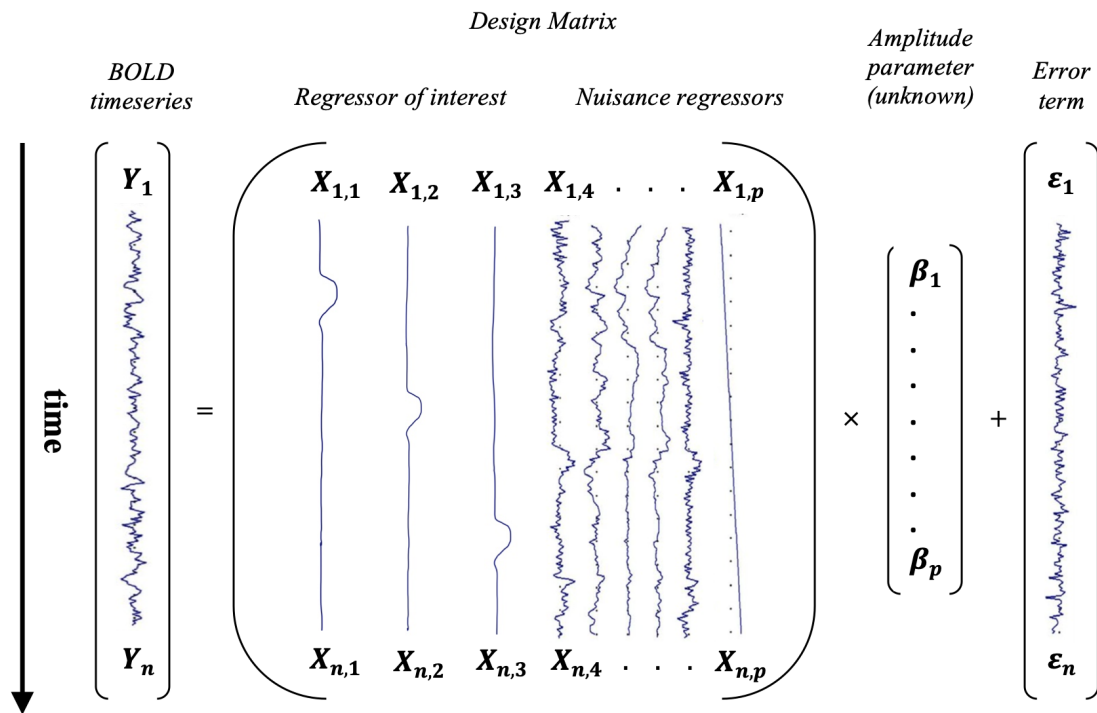


FIGURE 5.2: Application of the GLM on an imaginary voxel with time series Y .

The process of assessing statistical significance entails the formulation of a null hypothesis H_0 and an alternative hypothesis H_1 which could be expressed as:

- H_0 : There is no net BOLD signal effect in a voxel during the stimulation period compared to the fixation period (rest), $\beta = 0$
- H_1 : There is an effect on the BOLD signal in a voxel during the stimulation period compared to the fixation period (rest), $\beta \neq 0$

A result is considered statistically significant when the likelihood of making a Type 1 (false positive) error, which involves rejecting the null hypothesis, is lower than a predetermined probability threshold, typically denoted as the p-value [178]. The estimate for each β parameter determined by the GLM (described in Equation 5.4)

can be used to form the test statistic that is described by the following equation [178, 180]:

$$t_{\hat{\beta}} = \frac{\hat{\beta}}{SE_{\hat{\beta}}} \quad (5.6)$$

Where $\hat{\beta}$ has been previously defined in Equation 5.4 and $SE_{\hat{\beta}}$ is the standard error of the $\hat{\beta}$ parameter that can be calculated by measuring the square root of the variance of the $\hat{\beta}$ parameter described by Equation 5.5 [178, 180]. Thus Equation 5.6 can be rewritten as [178, 180]:

$$t_{\hat{\beta}} = \frac{\hat{\beta}}{\sqrt{\text{var}(\hat{\beta})}} \quad (5.7)$$

Assuming that the assumptions of the GLM are satisfied, the statistic $t_{\hat{\beta}}$ follows a Student's t-distribution [178]. The exact characteristics of this distribution depend on the degrees of freedom, which is calculated as the difference between the number of time points analysed and the number of independent regressors [178]. When the degrees of freedom approaches infinity, the t-distribution closely resembles the Gaussian or standard normal (z-) distribution. Consequently, in experiments with over 100 observations, z-values are reported instead of t-values [178, 182].

5.2.2 Applying the General Linear Model

To apply the GLM on the recorded fMRI data of each subject after passing through the preprocessing steps, the GLM was applied using the FEAT function in the FSL software library [183, 184].

The first-level analysis was first carried out for each stimulus and run for each subject. Through FSL a highpass filter was applied setting the cut-off to 60 s to remove the low-frequency drifts. Spatial smoothing full width half maximum (FWHM) of 5 mm was also applied to the data. This was applied to each volume to reduce the noise, where the signal of each voxel is averaged with the neighbouring voxel's signals weighted by a 5 mm Gaussian kernel at half maximum [185, 186].

The FEAT software uses FILM (FMRIB's Improved Linear Model) to apply the GLM first-level analysis [184]. This approach represents a robust and precise non-parametric method for estimating the autocorrelation of time series data.

Its purpose is to prewhiten the time series of each voxel, thereby enhancing the efficiency of the estimation process [178, 187].

The design matrix was created using the FEAT software. Six essential regressors were created (one for each stimulus frequency) corresponding to the six consecutive trials per run, during which the HRF response is active during the stimulation period and returns to baseline during a fixation and rest period. The HRF response for each regressor is also set to 0 or baseline during the stimulation period of the other trials. Thus, for a 22.8 s stimulation period, the HRF is spread out with a sustained peak whose magnitude corresponds to the duration of the stimulus. Subsequently, it gradually returns to the baseline level once the stimulus has concluded [181]. An appropriate HRF function was then selected to model the blurs and delays caused by the difference between the input function (the box-car stimulus waveform) and the output function (measured fMRI hemodynamic response). To do this a double-gamma HRF was selected to allow for post-stimulus undershoot [178, 181]. The design matrix, including the six essential regressors and six nuisance regressors, which are modelled by FEAT using the MCFLIRT motion correction algorithm, are shown in Figure 5.3 [188]. Since the design matrix contains six essential regressors, the GLM generates six amplitude estimates $(\beta_1, \beta_2, \dots, \beta_6)$ for each voxel corresponding to the six conditions (frequencies) that could be tested for statistical significance during one run. Thus, for each voxel, the GLM generates six contrasts that represent the model fit for each regressor.

Following the initial statistical analysis, the FEAT software generates a z-statistic (also known as z-score or z-value) image. Typically, this image is normally thresholded to reveal which individual voxels or clusters of voxels exhibit statistical “activation” at a specific significance level. In this study, cluster thresholding was employed, meaning that the z-statistic threshold was utilized to identify contiguous clusters of voxels. For each cluster, its estimated significance level, calculated using Gaussian random field theory, is compared to the cluster probability threshold [184]. The original structural image was masked by significant clusters to produce colour blobs for the SPMs. The z-statistic threshold in this study was set to a value of 1.5 and a p-value of 0.05 was used. The choice of Z-score in fMRI analysis can depend on factors such as the study design, the SNR in the data, and the specific hypotheses being tested. A z-score of 2 or 3 is commonly employed when

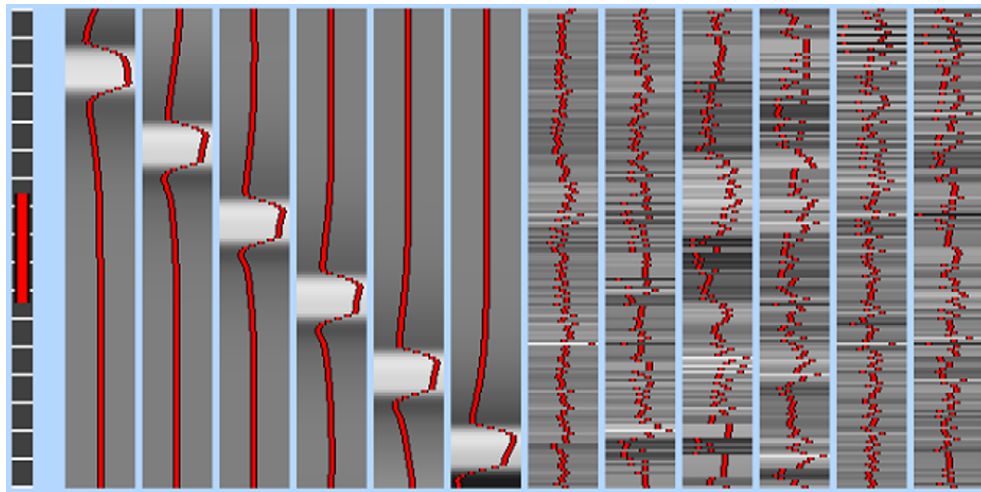
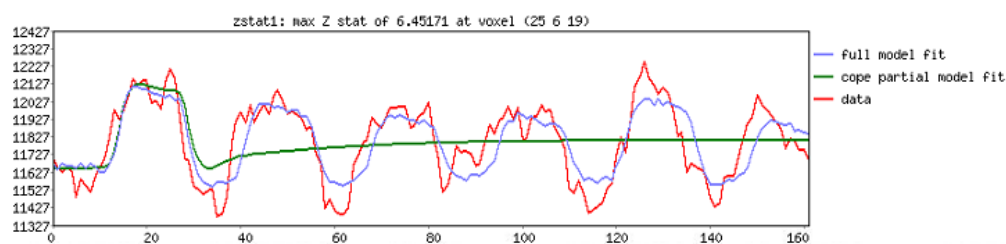


FIGURE 5.3: The design matrix in FEAT showing the six essential regressors in the first six columns and the six nuisance regressors in the last six columns. Columns 1-6 regressors describe the six trials during which the stimulus flickered at 7.5 Hz, 10 Hz, 15 Hz, 20 Hz, 25 Hz, 30 Hz respectively.

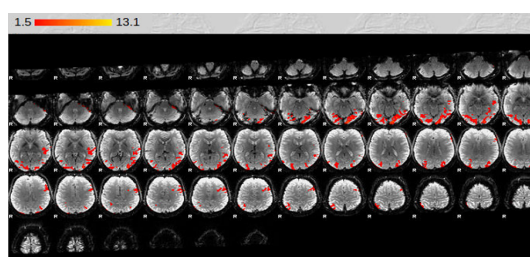
using the GLM however, after visually inspecting the SPMs obtained in this study, this z-score value was deemed too high to capture any activated clusters, thus this was lowered to a value of 1.5. In this project, a voxel will be therefore considered “activated” if its z-value exceeds the z-statistic threshold of 1.5 ($|z| > 1.5$).

After running the first-level analysis for each stimulus, run and subject, FEAT generates a web page report that includes a summary of the results. A set of time series plots of the full model fit (the estimated time series output by the GLM), the contrast of parameter estimate (COPE) partial model fit (the estimated time-series output for the corresponding contrast) and the data (original fMRI data) are displayed for peak z-value voxels for each contrast. Figure 5.4(a) shows the resulting time series plots for the black-white stimulus for Subject 6 showing the first contrast, where in this case the regressor represents the first trial when the stimulus was flickering at 7.5 Hz. This plot shows the time series for the voxel having coordinates (25, 6, 19) which obtained the maximum z-statistic for this contrast. Z-statistic thresholded values for each contrast, which are overlaid on each subject’s structural image, are generated, showing the activated clusters. The z-statistic range selected for rendering runs from red (minimum z-statistic after thresholding) to yellow (maximum z-statistic after thresholding). Figure 5.4(b) shows the z-statistic thresholded values for the black-white stimulus for Subject 6

showing the first contrast (7.5 Hz trial).



(a) Time series plots for the voxel located at (25 6 19). Plot showing the original fMRI data in red, the estimated time-series (COPE partial model fit) for the first contrast in green, the estimated fMRI data by the GLM (full model fit) in purple.



(b) Z-statistic thresholded values for the first contrast.

| Cluster List | | | | | | | | | | | | | | | |
|---------------|--------|----------|------------------------|-------|---------------|---------------|---------------|---------------|---------------|---------------|----------|------------------|------------------|------------------|-----------|
| Cluster Index | Voxels | P | -log ₁₀ (P) | Z-MAX | Z-MAX X (vox) | Z-MAX Y (vox) | Z-MAX Z (vox) | Z-COG X (vox) | Z-COG Y (vox) | Z-COG Z (vox) | COPE-MAX | COPE-MAX X (vox) | COPE-MAX Y (vox) | COPE-MAX Z (vox) | COPE-MEAN |
| 3 | 1758 | 2.78e-09 | 8.56 | 6.45 | 25 | 6 | 19 | 16.5 | 16.6 | 23.5 | 429 | 25 | 5 | 19 | 91.1 |
| 2 | 1253 | 4.77e-07 | 6.32 | 5.45 | 46 | 19 | 44 | 40.9 | 11.8 | 27.8 | 298 | 44 | 13 | 33 | 96.4 |
| 1 | 365 | 0.0474 | 1.32 | 3.32 | 11 | 45 | 40 | 9.97 | 46.5 | 38.1 | 276 | 7 | 46 | 36 | 99.3 |

| Local Maxima | | | | |
|---------------|------|----|----|----|
| Cluster Index | Z | x | y | z |
| 3 | 6.45 | 25 | 6 | 19 |
| 3 | 5.4 | 19 | 13 | 21 |
| 3 | 5.31 | 19 | 31 | 16 |
| 3 | 4.62 | 19 | 9 | 26 |
| 3 | 4.47 | 18 | 7 | 25 |
| 3 | 4.27 | 21 | 10 | 18 |
| 2 | 5.45 | 46 | 19 | 44 |
| 2 | 4.43 | 34 | 8 | 22 |
| 2 | 4.17 | 50 | 13 | 27 |
| 2 | 4.04 | 45 | 5 | 21 |
| 2 | 4.03 | 37 | 9 | 21 |
| 2 | 3.93 | 33 | 5 | 23 |
| 1 | 3.32 | 11 | 45 | 40 |
| 1 | 3.22 | 7 | 50 | 38 |
| 1 | 3.1 | 6 | 46 | 37 |
| 1 | 3.02 | 7 | 54 | 34 |
| 1 | 2.92 | 9 | 45 | 42 |
| 1 | 2.76 | 7 | 52 | 33 |

(c) Cluster details for the first contrast.

FIGURE 5.4: Results generated by FEAT for Subject 1, black-white stimulus, first contrast.

A table of cluster details and local maxima are also displayed for the generated GLM for each contrast as can be seen in Figure 5.4(c). These describe the number of voxels found in each thresholded cluster together with the X, Y, Z location of the voxel that obtained the maximum z-value, the X, Y, Z location of the centre of gravity of the voxels within that cluster, and information about the β parameter (COPE) determined by the GLM. This information includes the maximum value, mean value and the voxel location that obtained the maximum β value which is described by an X, Y, Z coordinate with respect to the structural image of the particular subject. A table describing the local maxima within each cluster is also generated, this describes the voxel coordinates that obtained the highest z-statistic values within that cluster.

Following the first-level analysis where the GLM was conducted on each stimulus run, a second-level analysis was done where the average of the two runs for each stimulus was calculated. Here, FEAT generates a web page report that includes a summary of the results showing the z-statistic images with the activated clusters and the corresponding table of the activated clusters and the details, similar to the results from the first-level analysis that were discussed in this section.

5.3 Results

A summary of the second-level analysis FEAT results obtained was generated using the FEATQuery tool [184]. This tool allows you to define a mask image from which it generates the mean statistical values and time series for that particular mask. In this study, the z-statistic result after thresholding for each second-level analysis FEAT output for each subject, stimulus and contrast, was analysed using FEATQuery. Here the MNI structural atlas space was used to mask the occipital, temporal, parietal and frontal lobes respectively to analyse the activations in each of these areas. For each mask applied, FEATQuery outputs the number of voxels activated in the masked image and the maximum z-value voxel obtained, with its corresponding coordinates in voxel (fMRI) space and mm (standard) space. A label for this coordinate generated by the Harvard-Oxford cortical structural atlas is also outputted. An example of such a result can be seen in Figure 5.5, where the occipital lobe was masked on the thresholded z-statistic results of the first contrast (7.5 Hz trial) of Subject 6.

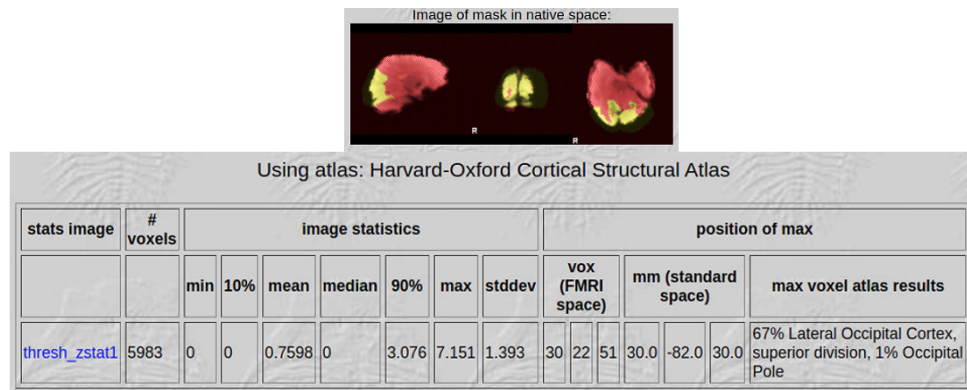


FIGURE 5.5: The FEATQuery output when applying an occipital lobe mask to the second-level analysis result of Subject 6, black-white stimulus, first contrast.

5.3.1 The Activated Cortical Brain Regions

The FEATQuery results of each subject, stimulus and contrast were first used to determine the cortical areas that are being activated in the brain when each subject was presented with a stimulus. To do this, the atlas location of the maximum z-value voxel from each of the four masks applied to each subject, stimulus and contrast was noted. Thus, the brain cortical area that was most frequently activated for each subject and stimulus when analysing the results across all frequencies (contrasts) was determined by the atlas location of the maximum z-value voxel. The results for this are tabulated in Table 5.1. These brain cortical areas are also shown on an MNI atlas brain image in Figure 5.6 for better visualisation.

The results presented in Table 5.1 suggest that the occipital lobe, which comprises the lateral occipital cortex, lingual gyrus, occipital fusiform gyrus, occipital pole and intracalcarine cortex, is the most frequently activated area for all stimuli types presented to all the subjects. However, activations in the parietal lobe (precuneus cortex and postcentral gyrus) have also been activated by Subjects 1, 2, 3 and 4 when exposed to colour and random dot stimuli, suggesting that these stimuli types may increase the generation of SSVEPs in these areas. Interestingly, the temporal lobe, which encompasses the medial occipitotemporal gyrus, has been found to be the most frequently activated area when displaying the black-white stimulus to Subject 1 only. Areas located in the frontal lobe are not the most frequently activated areas, across all subjects and stimuli and since no brain activations in this region are reported in Table 5.1.

TABLE 5.1: The most frequented location of the z-max voxels for all subjects and stimuli, analysed across all frequencies.

| Stimulus | Subject | | | | | |
|--------------|-------------------------------|--------------------------|--------------------------|--------------------------|--------------------------|--------------------------|
| | Subject 1 | Subject 2 | Subject 3 | Subject 4 | Subject 5 | Subject 6 |
| B-w | Medial occipitotemporal gyrus | Precuneus cortex | Lateral occipital cortex | Lateral occipital cortex | Lateral occipital cortex | Lateral occipital cortex |
| B-g | Lingual gyrus | Lateral occipital cortex | Lateral occipital cortex | Precuneus cortex | Lateral occipital cortex | Lingual gyrus |
| R-g | Precuneus cortex | Postcentral gyrus | Lateral occipital cortex | Lingual gyrus | Lingual gyrus | Occipital fusiform gyrus |
| Symbol | Lingual gyrus | Lateral occipital cortex | Intracalcarine cortex | Occipital fusiform gyrus | Lateral occipital cortex | Lingual gyrus |
| Text | Lingual gyrus | Lateral occipital cortex | Lateral occipital cortex | Occipital fusiform gyrus | Lateral occipital cortex | Intracalcarine cortex |
| Checkerboard | Occipital fusiform gyrus | Occipital pole | Lateral occipital cortex | Lateral occipital cortex | Lateral occipital cortex | Occipital pole |
| Random dot | Lingual gyrus | Lateral occipital cortex | Postcentral gyrus | Occipital pole | Occipital pole | Lateral occipital cortex |

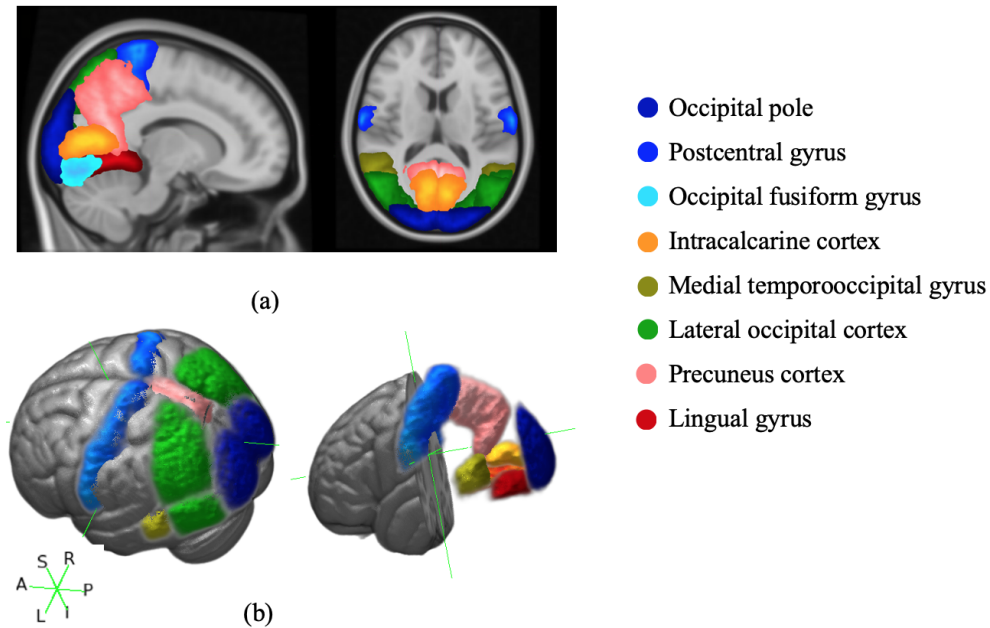


FIGURE 5.6: The brain cortical regions in Table 5.1 visualised on the MNI atlas brain image with the corresponding labels. (a) 2D axial and sagittal views of the MNI atlas template image having the coloured brain cortical regions (b) 3D-view of the MNI atlas image having the coloured brain cortical regions.

To analyse and visualise further the most frequently activated areas for each stimulus across all frequencies, the individual subjects' results were evaluated. For each subject and stimulus, the three most frequented areas, where the maximum z-value voxel was located, were mapped on an MNI atlas brain image to highlight the location of the cortical activations. Red symbolises the most frequently activated area, followed by green and yellow colours to mark the subsequent most frequently activated areas. The brain maps showing the most frequented location of the z-max voxel for Subject 1 can be seen in Figure 5.7. The rest of the brain visualisation maps for the other subjects can be seen in Appendix C.

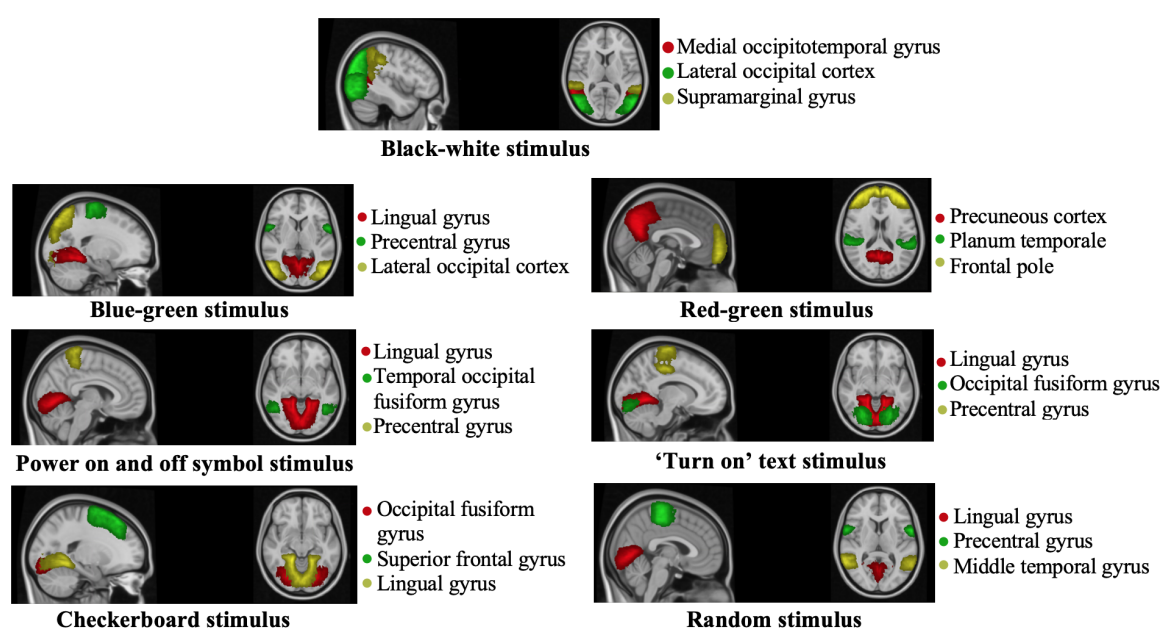


FIGURE 5.7: The three most frequently activated locations of the maximum z-value voxels for Subject 1, showing the results for each stimulus evaluated across the six frequencies. Red label shows the most frequented area, followed by the green and yellow labels.

Individual subjects' results suggest that the most frequently activated area of the brain, where the maximum z-value voxel is located, across all subjects and stimuli is the occipital lobe (lingual gyrus, lateral occipital cortex, occipital fusiform gyrus, intracalcarine cortex). Activations were found in the temporal, parietal and frontal lobe but these occur less frequently and consistently when compared to the occipital lobe. The temporal lobe which comprises the medial occipitotemporal gyrus, temporal occipital fusiform gyrus, middle and inferior temporal gyrus, and planum temporale is mostly activated when presenting the black-white stimulus in Subjects 1, 2 and 5 and when presenting the random dot stimulus in Subjects 1, 4 and 6. No temporal activations were observed with any stimulus for Subject 3.

When looking at areas from the parietal lobe which include the precentral gyrus, postcentral gyrus, precuneus cortex and supramarginal gyrus, it can be observed that these areas are activated by the blue-green stimulus for all subjects except Subject 6. Parietal areas are also activated in Subjects 1 and 5 when focusing on the random dot stimulus, and Subjects 3 and 4 when focusing on the power on and off symbol stimulus. No parietal areas were activated in Subject 6 when focusing on all stimuli types. Frontal areas of the brain (superior frontal gyrus, frontal pole and cingulate gyrus) were activated in Subjects 1, 3 and 5 when displaying the red-green stimulus. Activations in these areas were also noticed when displaying the random dot stimulus to Subjects 3 and 6, and when displaying the text stimulus to Subjects 4 and 5. The frontal lobe was not activated in Subject 2.

This section provides an in-depth analysis for each subject of the brain cortical areas that are activated when subjects were presented stimuli with different colours, shapes and textures at different frequencies. Since these results suggest that the most frequently activated areas where the maximum z-value voxel is located in the occipital lobe, it can be said that the strongest BOLD response is activated in this area of the brain. However, since frequently activated areas were also particularly observed in temporal and parietal lobes, a strong BOLD response can also be found in these areas at specific stimuli properties. The evaluated individual's subject results indicate that inter-subject variability is present in the recorded fMRI data. These findings are further described in the Discussion, Chapter 7.

5.3.2 Number of Activated Voxels in Different Regions

The results from FEATQuery highlight the number of voxels in each brain mask applied (at the occipital, temporal, parietal and frontal lobes) which are activated ($|z| > 1.5$) for a particular subject, stimulus and frequency. To summarise these results further, Table 5.2 shows the average number of voxels activated across all subjects in each brain mask for each stimulus and frequency. For each frequency, the brain mask with the largest number of activated voxels is highlighted in bold text in this table. For each stimulus, the sum of the number of voxels activated in each brain mask across all frequencies is also displayed. The results were also presented using pie charts (Figure 5.8), which for each stimulus show the total number of activated voxels in each brain mask activated across all frequencies.

TABLE 5.2: The average activated number of voxels across the six subjects.

| Black-white stimulus | | | | |
|----------------------------------|-------------------------|----------|-------------|-------------|
| Frequency (Hz) | No. of voxels activated | | | |
| | Occipital | Temporal | Parietal | Frontal |
| 7.5 | 1741 | 897 | 3936 | 3037 |
| 10 | 1829 | 968 | 2149 | 2782 |
| 15 | 3028 | 1122 | 3996 | 4537 |
| 20 | 2172 | 940 | 4732 | 3473 |
| 24 | 3146 | 1292 | 5167 | 3777 |
| 30 | 2558 | 992 | 2692 | 2901 |
| Total voxels activated: | 14474 | 6211 | 22672 | 20507 |
| Blue-green stimulus | | | | |
| Frequency (Hz) | No. of voxels activated | | | |
| | Occipital | Temporal | Parietal | Frontal |
| 7.5 | 3150 | 2065 | 4383 | 3936 |
| 10 | 3560 | 2325 | 4633 | 7021 |
| 15 | 2786 | 1207 | 2553 | 2078 |
| 20 | 2575 | 794 | 3272 | 2285 |
| 24 | 1273 | 799 | 1667 | 2364 |
| 30 | 2660 | 1089 | 3686 | 3423 |
| Total voxels activated: | 16004 | 8279 | 20194 | 21107 |
| Red-green stimulus | | | | |
| Frequency (Hz) | No. of voxels activated | | | |
| | Occipital | Temporal | Parietal | Frontal |
| 7.5 | 250 | 245 | 1540 | 2033 |
| 10 | 704 | 839 | 2613 | 2876 |
| 15 | 1685 | 729 | 3240 | 2532 |
| 20 | 3463 | 1326 | 3889 | 2570 |
| 24 | 4016 | 1436 | 5660 | 4385 |
| 30 | 2902 | 869 | 3045 | 3309 |
| Total voxels activated: | 13020 | 5444 | 19987 | 17705 |
| Power on and off symbol stimulus | | | | |
| Frequency (Hz) | No. of voxels activated | | | |
| | Occipital | Temporal | Parietal | Frontal |
| 7.5 | 5268 | 2250 | 5014 | 5341 |
| 10 | 3841 | 802 | 3012 | 4518 |
| 15 | 5992 | 2188 | 8086 | 6444 |
| 20 | 2756 | 827 | 2790 | 3540 |
| 24 | 4150 | 1316 | 6047 | 3569 |
| 30 | 2841 | 879 | 3567 | 3370 |
| Total voxels activated: | 24848 | 8262 | 28516 | 26782 |
| 'Turn on' text stimulus | | | | |
| Frequency (Hz) | No. of voxels activated | | | |
| | Occipital | Temporal | Parietal | Frontal |
| 7.5 | 3752 | 916 | 2149 | 2028 |
| 10 | 5409 | 1292 | 4823 | 4603 |
| 15 | 3511 | 766 | 3636 | 2432 |
| 20 | 3731 | 1629 | 3978 | 5042 |
| 24 | 5585 | 1267 | 4751 | 4328 |
| 30 | 5947 | 1449 | 6095 | 4024 |
| Total voxels activated: | 27935 | 7319 | 25432 | 22457 |
| Checkerboard stimulus | | | | |
| Frequency (Hz) | No. of voxels activated | | | |
| | Occipital | Temporal | Parietal | Frontal |
| 7.5 | 3709 | 1349 | 4752 | 3972 |
| 10 | 6359 | 2002 | 6006 | 7734 |
| 15 | 3638 | 905 | 3760 | 2640 |
| 20 | 2765 | 1193 | 3376 | 4097 |
| 24 | 5522 | 1101 | 5378 | 4243 |
| 30 | 2153 | 1121 | 2870 | 3290 |
| Total voxels activated: | 24146 | 7671 | 26142 | 25976 |
| Random dot stimulus | | | | |
| Frequency (Hz) | No. of voxels activated | | | |
| | Occipital | Temporal | Parietal | Frontal |
| 7.5 | 4591 | 620 | 4495 | 4270 |
| 10 | 5471 | 1232 | 6179 | 5004 |
| 15 | 6362 | 1788 | 6153 | 6047 |
| 20 | 3322 | 927 | 3711 | 2586 |
| 24 | 3269 | 841 | 4959 | 2985 |
| 30 | 3529 | 1084 | 4711 | 4276 |
| Total voxels activated: | 26544 | 6492 | 30208 | 25168 |

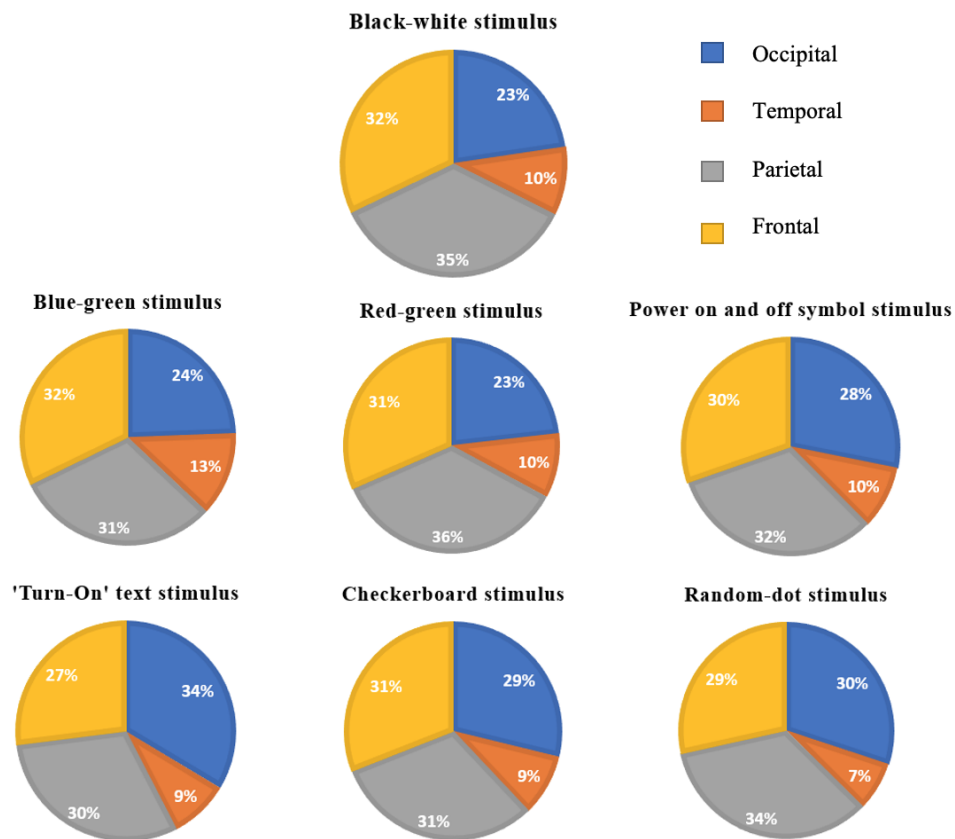


FIGURE 5.8: Pie chart for each stimulus showing the average number of voxels activated in each brain mask evaluated across all subjects and frequencies.

The largest number of activated voxels for each frequency per stimulus (highlighted in bold text in Table 5.1), suggests that the parietal and frontal lobes have the highest number of activated voxels when presenting all the stimuli at any frequency except the blue-green 15 Hz stimulus and the 'Turn On' text 7.5 Hz, 10 Hz and 24 Hz stimuli, where the maximum number of activated voxels was located in the occipital lobe. No frequency across all stimuli obtained the largest number of activated voxels to be located in the temporal lobe.

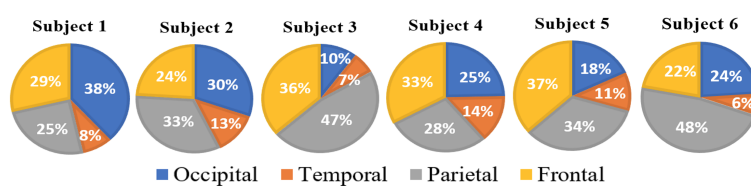
The pie charts for each stimulus shown in Figure 5.8 show that the temporal lobe has the least amount of activated voxels (across all frequencies) when compared to the number of activated voxels in the occipital, parietal and frontal lobes. Across the different stimuli, the blue-green stimulus has the largest number of activated voxels in the temporal lobe (13%) and the random dot stimulus has the least number of activated voxels in the temporal lobe (7%). Similar to the observations seen when looking at the number of voxels activated in the individual frequencies per stimulus, Figure 5.8, which shows the number of voxels activated across the

six frequencies, indicate that the parietal and frontal lobes across all the seven stimuli have the highest number of voxels activated. Particularly, there is a higher activation in the parietal lobe in the black-white and red-green stimulus obtaining 35% and 36% of the total activated voxels to be located in this area respectively. These same stimuli have also obtained the lowest number of voxels activated in the occipital lobe (23%) compared to the other stimuli. The highest number of activated voxels in the occipital lobe was obtained by the ‘Turn On’ text stimulus (34%).

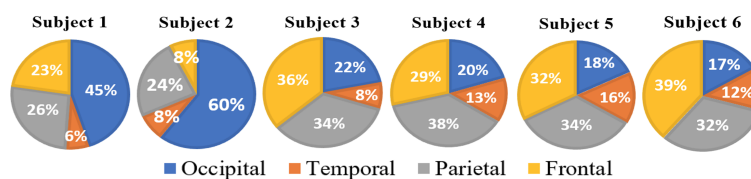
To further analyse the number of voxels activated in each brain mask per subject per stimulus, individual pie plots for each subject and stimulus showing the number of activated voxels in each brain mask across all frequencies were generated. These are shown in Figure 5.9.

The pie charts in Figure 5.9 suggest that the number of voxels activated in each of the four brain masks show a similar behaviour for each stimulus for Subjects 3, 4, and 6. This is because such subjects always obtained the highest number of activated voxels in the parietal and frontal regions followed by the occipital and the temporal region. However, Subjects 1 and 2 exhibited a different behaviour. For Subject 1, the highest number of activated voxels in the occipital region increases for the black-white and blue-green stimuli, obtaining 38% and 45% of voxels activated in this area respectively. The number of activated voxels in the occipital region, however, decreases drastically to 2% in the red-green stimulus for this same subject. Subject 2 also did not obtain a similar behaviour for all the stimuli since there is a large increase in the number of voxels activated in the occipital lobe for the blue-green stimulus reaching 60%. Moreover, Subject 2 obtained a high number of voxels activated in the occipital region for the text, checkerboard and random dot stimuli surpassing the number of voxels activated in the parietal and frontal lobes. This behaviour was also noticed in Subject 5 who also obtained high activations in the occipital region for the text, checkerboard and random dot stimuli.

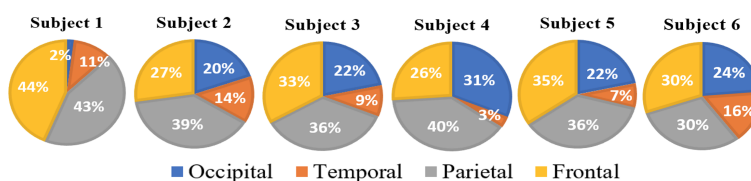
The variation in the number of activated voxels within each brain mask results between the subjects suggest that there is inter-subject variability. However, such findings indicate that apart from the occipital region, the parietal and frontal areas of the brain are also activated when subjects are presented RVS. These results are further explained in Chapter 7.



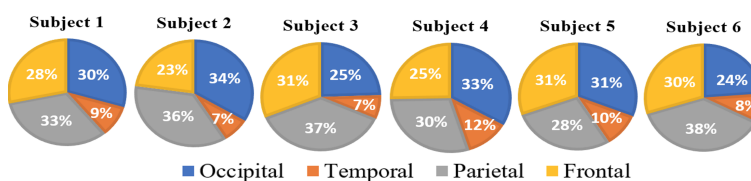
(a) Black-white stimulus



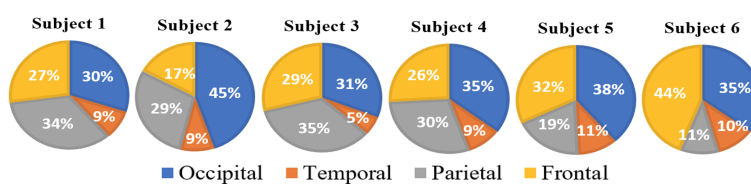
(b) Blue-green stimulus



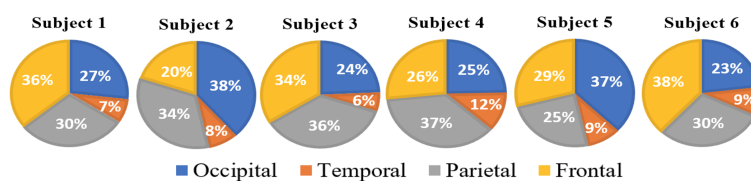
(c) Red-green stimulus



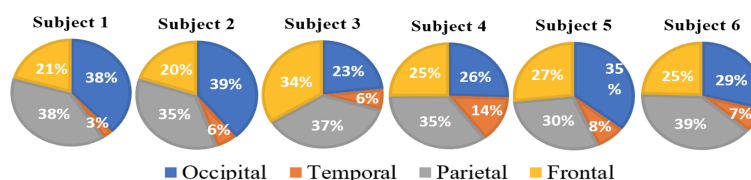
(d) Power on and off symbol stimulus



(e) 'Turn On' text stimulus



(f) Checkerboard stimulus

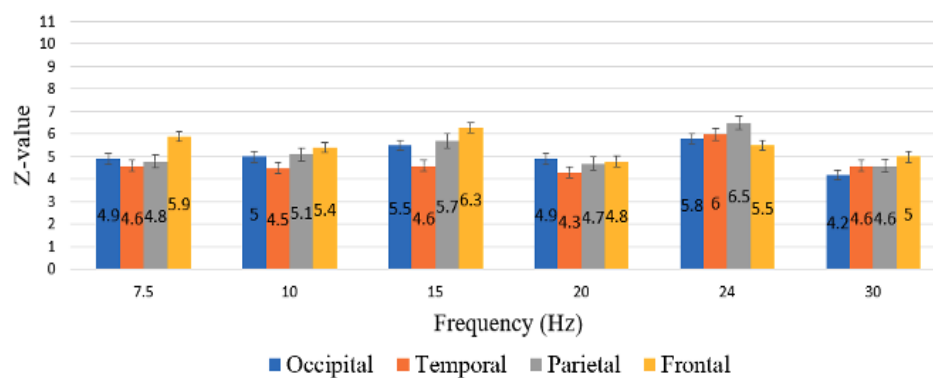


(g) Random dot stimulus

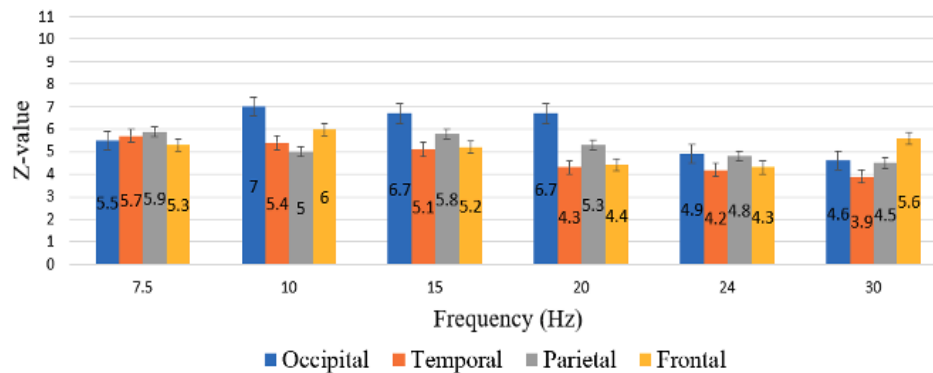
FIGURE 5.9: Pie charts showing the number of activated voxels in each brain mask evaluated for each subject across all frequencies.

5.3.3 Z-Statistic Variation Across Brain Regions and Frequencies

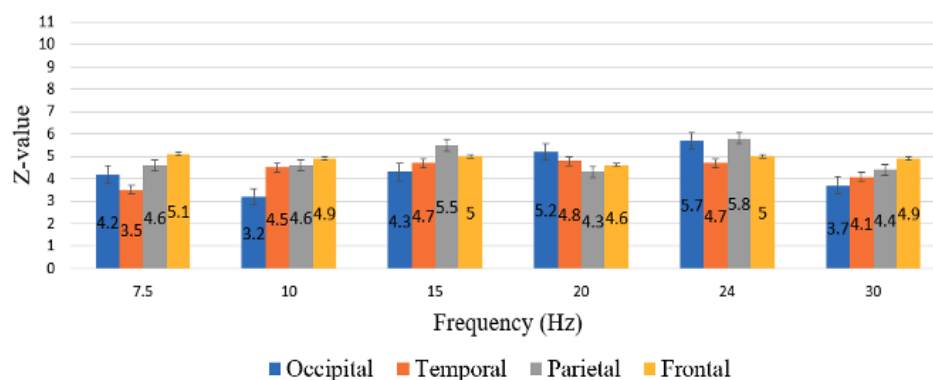
As described in the beginning of Section 5.3, FEATQuery outputs the value of the maximum z-value found in each brain mask. To summarize the results, the maximum z-value for each stimulus-frequency condition was averaged across all subjects to plot the bar graphs for each stimulus, seen in Figure 5.10. These explain how the maximum z-value varies across frequencies and brain masks.



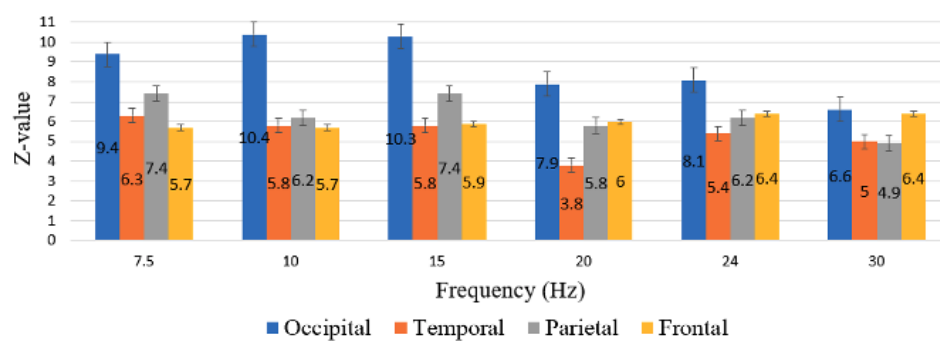
(a) Black-white stimulus



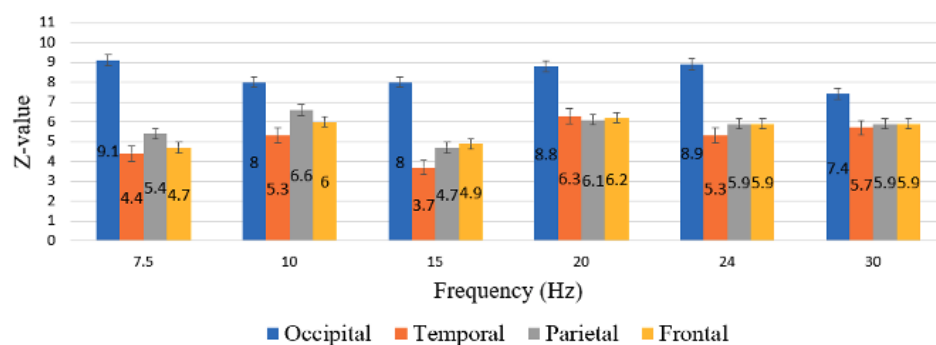
(b) Blue-green stimulus



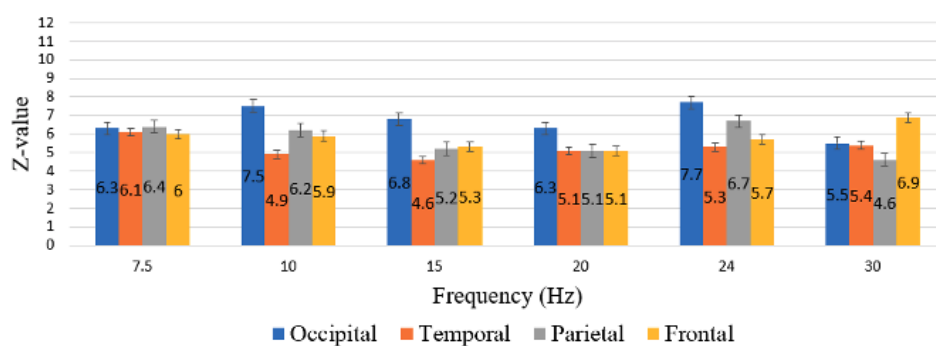
(c) Red-green stimulus



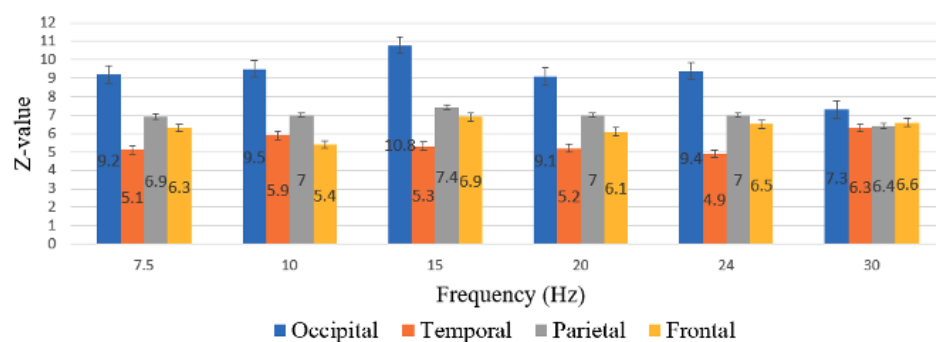
(d) Power on and off symbol stimulus



(e) 'Turn On' text stimulus



(f) Checkerboard stimulus



(g) Random dot stimulus

FIGURE 5.10: Bar graphs for each stimulus showing the mean value of the maximum z-statistic across all subjects obtained in each brain mask and frequency.

Results from the black-white stimulus presented in Figure 5.10(a), show that the highest values for the z-statistic were obtained in the frontal lobe for frequencies in the range of 7.5 Hz - 15 Hz. For the higher frequencies (20 Hz, 24 Hz, 30 Hz), the area from where the highest z-statistic is obtained varies. Results for the blue-green stimulus presented in Figure 5.10(b), show that the highest z-statistic was obtained in the occipital lobe for the 10 Hz - 24 Hz frequency range, with the highest values obtained for the 10 Hz - 20 Hz frequencies. Results for the red-green stimulus do not show a particular brain region or frequency that obtained high z-statistic values, thus no clear observations can be made from this result. The power on and off symbol stimulus however obtained very high z-statistic values in the occipital lobe across all six frequencies, reaching the highest values in the 7.5 Hz - 15 Hz frequency range and the lowest at the 30 Hz stimulus. Similar results were also seen from the 'Turn On' text stimulus which obtained the highest z-statistic values in the occipital lobe having the largest value at the 7.5 Hz stimulus and the lowest value at the 30 Hz frequency. A high z-statistic value in the occipital lobe was also seen when presenting the checkerboard stimulus at frequencies ranging from 10 Hz - 24 Hz. The random dot stimulus, similar to the results of the shape stimuli (power on and off symbol stimulus and 'Turn On' text stimulus) obtained very high z-statistic values in the occipital lobe for all frequencies. The highest value of the z-statistic was seen at the 15 Hz frequency and the lowest value was seen at the 30 Hz frequency.

A voxel having a high z-statistic value indicates that a strong BOLD response is present at that voxel. Consequently, the previous paragraph indicates that the occipital lobe exhibits the strongest BOLD response for most stimuli, except for the black-white and red-green stimuli. This response is prominent between 7.5 Hz and 24 Hz but diminishes at 30 Hz. The highest z-values at the occipital lobe were obtained for the power on and off stimulus and the random dot stimulus. The z-statistic values in the parietal lobe are lower than in the occipital lobe, although some stimuli elicit higher values in this area at specific frequencies compared to the black-white stimulus: symbol (7.5 Hz - 20 Hz), text (7.5 Hz and 10 Hz), checkerboard (7.5 Hz and 10 Hz), and random dot (7.5 Hz - 30 Hz). Similarly, in the frontal areas, the symbol (20 Hz - 30 Hz) and random dot (15 Hz - 30 Hz) stimuli evoke greater responses than the black-white stimulus. In the temporal regions, the blue-green (7.5 Hz - 15 Hz), symbol (7.5 Hz - 15 Hz), and random dot (7.5 Hz - 20 Hz) stimuli generate increased BOLD responses compared to the

black-white stimulus. Such results may indicate that certain stimuli parameters may evoke a stronger SSVEP response in the brain than the standard black-white stimulus, as further discussed in Chapter 7.

5.4 Chapter Summary

The results from the general linear model (GLM) were evaluated by applying brain masks to the z-statistic thresholded results for each subject, stimulus and frequency at the four major lobes of the brain (occipital, temporal, parietal, frontal lobe). From this, an in-depth analysis on the most frequently activated cortical regions in the brain for each subject was evaluated by analysing the location of the maximum z-value voxel from each of these four areas. Results across all subjects concluded that the occipital lobe is the most frequently activated area for all stimuli types.

The results were also evaluated by noting the number of voxels that had a statistically significant z-statistic value in each of the brain masks. These results show that for three subjects, the frontal and parietal lobes have the largest number of activated voxels, followed by the occipital and temporal regions. However, this activity was not observed in the other three subjects.

The highest maximum z-value voxels were obtained by the power on and off symbol and random dot stimulus which were located in the occipital lobe. Both the blue-green and checkerboard stimuli also obtained the highest maximum z-value voxels in the occipital lobe having a value greater than the black-white stimulus. These results also show that the 30 Hz frequency obtained the lowest z-value when compared to the other frequencies. The z-score values at the non-occipital areas (temporal, frontal and parietal lobe) were lower than the z-value at the occipital lobe for five stimuli suggesting that the BOLD response at these areas is weaker.

The results described in this chapter are further analysed in Chapter 7. The next chapter uses the same RVS presented in this chapter to analyse the SSVEP response using a high-channel EEG setup which allows a better temporal and spectral analysis of the SSVEP in the brain.

Chapter 6

EEG Setup and Analysis

6.1 Introduction

This chapter describes the setup and steps taken to design and carry out an EEG study to analyse the SSVEP on the scalp when subjects are exposed to different stimuli properties and frequencies. A description of the techniques and methods used to analyse the EEG data is then given, which is followed by an in-depth explanation and analysis of the results obtained.

6.2 Objectives of the EEG Analysis

Following the functional MRI study, an EEG study was conducted to analyse the SSVEP signals in the brain with the following aims:

- To design an experimental protocol and carry out EEG data recording sessions on human subjects.
- To localise the SSVEP on the scalp when presenting stimuli with different parameters, including colour, shape, and texture.
- To investigate spatial and amplitude variations in brain activity in response to changes in stimulus properties and frequency.
- To analyse if the brain's response to a particular stimulus parameter is more localised and/or can increase the strength of the SSVEP in non-occipital areas to adequately control SSVEP-based BCI systems.

- To compare the SSVEP response recorded from the whole scalp in the EEG study with the cortical brain-activated regions when presenting RVS determined by the fMRI study, to get a more comprehensive understanding of the brain's response to flickering stimuli.

6.3 System Architecture

To conduct the EEG study, the BioSemi ActiveTwo system was used to record the EEG data from human subjects [189]. Together with this system, a 24" LCD monitor having a vertical refresh rate of 60 Hz and a resolution of 1920×1080 pixels was utilised. The PsychoPy software was again used to create and render the RVS on the LCD monitor and the BioSemi ActiView data acquisition software was used to acquire the EEG signals [155, 190]. The correct synchronisation between these two softwares was ensured via a triggering system, which will be explained in more detail in this section. All recorded data was then processed and analysed offline using the MATLAB software [191].

6.3.1 Hardware Description

The BioSemi ActiveTwo system is a biopotential measurement system, consisting of a direct current (DC) amplifier with a rechargeable battery unit, an EEG head cap, EEG active electrodes, a USB receiver and trigger box, an ST-ST 62.5 fibre optic cable, a USB 2.0 cable and an LPT1 trigger cable [189]. The BioSemi ActiveTwo system can withstand up to 256 channels (electrodes), which are suitable for EEG, electrocardiogram (ECG) and electromyography (EMG) applications.

The BioSemi pin-type active Ag-AgCl electrodes provide low-noise measurements and excellent DC-stability (low drifts) [192]. The BioSemi head cap indicates the different electrode positions conforming to the 10-20 electrode system and the MCN, to facilitate the electrode placement. Furthermore, the cap ensures that there is adequate contact between the electrodes and the skin, and that the electrodes are positioned correctly. The SignaGel electrolyte is placed between the electrodes and the scalp to increase conductivity. For this study, a 64-channel (electrode) EEG data acquisition system was utilised. This high number of channels was chosen such that the analysis of SSVEPs covers a large surface area of the head, providing

a relatively high spatial resolution.

The BioSemi DC amplifier is a compact, energy-efficient front-end system with galvanic isolation. It can digitise up to 256 sensor signals with a high resolution of 24 bits [193]. The amplifier is operated with a battery power supply, and all the digital outputs of the analogue-to-digital converters (ADCs) are digitally multiplexed and sent to the USB receiver via a single optical fibre for optimal interference rejection and subject safety [193].

The USB receiver takes the optical data from the DC amplifier and transforms it into a USB 2.0 output to stream the EEG data to the computer running the BioSemi ActiView data acquisition software [194]. Furthermore, the receiver is equipped with a trigger port featuring 16 separate trigger inputs and 15 independent trigger outputs to allow for event-related potential (ERP) measurements and event logging [194].

6.3.2 Software Description

The BioSemi ActiView software, which is the acquisition programme for the ActiveTwo system, was used to configure the hardware and setup [190]. Through this software, a configuration file with the amplifier parameters was loaded. This includes the appropriate 64-channel labels for the head cap, the sampling rate and bandwidth. For this study, a high sample rate of 2048 Hz and a bandwidth of 400 Hz were set for each channel. The BioSemi system also calculates the electrode impedance offsets, which are viewed on the ActiView software. Thus before starting any data collection, the offsets at each active electrode, which are displayed through the ActiView software, were checked to make sure that they are between ± 40 mV at rest to ensure proper connection between the scalp and the electrodes [195]. All EEG data recorded in ActiView was saved in the BioSemi data format (BDF), which was then converted to the MAT-file format to be loaded in MATLAB for further processing [196].

The PsychoPy software, which was also used in the fMRI study, was utilised to create and render the RVS with the different parameters [155]. This was configured to send triggers via the BioSemi serial adapter, which are then recorded and saved by the BioSemi ActiView software during the data recording session.

6.4 Subjects and Experimental Setup

The same six subjects that carried out the fMRI study (three males and three females, age range 22 - 28) carried out the EEG study. The same experimental protocol used in the fMRI study for each subject was also performed in the EEG study. This was done such that the findings from both recording modalities could be compared to each other. Figure 6.1 shows the setup used to conduct the EEG study.

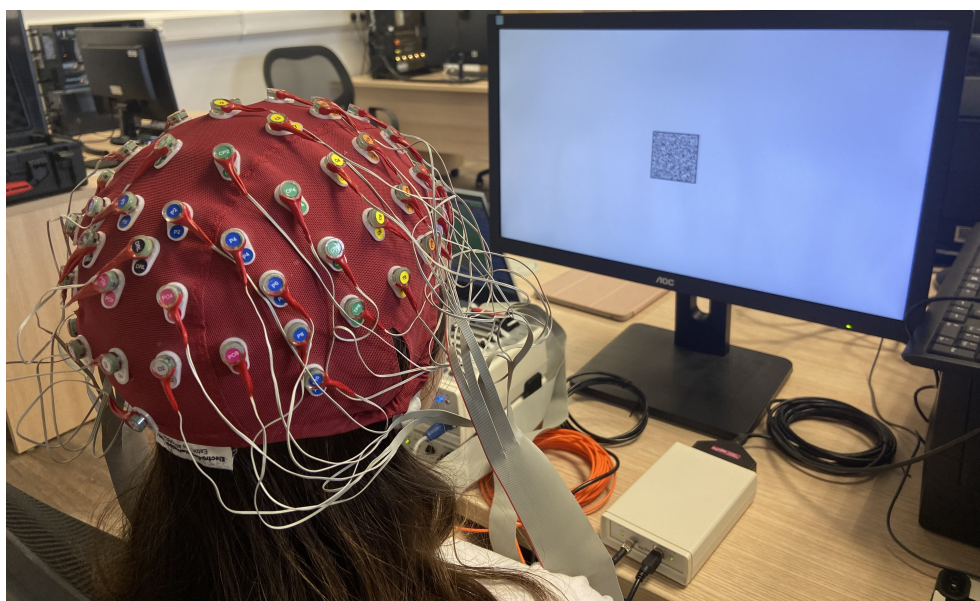


FIGURE 6.1: EEG data acquisition setup showing the subject focusing on the RVS displayed on an LCD monitor screen.

6.4.1 Data Acquisition

All participating subjects were asked to read and sign a consent form that was approved by the University Research Ethics Committee (UREC) of the University of Malta, prior to each recording session. The RVS displayed on the LCD monitor were presented to each subject at approximately eye level while being placed 30 cm away from the screen. Before the data acquisition session, the subjects were instructed to focus their attention on the RVS, restrict their physical movement, and blink as little as possible. Data was recorded from 64 EEG electrodes placed around the whole scalp whose positions are described in Figure 6.2. The BioSemi system utilizes two extra electrodes referred to as the common mode sense (CMS) active electrode and the driven right leg (DRL) passive electrode, effectively taking

the place of the traditional ‘ground’ electrode found in standard EEG recording systems [197]. These CMS and DRL electrodes create a feedback loop that aims to align the subject’s average potential with the ADC reference voltage within the DC amplifier [197]. The Cz electrode, which is located at the top of the head, was chosen to be the reference electrode.

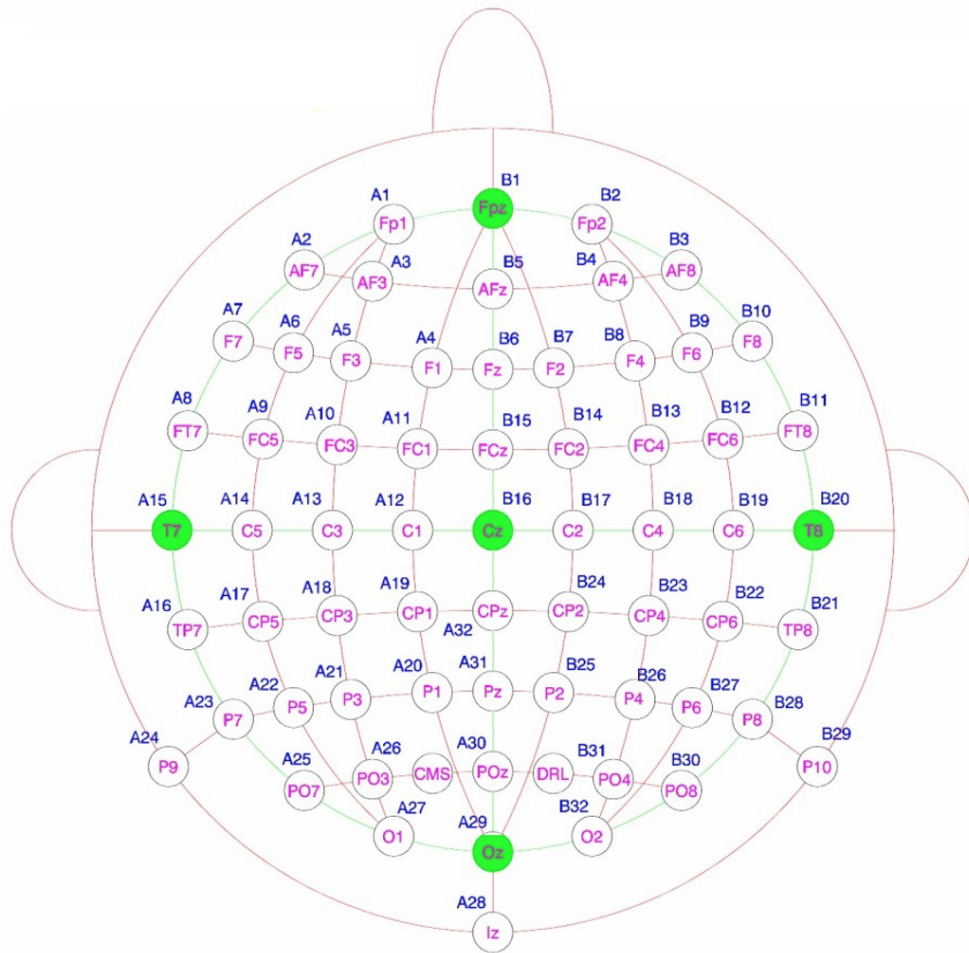


FIGURE 6.2: The 64-channel BioSemi head cap with the corresponding 10-20 system and MCN layout labels, and the CMS and DRL electrodes.

6.4.2 Experimental Paradigm

The same experimental paradigm used in the fMRI study previously explained in Section 4.6.1, and described via the flowchart in Figure 4.9 was implemented in this EEG study. However, the ‘pre-scanning session’ and the first session (which in the fMRI study was used to record structural images of the brain and gradient-echo maps) were discarded. Consequently, the experiment began by describing the

instructions to the participants to focus on the screen and minimize movements and blinking as much as possible. This was followed by the colour stimuli session where the black-white control stimulus, blue-green stimulus and red-green stimulus were shown to the subject at each of the six different frequencies (7.5 Hz, 10 Hz, 15 Hz, 20 Hz, 24 Hz and 30 Hz). Thus, each stimulus was presented for six trials (one trial for each frequency), which were repeated twice for a total of two runs. This session lasted a total of 25 minutes.

The colour stimuli session was followed by the shape stimuli session, where the power on and off symbol stimulus and ‘Turn On’ text stimulus were shown, and texture stimuli session, where the checkerboard and random dot stimuli were individually rendered. Each stimulus in these sessions was presented for six trials (one trial per frequency), and this was presented twice for a total of two trials per stimulus-frequency combination. Both of these sessions lasted 16 minutes. To keep the same 12° visual angle that was used in the fMRI study, the stimulus size for the EEG study was set to 6.3 cm, and each subject was placed 30 cm away from the LCD monitor.

As described in Section 4.6.1, each trial consisted of a 15.2 s fixation period, followed by a 22.8 s stimulus period and a 2.04 s rest period. To ensure that the PsychoPy code used to create the experiment paradigm and the data recording acquisition session from the BioSemi ActiView software were synchronised, the PsychoPy code was configured to send a trigger at the start of every fixation, stimulus and rest period, respectively. The timing of these triggers was then later used when organising the recorded data, to be able to separate the EEG data recorded during each period. Breaks were given to the subject between the colour, shape and texture recording session since it is tiring to look at RVS for a long period of time.

6.5 Data Analysis

The collected raw EEG data from each subject was first preprocessed as will be explained in this section. Specific algorithms were then applied to observe the power of the SSVEP response with different stimuli parameters and frequency values. Statistical analysis was used to compare the strength of the SSVEP response elicited by stimuli properties with the response evoked during the control condition.

6.5.1 Preprocessing

The EEG data from each of the 64 channels in the time domain was referenced to the Cz electrode (that is located at the top of the head), by taking the potential value recorded from each active electrode and subtracting it from the potential at the Cz electrode. This type of technique is called monopolar or unipolar recording, and it is essential to cancel out environmental noise from the recorded data [198].

Apart from SSVEPs, the EEG data collected from the scalp typically contains other types of electrical signals including noise and physiological artefacts, which are crucial to remove for further accurate analysis. Digital filters were applied to the recorded data to remove these unwanted components. This kind of interference encompasses various sources of noise, including the 50 Hz power line frequency, cardiac signals like the ECG, motion artefacts generated by muscle contractions (EMG), eye movement-related signals stemming from eyeball motion (electrooculogram (EOG)), and changes in skin impedance due to the insulating properties of the outer skin layer and the ionic potential of sweat glands [199]. Consequently, a bandpass filter having a passband between 2 Hz - 100 Hz was employed in this study [110, 200, 201]. This ensured that factors such as sweating and drifts in electrode impedance, which can result in slow changes in the recorded voltage, were eliminated. Furthermore, frequencies above 100 Hz were suppressed as these frequencies are often generated due to the contraction of muscles [199]. The power line frequency was eliminated by applying a notch filter at 50 Hz.

6.5.2 Feature Extraction

In the feature extraction phase, characteristics of the preprocessed EEG data are extracted for the different SSVEPs that are evoked when the RVS are presented to the subjects. Since SSVEPs are elicited by periodic stimulation, making them periodic signals, their spectral content is located around the stimulation frequency and its harmonics. Thus to distinguish the SSVEP signals, the EEG data is transformed from the time to the frequency domain. In this way, the power of the signal can be analysed which facilitates better analysis and description of the signal's frequency characteristics.

6.5.2.1 Fast Fourier Transform

Spectral analysis was conducted by applying the Fourier transform (FT) to transform the EEG data recorded in the time domain into the frequency domain. When working with real EEG data it is necessary to approximate the FT on discrete vectors of data. Therefore, the discrete Fourier transform (DFT) is employed to find the spectrum of a finite-duration signal [202].

For a positive integer N and a discrete-time signal $x[n]$, the N -point FT X_k from $n = 0$ to $n = N - 1$ can be computed according to the formula [202, 203]:

$$X_k = \sum_{n=0}^{N-1} x[n] e^{-\frac{j2\pi kn}{N}} \quad (6.1)$$

Where $k = 0, 1, \dots, N - 1$. For each value of k , the direct computation of $x[n]$ requires N^2 complex multiplications and $N^2 - 1$ complex additions to compute all N values. This makes the direct computation of FT inefficient since it does not exploit the periodicity properties and symmetry of the phase factor ($e^{-\frac{j2\pi kn}{N}}$) [202, 203]. For this reason, an implementation of the DFT known as the fast Fourier transform (FFT), which is more efficient and provides a faster computation time, is utilised. This is done by applying a radix-2 FFT algorithm, which requires $(N/2)\log_2 N$ multiplications and $N\log_2 N$ complex additions to compute the same result [202, 203].

In a real-time BCI system, the N -point FFT is applied to the EEG data using moving windows having a fixed time period s and L samples [204]. For a sampling frequency f_s , $L = s \times f_s$ such that if L is less than the N , zero-padding is done as a computationally efficient method to insert a large number of frequency bins [204].

6.5.2.2 Power Spectral Density

Electroencephalography (EEG) signals are considered as finite-energy signals having finite average power and, hence, are characterised by a power density spectrum. The periodogram is used to find an estimate of the power spectral density (PSD), and is given by [202]:

$$PSD_k = \frac{1}{N} \left| \sum_{n=1}^{N-1} x[n] e^{-\frac{j2\pi kn}{N}} \right|^2 \quad (6.2)$$

This computes a real-valued double-sided spectrum that is symmetrical along the DC value. To analyse the PSD, it is only required to look at either the positive or negative frequencies. The periodogram provides an asymptotically unbiased estimate of the true PSD. This distortion mainly stems from two factors: spectral smoothing, which spreads the sinusoidal power across a range of frequencies, and power leakage through the side lobes [204]. To mitigate the variance and noise associated with the periodogram, Welch's method is employed [204].

With this method, the discrete time signal $x[n]$ is divided into K segments of M samples each which overlap each other. Each segment is then windowed after which the periodogram is computed for each segment. Finally, an average of these periodograms is taken to obtain Welch's PSD estimate [202].

The choice of window and the length of the data segments M , affect the frequency resolution of the power spectrum. Different window shapes exist having different main lobe widths and peak side lobes, these include: the rectangular, Bartlett, Hanning, Hamming and Blackman windows. As the width of the main lobe increases, the spectral smoothing is increased, which in turn reduces the spectral resolution. The Hamming window was used in this analysis to strike a balance between achieving high resolution and minimizing spectral leakage.

From the PSD spectrum, peaks are expected to be found at the frequency components corresponding to the stimulus' fundamental frequency and its harmonics.

6.5.2.3 Signal-to-noise Ratio

The signal-to-noise ratio (SNR) depicts how large the amplitude of the evoked SSVEP response is in relation to the background activity and thus it describes the relationship between the signal level and the noise level. Background activity refers to the activity in the brain when a subject is in a relaxed state and no stimuli are presented. This background activity in EEG data usually appears as alpha frequency components (8 Hz - 12 Hz), which magnitudes vary from subject to subject. Such frequency components can therefore be easily misinterpreted for an

SSVEP response due to RVS. Thus, it is essential to cancel out this background activity and enhance any SSVEP peaks by estimating the SNR using the following equation [204]:

$$SNR = \frac{PSD_S(f)}{PSD_B(f)} \quad (6.3)$$

Here $PSD_S(f)$ is the PSD estimated for EEG data recorded during a stimulation period, and $PSD_B(f)$ is the PSD estimated during a baseline period (or fixation period). The higher the SNR amplitude, the better it is to detect and discriminate the frequency components at the fundamental and harmonics of the RVS, implying that a strong SSVEP response is present.

6.5.2.4 Z-score

The z-score statistical measure is another way of how the PSD during stimulation is compared to the baseline PSD to obtain a more objective estimation of the power change due to the RVS [205]. Hence, the z-score is applied to calculate the SSVEP signal strength as it rescales the data about the mean. A z-score that is equal or above 2, specifies that the observation is above the mean and therefore significant at the 95% level, while a z-score below -2 indicates that the observation is below the mean [205]. This corresponds to the common significance level of 0.05 used in hypothesis testing. Using a Z-score threshold of 2 also provides consistency and comparability across different studies and analysis, as this value is most commonly used in EEG studies [114, 205, 206]. Furthermore, a Z-score of 2 strikes a balance between sensitivity and specificity since it allows for the identification of potential deviations from the mean while minimising the risk of overinterpreting normal variability as significant [205].

The z-score is calculated by subtracting the PSD mean of all baseline trials μ from the PSD x of a single trial during the stimulation period, and dividing the result by the baseline PSD standard deviation σ of all trials as shown by the following equation:

$$z\text{-score} = \frac{x - \mu}{\sigma} \quad (6.4)$$

6.5.3 Statistical Analysis

In this study, statistical analysis was applied to understand if the SSVEP response generated by the different stimuli properties applied at different frequencies is statistically significant over the SSVEP response generated by the control condition (black-white stimulus). This was evaluated over all the EEG collected from the 64 channels placed across the whole scalp. To do this, non-parametric permutation-based statistics were applied, as will be explained in this section.

6.5.3.1 Permutation-based Statistics

Non-parametric permutation testing is a valuable framework for evaluating the statistical significance of EEG data across different channels. This method provides two main advantages: (i) it does not rely on any assumption about the data distribution or its parameters and (ii) it allows for straightforward corrections for multiple comparisons in the analysis [207]. The non-parametric permutation-based statistic exhibits greater flexibility than z-score analysis in the context of EEG experiments featuring multiple conditions, repeated measures, or factors that pose challenges to traditional parametric methods. Permutation-based statistics provide a comprehensive overview, revealing statistically significant SNR values for each tested stimulus-frequency condition across all 64 electrode positions. This holistic perspective contrasts with the z-score approach, where individual data from each electrode requires separate analysis, delaying the immediate identification of electrodes with significant SNR values for each stimulus-frequency condition.

Non-parametric permutation testing creates a null hypothesis distribution from the data available. This is achieved by repeatedly shuffling conditions over trials or subjects for a number of iterations and each time recalculating the test statistic [207, 208]. The null hypothesis values for each iteration form a distribution of test statistics obtained under the null hypothesis [207, 208]. The test statistic of two conditions is taken as the difference between the means of the two populations ($\mu_{population\ 1}$ and $\mu_{population\ 2}$) as described by Equation 6.5.

$$Test\ statistic = \mu_{population\ 1} - \mu_{population\ 2} \quad (6.5)$$

To understand this better, consider an EEG dataset having two conditions, A and B, where the hypothesis is that frontal gamma power is higher in condition

A compared to condition B. This hypothesis can be evaluated by conducting the difference of the gamma power between the two conditions. The null hypothesis for this scenario is that there is no difference in frontal gamma power between the two conditions. In other words, this can be interpreted as stating that if trials were randomly labelled as either condition A or condition B, the test statistic would exhibit the same value as the test statistic before the random labelling [207]. Essentially, under the null hypothesis, a trial originally assigned to condition A could be labelled as condition B, and vice versa, without affecting the test statistic [207]. Thus, the test statistic across these “conditions” is obtained after labels from many trials have been swapped (shuffled). If there is no difference between the conditions, the label swapping has no impact on the test statistic, and the test statistic value is expected to be zero [207]. If the test statistic deviates from zero, this deviation is attributed to either the presence of outliers or sampling error that coincidentally ended up in one condition [207].

This process generates one null hypothesis test statistic value. This procedure is repeated for numerous iterations, forming a distribution of test statistic values under the null hypothesis [207, 208]. To assess statistical significance, the observed test statistic (associated with unshuffled data) is compared to this distribution of null hypothesis test statistic values obtained from the shuffled data [207]. A p -value associated with the observed test statistic is then calculated. One way of doing this is by comparing the observed test statistic to the statistical properties of the null hypothesis distribution by subtracting the mean of the null hypothesis distribution from the observed statistic value and then dividing by the standard deviation of the null hypothesis distribution [207]. This is commonly known as the standard z-score given by [207]:

$$z\text{-score} = \frac{v_e - \overline{V}_n}{std(V_n)} \quad (6.6)$$

Where v_e is the observed-effect test statistic and \overline{V}_n is a vector containing the mean values of the null hypothesis test statistics [207].

6.5.3.2 Correction for Multiple Comparisons

To correct for multiple comparisons, this study employed pixel-based statistics [207]. This method involves creating a distribution containing the test statistic

from each iteration of permutation testing with the most extreme statistical values [207]. Pixel-based multiple-comparisons correction involves conducting permutation testing using the procedures outlined in Section 6.5.3.1 to generate test statistic values under the null hypothesis. However, during each iteration of permutation testing, the two most extreme null hypothesis test statistic values are recorded; these are the largest positive and negative values. After completing all iterations, two distributions are formed; one containing the largest positive test statistic values and the other containing the largest negative test statistic values. The statistical threshold is defined as the value corresponding to the 97.5th percentile of the largest values and the value corresponding to the 2.5th percentile of the smallest values, thereby establishing the upper and lower bounds of the threshold at a significance level of $p = 0.05$ [207].

6.5.3.3 Stationary Signals

To keep the same experimental protocol as the fMRI experiment, for each stimulus-frequency condition, the EEG data for two trials of 22.8 s each was recorded. However, in EEG analysis, this trial length is deemed long since the SSVEP response from EEG can be detected from short trial lengths of 1 s - 2 s [92]. Thus, to increase the number of trials of stimulation periods for each stimulus-frequency condition which will be used in the permutation-based statistics, each 22.8 s trial was divided into five, four-second trials. To do this, however, the recorded time series EEG data during the stimulation period had to be proved for stationarity to verify that the mean and variance of the SSVEP response does not vary over time. The first 2.8 s of each 22.8 s trial was excluded from the analyses to (i) allow for the steady-state response to stabilize, (ii) eliminate the transient phase, which can distort the signal estimate, and (iii) discard any data that is expected to be dominated by responses related to the stimulus onset.

To check for stationarity of the time series data, the Augmented Dickey-Fuller (ADF) test and Kwiatkowski-Phillips-Schmidt-Shin (KPSS) statistical test were used. Both statistical tests were employed since they are sensitive to different types of stationarity. While the ADF test is useful for detecting non-stationarity due to trends in the data such as linear trends, the KPSS test is useful for detecting non-stationarity when the data deviates from a stationary process due to a unit root around a mean. Thus using both tests helps in providing information about

the type of non-stationarity (around a mean or linear trend) which gives a better interpretation of the results. Furthermore, it is common for EEG studies to utilise both tests to check for stationarity [209, 210].

The ADF test is a version of the statistical test known as a unit root test [211, 212]. A unit root is a characteristic of certain stochastic processes that can cause difficulties in statistical inference when dealing with time series models. Specifically, a unit root indicates that the process is non-stationary. Thus, an ADF test is conducted with the assumptions that [211, 212]:

- Null hypothesis H_o : The time series data is non-stationary or has a unit root.
- Alternate hypothesis H_A : The time series is stationary or has no unit root.

The null hypothesis H_o is rejected if the test statistic is smaller than the critical value and if the p -value is less than 0.05. In this case, the time series data does not have a unit root (it is stationary) and is not time-dependent [211].

The KPSS test is another form of unit root test designed to assess the stationarity of a given series with respect to a deterministic trend [211]. The following assumptions are used to conduct a KPSS test [211, 212]:

- Null hypothesis H_o : The time series is stationary or has no unit root.
- Alternate hypothesis H_A : The time series data is non-stationary or has a unit root.

The null hypothesis H_o fails to be rejected if the test statistic is smaller than the critical value and the p -value is less than 0.05. In this case, the time series data does not have a unit root, meaning that it is stationary [211].

Both the ADF and KPSS tests were implemented in MATLAB using the ‘adftest’ and ‘kpsstest’ functions, respectively, and it was determined that the SSVEP response in each of the 22.8 s trials at each of the 64 channels was stationary. This is because the ADF test function returns a value of 1, indicating rejection of the unit-root null model in favour of the alternative hypothesis. Conversely, the KPSS test function returns a value of 0 indicating failure to reject the trend-stationary null hypothesis. Hence, each of the two 22.8 s trials for each stimulus-frequency

condition, (after eliminating the first 2.8 s of data), was divided into five, four-second trials to remain with 10 trials per stimulus-frequency condition. This structuring of trials is explained in Figure 6.3.

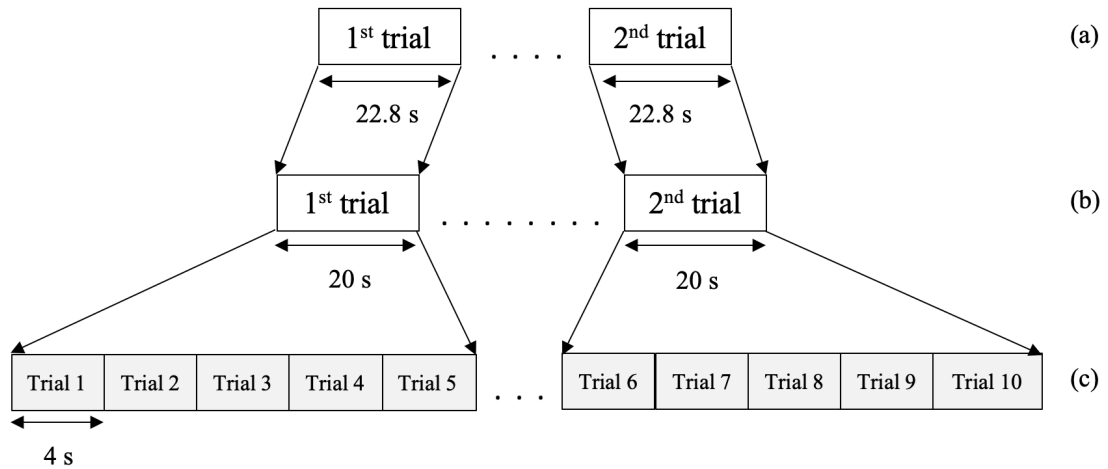


FIGURE 6.3: Protocol of trial structuring: (a) Two 22.8 s trials for each stimulus-frequency condition (b) Discarding the first 2.8 s (c) Dividing the 20 s trials into 10 four-second trials.

6.6 Results

This section uses the SNR, z-score and permutation-based statistics to present the results and observations obtained after preprocessing the raw EEG data. Focus is given on analysing the strength of the SSVEP response generated by the stimuli with different properties and comparing this to the strength of the SSVEP evoked by the black-white stimulus.

6.6.1 Single Trial Analysis

The EEG signal after passing through the preprocessing steps described in Section 6.5.1, which includes the process of referencing to the Cz channel and filtering, is shown in Figure 6.4 as an example. This signal was obtained from the Oz channel of Subject 2 when the subject focused on the 7.5 Hz black-white stimulus during one 22.8 s trial.

As explained in Section 6.5.3.3, the ADF and KPSS tests were applied to generate 10 four-second trials for each stimulus-frequency condition presented to the user.

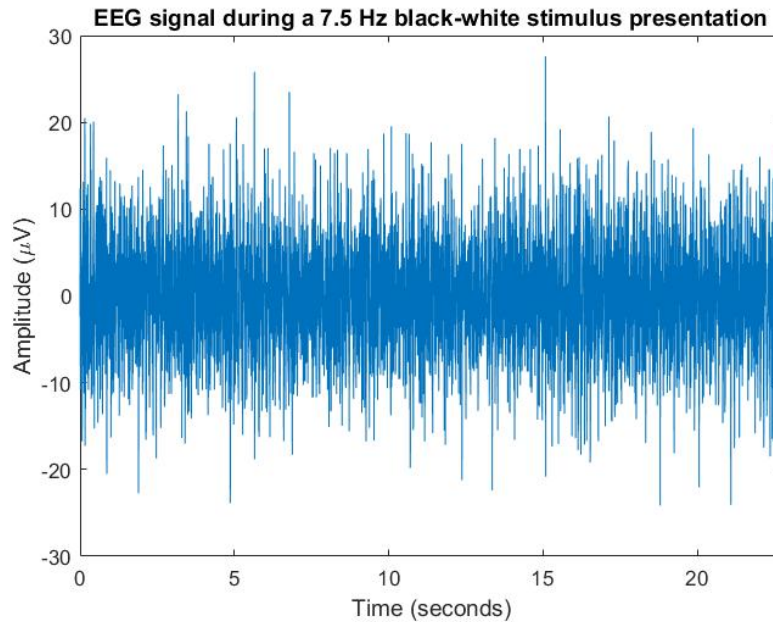


FIGURE 6.4: The time-domain EEG signal for one 22.8 s trial for the 7.5 Hz black-white stimulus period of Subject 2 at the Oz channel.

The 15.2 s fixation period that was shown prior to each stimulation period, which contains the baseline EEG data (resting EEG data), was also further divided into shorter trials. To generate 10 four-second trials of baseline data for each subject, the first four fixation periods that were shown prior to the black-white stimulus were used. The first 2.8 s data of these periods were discarded, and with the remaining 12.4 s data, three four-second trials could be extracted from the first three 15.2 s fixation periods, and one four-second trial was then extracted from the fourth fixation period to obtain a total of 10 four-second fixation period trials for each subject.

The EEG waveform for each fixation and stimulus period trial at each of the 64 channels was then evaluated in the frequency domain to observe the frequency content and the elicited SSVEP response (in the case of a stimulation period trial) more clearly. The PSD using Welch's method was applied to each of the 4 s stimulus-frequency condition trial and fixation period trial, where the data was divided into three segments with a 50% overlap. The 'pwelch' MATLAB function was used to apply this.

After applying the PSD to each trial at each channel, the SNR for each of the stimulus-frequency condition trials could be evaluated. Equation 6.3 was used to perform this by dividing the PSD of each of the 10 four-second stimulation

periods trials for each stimulus-frequency condition for a particular subject with each of the PSD of the 4 s fixation period trial for that particular subject. To summarise the results of the six individual subjects, the mean SNR for each of the 10 stimulus-frequency condition trials across the six subjects for each of the 64 channels was evaluated. Figure 6.5 shows the SNR averaged across the six subjects for one 4 s trial for the 10 Hz black-white stimulus at the Oz channel. Peaks can be clearly seen at 10 Hz up to the 4th harmonic (40 Hz), showing that an SSVEP response is present during this trial at the Oz channel.

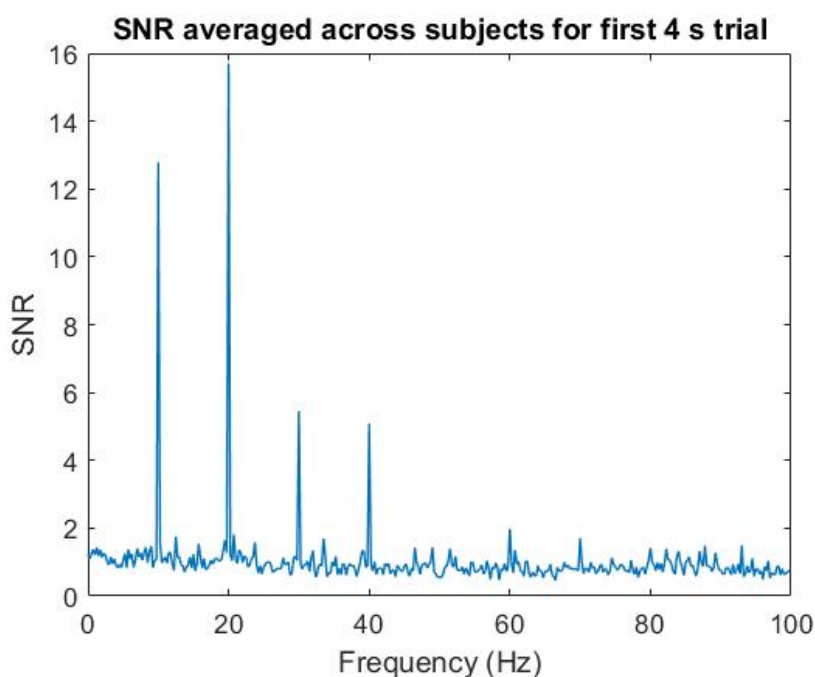


FIGURE 6.5: The SNR averaged across the 6 subjects for one 4 s trial when presenting the 10 Hz black-white stimulus at the Oz channel.

6.6.2 Permutation-based Statistics

The 10 SNR trials for each stimulus-frequency condition were then used to determine if the SNR evoked by the colour, shape and texture stimuli is statistically significantly better than the black-white stimulus condition (control condition) at each of the six frequencies and their corresponding two harmonics. This was done by applying permutation pixel-based statistics. Only the fundamental frequency and two harmonics were considered in this analysis since higher harmonics cannot be detected for the 30 Hz flickering stimulus due to the bandpass filter applied in

the preprocessing stage having a cut-off frequency at 100 Hz.

Two conditions were considered for each permutation-based test applied:

- Condition 1: 10 SNR trials for each of the 64 channels, averaged across the six subjects for the black-white stimulus for each frequency (7.5 Hz, 10 Hz, 15 Hz, 20 Hz, 24 Hz and 30 Hz) and its two harmonics, respectively.
- Condition 2: 10 SNR trials for each of the 64 channels, averaged across the six subjects for each of the blue-green, red-green, power on and off symbol stimulus, ‘Turn On’ text stimulus, checkerboard stimulus and random dot stimulus for each frequency (7.5 Hz, 10 Hz, 15 Hz, 20 Hz, 24 Hz and 30 Hz) and its two harmonics, respectively.

From the above two conditions, the following hypothesis could be generated:

- Null hypothesis H_o : There is no difference in the SNR power between the two conditions for a particular stimulus property (blue-green, red-green, power on and off symbol stimulus, ‘Turn On’ text stimulus, checkerboard stimulus or random dot stimulus) at a specific frequency (7.5 Hz, 10 Hz, 15 Hz, 20 Hz, 24 Hz or 30 Hz).
- Alternate hypothesis H_A : There is a difference in the SNR power between the two conditions for a particular stimulus at a specific frequency.

For each stimulus-frequency condition, pixel-based statistics were applied by randomly shuffling the condition labels of the SNR trials of conditions 1 and 2. This was done for a total of 1000 iterations, each time calculating the z-value and storing only the maximum and minimum values to employ the pixel-based multiple-comparison correction. For a p -value set to 0.05, the statistical threshold was defined as the 2.5th percentile of the smallest values and the 97.5th percentile of the largest values. Using these thresholds, the original z-values between the unshuffled conditions 1 and 2 could be masked such that any SNR value at each channel that has a magnitude greater than the upper threshold or smaller than the lower threshold can be considered as statistically significant, and therefore it can be said that the null hypothesis can be rejected.

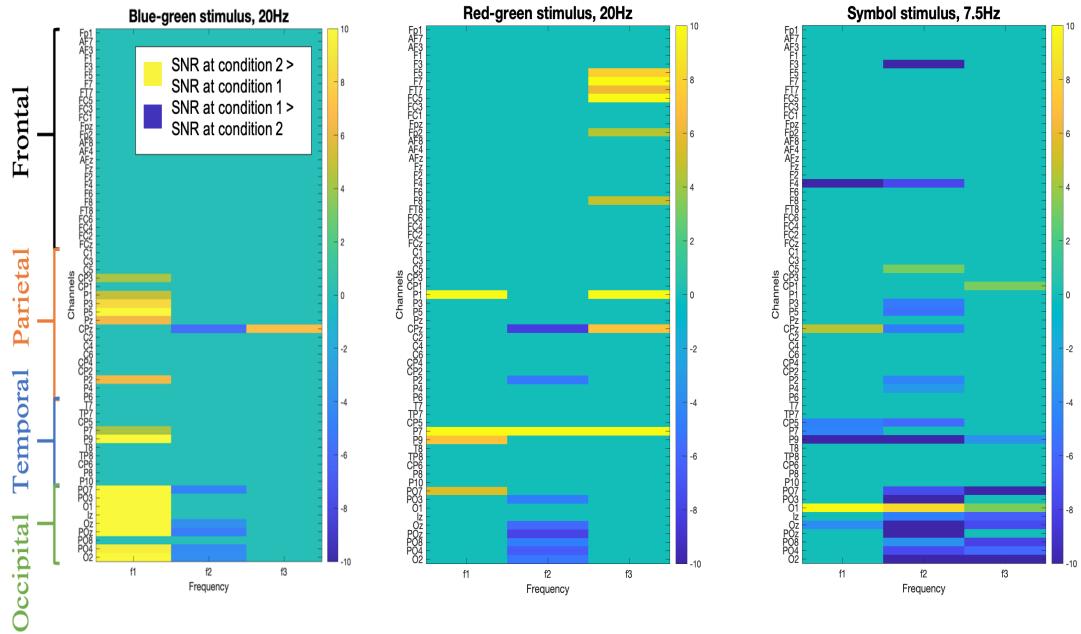
The results after applying permutation-based statistics on each stimulus-frequency condition were visualised by plotting the resulting z-values at the fundamental

frequency (f_1) and two harmonics (f_2 , f_3) at each of the 64 channels which exceed the threshold. Figure 6.6 shows the results for the frequency that obtained the most statistically significant activations for each stimulus. Positive z-values (yellow colour) indicate that the SNR at the stimulus parameter being tested (condition 2) is statistically significantly greater than that of the black-white stimulus (condition 1) and vice versa for negative z-values (dark blue colour), meaning that the SNR at condition 1 is statistically significantly greater than that of condition 2. A colour map was used to illustrate the strength of the difference in SNR, i.e. the brighter the yellow is or the darker the blue colour is, the greater the difference in SNR values. The 64 channels are organised according to the frontal, parietal, temporal and occipital lobes, marked on the left-hand side of Figures 6.6(a) and 6.6(d).

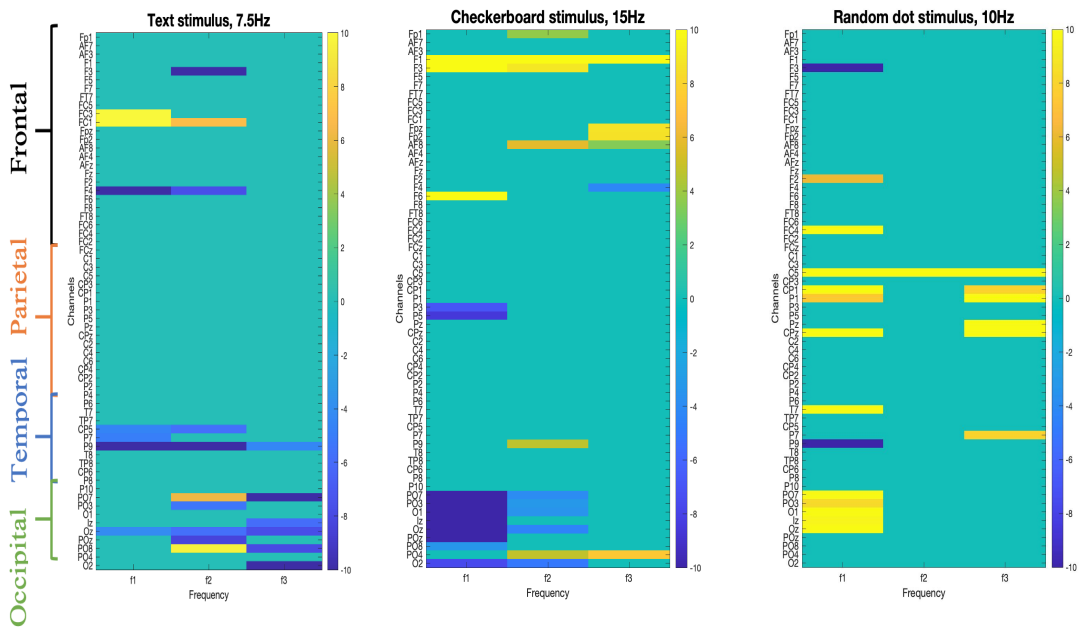
6.6.2.1 Results from Permutation-based Statistics

After analysing the visualisation plots for each stimulus-frequency condition, generalised observations could be made which will be discussed in the following paragraphs. The blue-green stimulus results indicate the strongest observations at the occipital region since for the 10 Hz - 24 Hz frequencies, the SNR at the first harmonic was statistically significantly greater than that of the black-white stimulus. It was also noted that across all frequencies (7.5 Hz - 30 Hz), the blue-green stimulus obtained a statistically significant larger SNR response at the P7 and P9 channels, which are located at the left behind the ear regions. Figure 6.6(a) shows the resulting permutation-based statistics results for the 64 channels for the 20 Hz stimulus, which indicates the clear statistically significant greater SNR values of the blue-green stimulus (shown by the yellow colour), at the occipital, P7 and P9 channels. For this frequency, the SNR at the blue-green stimulus was also statistically significantly higher at some left parietal channels.

Results after applying permutation-based statistics on the red-green stimulus show that the SNR at the red-green stimulus was statistically significantly stronger at the left temporal regions (channels P7 and P9) at the 10 Hz - 20 Hz frequencies. Figure 6.6(b) presents the result for the 20 Hz frequency, showing statistically significantly higher SNR at three harmonics for the P7 channel and one harmonic at the P9 channel. Such figure also shows a statistically significant stronger SNR at the third harmonic for frontal channels, which was also observed for the 30 Hz frequency.



(a) 20 Hz, blue-green stimulus (b) 20 Hz, red-green stimulus (c) 7.5 Hz, Power on and off symbol stimulus



(d) 7.5 Hz, 'Turn On' text stimulus (e) 15 Hz, checkerboard stimulus (f) 10 Hz, random dot stimulus

FIGURE 6.6: Permutation-based statistic results for the frequency that obtained the most statistically significant activations for each stimulus. Yellow labels represent that the SNR values at the tested stimulus condition (condition 2) are statistically significantly greater than the SNR values at the black-white stimulus condition (condition 1). Blue labels indicate that the SNR values at the black-white condition (condition 1) are statistically significantly greater than the SNR values at the tested stimulus condition (condition 2). f_1 , f_2 and f_3 indicate the SNR value at the first, second and third harmonic respectively.

After analysing all the frequencies for the symbol stimulus, it was observed that no consistent channels for the symbol stimulus across the six frequencies have an SNR that is statistically significantly higher than the SNR generated by the black-white stimulus (indicated in the visual plots by the yellow colour). Notable observations could only be made at the occipital region, where the SNR for the black-white stimulus was statistically significantly higher than the SNR generated by the symbol stimulus (indicated in the visual plots by the blue colour) for the 7.5 Hz and 15 Hz - 24 Hz stimuli. This can be seen by the blue labels in Figure 6.6(c), which shows the result for the 7.5 Hz stimulus. In this case, the black-white stimulus was also statistically significantly stronger at some temporal and parietal regions. Like the symbol stimulus, after observing the results for all the frequencies, it was noticed that no consistent channels of the text stimulus across the frequencies obtain an SNR that was statistically significantly higher than the black-white stimulus SNR. However, the black-white stimulus SNR was statistically significantly larger than the text stimulus SNR at the occipital regions for the 7.5 Hz and 15 Hz - 24 Hz stimuli. This can be seen in Figure 6.6(d) by the presence of the blue labels, which shows the result for the 7.5 Hz. Here, the SNR at the black-white stimulus was also statistically significantly stronger at some temporal channels.

The results from all the frequencies for the checkerboard stimulus show that the SNR of the black-white stimulus was statistically significantly higher for the 7.5 Hz - 15 Hz and 24 Hz frequencies at the occipital region. Conversely, the SNR values at the checkerboard stimulus were statistically significantly stronger than the black-white stimulus SNR for frontal channels at 15 Hz - 30 Hz. This observation can be seen for the 15 Hz stimulus in Figure 6.6(e) by the blue labels at the occipital electrodes and the yellow labels at the frontal electrodes. For the random dot stimulus, stronger SNR statistically significant values than the black-white stimulus were observed for the occipital and parietal channels at the 7.5 Hz and 10 Hz stimuli. Figure 6.6(f) presents the results for the 10 Hz stimulus, showing statistically significant results for the random dot stimulus at the occipital regions at the first harmonic and parietal regions at different harmonics. Similar to the checkerboard stimulus, for the 24 Hz and 30 Hz stimulus, the SNR values at frontal electrodes for the random dot stimulus were also statistically significantly stronger than the black-white stimulus SNR.

To summarise, the observations from the permutation-based statistics show that the black-white stimulus SNR was almost always statistically significantly stronger than the SNR values from the symbol and text stimuli. This suggests that such stimuli do not improve the SSVEP response when compared to the control condition. However, the blue-green stimulus is statistically significantly stronger than the black-white stimulus at the occipital region (10 Hz - 24 Hz) and left temporal regions (7.5 Hz - 30 Hz). The SNR at the left temporal regions was also statistically significantly larger than the black-white stimulus for the red-green stimulus (10 Hz - 20 Hz). The random dot stimulus was statistically significantly stronger at occipital and parietal areas for the 7.5 Hz and 10 Hz frequencies. Both the checkerboard and random dot stimuli were statistically significantly higher at frontal areas for the 24 Hz and 30 Hz frequencies. These results are further discussed in Chapter 7.

6.6.3 SNR Topographic Maps

To visualise and better understand how the SNR varies across each stimulus-frequency condition, the average SNR taken across all subjects was plotted on topographic maps. This was done by taking the average SNR across the 10 trials for each stimulus-frequency condition for each subject and subsequently using these results to obtain the average SNR across the six subjects. This was followed by generating the sum of power at the fundamental frequency of the stimulus and its two harmonics. The results of the sum of power at each of the 64 channels were plotted on a topographical 2D EEG map showing the 64 electrode locations. Figure 6.7 shows the average SNR topographic maps obtained for each of the six frequencies for each of the seven stimuli. The colours on the topographic maps indicate the magnitude of the SNR power; the brighter the yellow colour, the larger the SNR is, and hence, the stronger the SSVEP response is over that area.

From the black-white stimulus topographic maps shown in Figure 6.7(a), it can be seen that there are clear high SNR values obtained at the occipital electrodes for the 7.5 Hz - 20 Hz frequencies. The SNR at these frequency ranges decreases at the parietal-occipital and temporal areas and becomes very low at the central-parietal and frontal regions. The SNR value at occipital, temporal and parietal areas, drops for the 24 Hz and 30 Hz frequencies. Interestingly, high SNR values can also be seen in the left temporal areas for the 7.5 Hz frequency only. Similar to the black-white stimulus, the blue-green stimulus topographic maps (shown in Figure

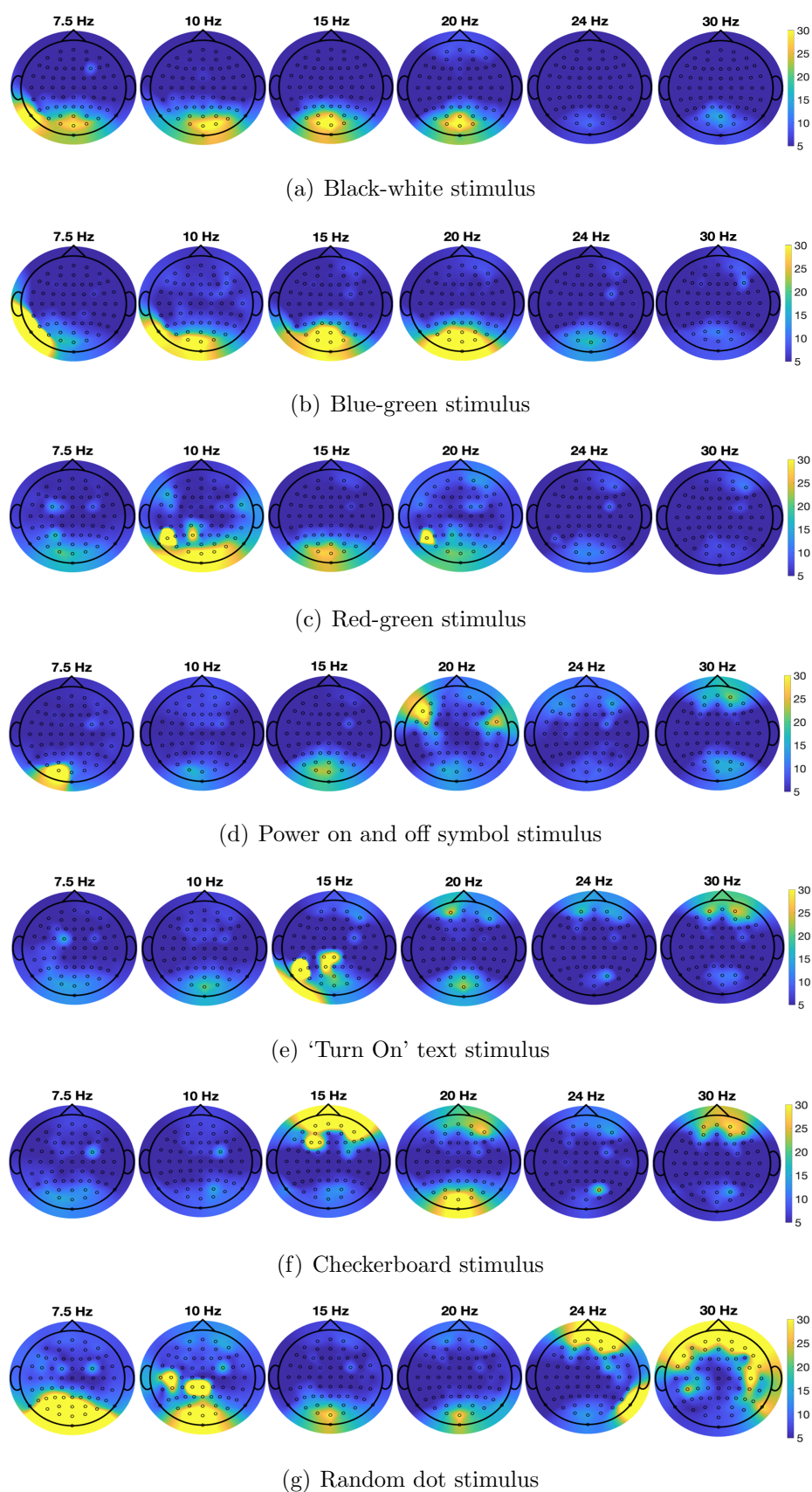


FIGURE 6.7: EEG topographic maps showing the SNR power for the different stimuli at each of the six frequencies.

6.7(b)) also show that the highest SNR was obtained at the occipital areas for the 10 Hz - 20 Hz stimuli. At the 7.5 Hz and 10 Hz frequencies, the SNR at the left behind the ear regions has higher values than the occipital electrodes. Comparing the SNR-activated areas of the blue-green stimulus with the black-white stimulus, it can be observed that the blue-green stimulus obtained a higher SNR in the occipital electrodes for 10 Hz - 24 Hz frequencies and left temporal electrodes at 7.5 Hz - 10 Hz.

The red-green stimulus whose results are seen in Figure 6.7(c), obtained high SNR values at the occipital regions for the 10 Hz and 15 Hz stimuli. Although for the 7.5 Hz and 20 Hz frequencies, the SNR value at the occipital areas is still the highest when compared to the temporal, parietal and frontal areas, the SNR value is decreased when compared to the black-white stimulus. It can also be noticed that for the 10 Hz and 20 Hz frequencies, the SNR value increases for some frontal electrodes. Similar to the blue-green stimulus, the SNR values at the occipital region for the 24 Hz frequency are larger than that of the black-white stimuli. Similar to the black-white and blue-green stimuli, the lowest SNR values at the occipital, temporal and frontal regions were obtained for the 24 Hz and 30 Hz frequencies.

By looking at the SNR topographic maps of the shape stimuli shown in Figures 6.7(d) and 6.7(e), it can be observed that the SNR values at the occipital areas for the 7.5 Hz - 20 Hz stimuli decrease when compared to the results from the colour stimuli. For the power on and off symbol stimulus, an increase in the SNR at frontal areas is observed for the 20 Hz - 30 Hz frequencies and at some of these electrodes, the SNR value is larger than that at the occipital region. For the 'Turn On' text stimulus, high SNR at frontal electrodes was also found for most frequencies (10 Hz - 30 Hz); however for the lowest frequencies 7.5 Hz - 15 Hz the SNR values at the occipital electrodes are greater than that of the frontal electrodes which cannot be said for the 20 Hz - 30 Hz frequencies.

The checkerboard stimulus topographic maps show that high SNR values are present at frontal areas across all frequencies when compared to the colour stimuli, particularly the magnitude increases for the 15 Hz - 30 Hz frequencies. The SNR value at the occipital areas is higher than that found at the frontal areas for only the 7.5 Hz, 10 Hz and 20 Hz frequencies. Like the checkerboard stimulus, high

SNR values for the random dot stimulus at the frontal electrodes are found at all frequencies, becoming more dominant for the 24 Hz and 30 Hz frequencies. The SNR values at the occipital lobe are greater than that present at the frontal lobe for the 7.5 Hz - 20 Hz frequencies, while the contrary can be said for the 24 Hz and 30 Hz frequencies. Interestingly, a high SNR at the left behind the ear and parietal regions can be observed for the 7.5 Hz and 10 Hz frequency.

The SNR topographic maps indicate that high SNR values can be obtained from the occipital lobe for all the stimuli properties tested for the 7.5 Hz - 20 Hz, suggesting that this region is good for detecting strong SSVEPs to control SSVEP-based BCIs. The SNR magnitude at the occipital, temporal and parietal regions was also observed to significantly drop for the 24 Hz and 30 Hz for all the stimuli. When compared to the black-white stimulus, higher SNR amplitudes were observed in the occipital and temporal areas for the blue-green and red-green stimuli, the frontal electrodes for the symbol stimuli and texture stimuli, and the occipital, temporal and parietal areas for the random-dot stimulus. These results are evaluated further using the z-score analysis which is described in the next section.

6.6.4 Z-score Analysis

To better interpret the results from the SNR topographic maps the z-score was used. This measure has an advantage over the SNR as it defines a threshold to identify whether the SSVEP response is significant or otherwise. Hence, this measure was used to observe the SSVEP response at different channels. Z-score analysis offers a notable advantage over permutation-based statistics allowing for the visualisation of z-score values across the entire frequency spectrum, facilitating direct comparisons between different frequencies. In contrast, permutation-based statistics determine significance only at the fundamental frequency and its two harmonics, restricting the ability to compare z-score values across the entire frequency range. The higher the z-score value at the stimulus' flickering frequency and harmonics, the stronger is the evoked SSVEP response by that stimulus-frequency condition. The z-score was calculated by using the average PSD of the 10 trials for each stimulus-frequency condition for each subject. The average z-score across the six subjects was then calculated from these values.

6.6.4.1 Analysis of the SNR Topographic Maps Using Z-score

The z-score was first observed at the four major areas of the brain (occipital, parietal, temporal, frontal areas), to see how this corresponds to the yellow and blue colours depicted by the topographic maps which describe the SNR values at different electrode positions. Consequently, the z-score at the Oz, T7, Cpz and Fpz electrodes for the 15 Hz black-white stimulus is presented in Figure 6.8 as an example to explain how the results from the z-score were interpreted. From this figure, it can be noticed that the z-score exceeds the threshold of 2 at the Oz channel for three harmonics (15 Hz, 30 Hz, 45 Hz) which in the SNR topographic maps has a yellow colour. The z-score magnitude at the fundamental frequency and harmonics decreases drastically at the Cpz electrode, and the threshold is not exceeded. For the T7 and Fpz electrodes, the z-score at the fundamental and harmonic frequencies did not exceed the threshold, suggesting that such channels cannot evoke a statistically significant SSVEP response.

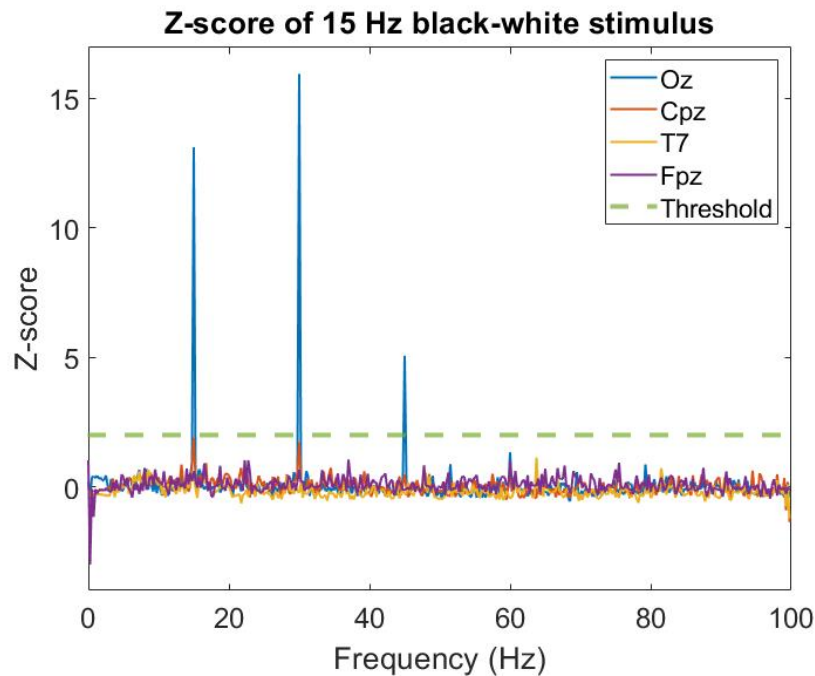


FIGURE 6.8: Z-score evaluated at the Oz, T7, Cpz and Fpz channels for the 15 Hz black-white stimulus.

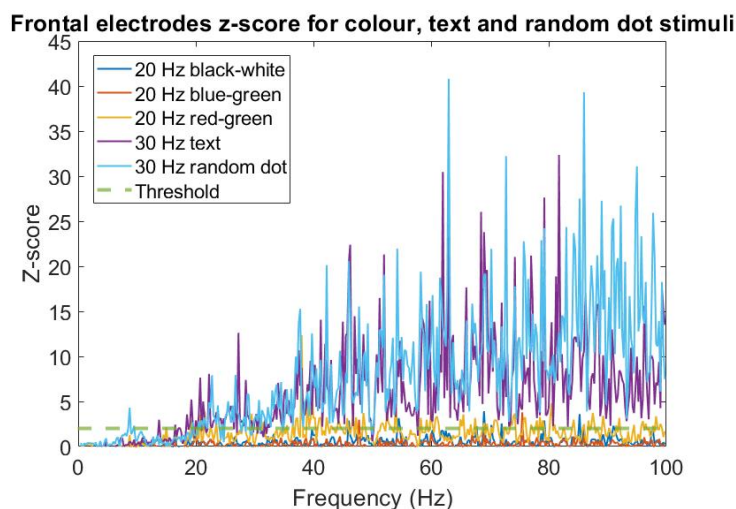
From the SNR topographic maps of Figure 6.7 it was observed that the shape (symbol and text stimuli) and texture (checkerboard and random dot stimuli) stimuli have relatively high SNR values at some frontal electrodes at different

frequencies. Thus, to further understand the magnitude of this SNR and how it compares to the different stimuli tested, the z-score analysis was decided to be used. Particularly, the z-score of the frontal electrode that obtained the highest SNR magnitudes for each stimulus as seen from Figure 6.7 was plotted. These electrodes were the Fpz at 20 Hz for the black-white and blue-green stimuli whose SNR is shown in Figure 6.7(a) and Figure 6.7(b) respectively, electrode Fp2 at 20 Hz for the red-green stimulus shown in Figure 6.7(c), electrode F7 at 20 Hz for the symbol stimulus shown in Figure 6.7(d), channel Fp2 at 30 Hz for the text stimulus shown in Figure 6.7(e), electrode Fpz at 15 Hz for the checkerboard stimulus shown in Figure 6.7(f) and electrode Fpz at 30 Hz for the random dot stimulus shown in Figure 6.7(g). The z-score at these channels is plotted in Figure 6.9.

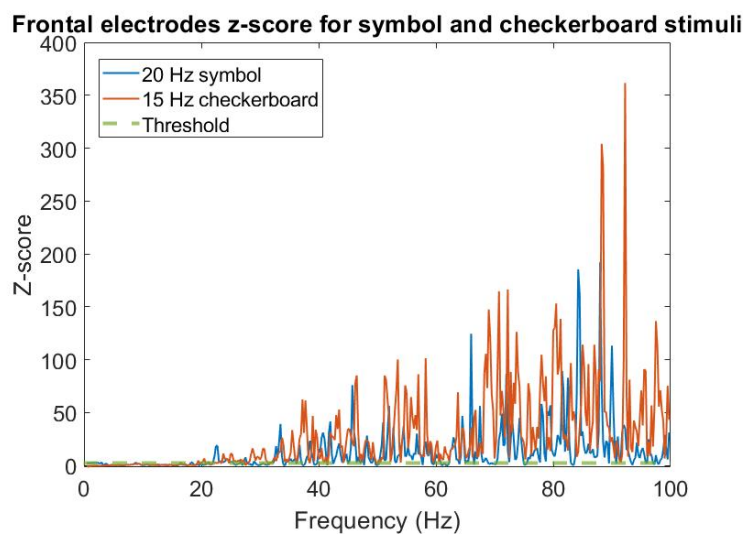
From these two plots, it can be seen that the activity at the frontal channels at all stimuli is not harmonically related since no distinct peaks can be observed at the fundamental frequency and harmonics. This suggests that the SSVEP response is not elicited in frontal areas of the brain. This observation will be further discussed in Chapter 7. The z-score shown in Figure 6.9(a) and Figure 6.9(b) highlights the difference in the magnitudes of the z-score. This is because the z-score amplitudes for the symbol and checkerboard stimuli shown in Figure 6.9(b) are very high when compared to the z-scores of the black-white, blue-green, red-green, text and random dot stimuli displayed in Figure 6.9(a). Such results suggest that stronger frontal activity is present for the symbol and checkerboard stimuli.

The SNR topographic maps in Figure 6.7 show that the SNR magnitude activity at the frontal electrodes varies with the different frequency values (7.5 Hz, 10 Hz, 15 Hz, 20 Hz, 24 Hz, 30 Hz). This can particularly be observed in the symbol and text stimuli, where the 20 Hz - 30 Hz frequencies seem to have higher frontal activity than the lower 7.5 Hz - 15 Hz frequencies. The z-score was therefore used to analyse the activity at the frontal channels across all frequencies for each stimulus. Figure 6.10 shows the z-score value at the Fpz channel for the 10 Hz, 24 Hz, and 30 Hz frequencies for the random dot stimulus. Here, it can be seen that the z-score at this channel is very noisy for all of the three frequencies whose magnitude increases greatly above 50 Hz. However, when looking at the topographic map shown in Figure 6.7(g), the SNR values at the Fpz channel for the 24 Hz and 30 Hz, are significantly higher than that at 10 Hz. One reason for this is that the sum of the

powers at the three harmonics for low frequencies does not exceed 50 Hz, thus, the high SNR magnitudes observed at frequencies beyond 50 Hz at the frontal electrodes are not captured. Therefore, the high frontal activity captured by some channels at the frontal electrodes for some stimuli, although not visible in the SNR topographic maps, is present across all the frequencies.



(a) Z-score at the Fpz channel for the black-white, blue-green and random-dot stimuli and the Fp2 channel for the red-green and text stimuli.



(b) Z-score at the F7 channel for the symbol stimulus and Fpz for the checkerboard stimulus.

FIGURE 6.9: Z-score plots for the frontal electrodes that obtained the highest SNR values for each stimulus.

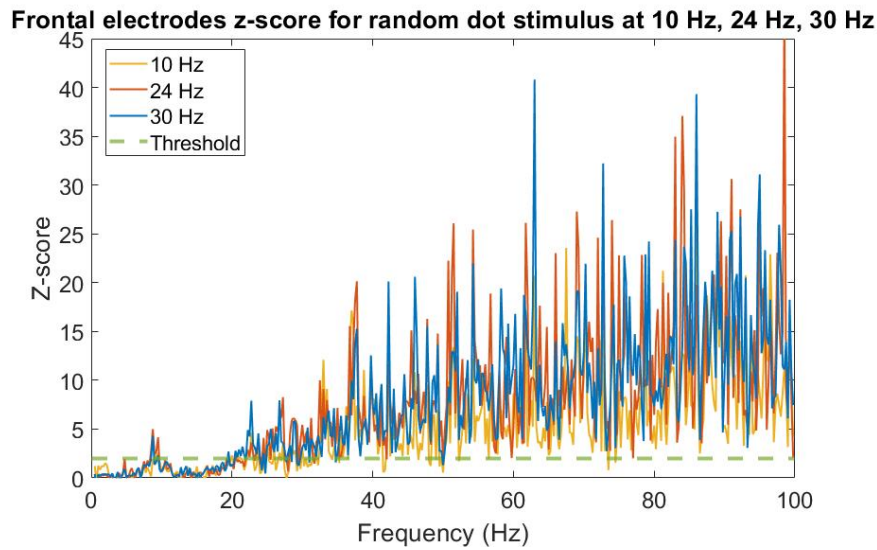


FIGURE 6.10: Z-score plots for the Fpz channel from the random dot stimulus for the 10 Hz, 24 Hz and 30 Hz frequencies.

6.6.4.2 Analysis of Stimuli Properties Using Z-score

The results from the SNR topographic maps shown in Figure 6.7 indicate that some stimuli properties may lead to higher SNR values in the occipital, behind the ear/temporal and parietal regions when compared to the black-white stimulus. The z-score at these stimuli-frequency conditions was used to compare the strength of the SSVEP generated to that of the black-white stimulus, and it was used to identify if the SSVEP response is statistically significant which was the case when exceeding the threshold of 2.

From the SNR topographic maps in Figure 6.7, high SNRs in the occipital areas (channels PO7, PO3, O1, POz, Oz, Iz, O2, PO4, PO8) were seen to be generated by the blue-green, red-green and random dot stimuli. In fact, through the z-score it was confirmed that occipital channels at the 10 Hz - 24 Hz blue-green stimulus, 10 Hz and 24 Hz red-green stimulus, and 7.5 Hz and 10 Hz random dot stimulus obtained a z-score that exceeds the threshold and a higher z-score than the black-white stimulus. This suggests that such stimuli conditions and frequencies evoke a higher SSVEP response than the standard black-white stimulus. Furthermore, it was determined that at 10 Hz, the random dot stimulus obtains the highest SNR when compared to the blue-green and red-green stimulus, and at 24 Hz the red-green stimulus obtains the highest SNR magnitude when compared to the blue-green stimulus. Figure 6.11(a) shows the average z-score for the 20 Hz blue-green

stimulus and the 20 Hz black-white stimulus at the Oz channel, where it can be observed that the magnitude of the SSVEP at the fundamental frequency (20 Hz) of the blue-green stimulus is much larger than that obtained by the black-white stimulus. The example shown through this figure highlights how the z-score magnitude at this stimulus-frequency condition exceeds that of the black-white stimulus.

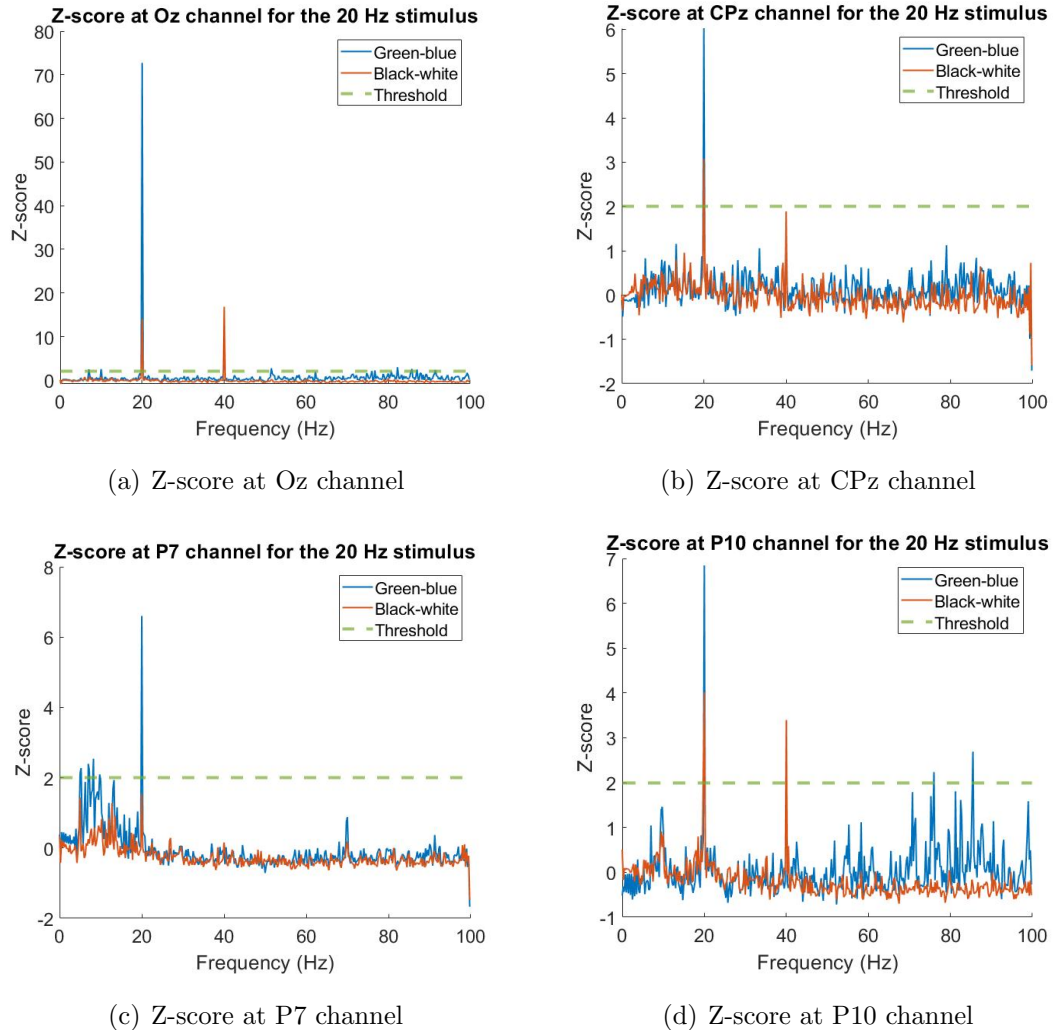


FIGURE 6.11: Z-score generated by the 20 Hz blue-green stimulus compared with the 20 Hz black-white stimulus at the Oz, CPz, P7 and P10 channels. The blue and orange plots show the result from the blue-green stimulus and the black-white stimulus, respectively. The threshold of 2 is marked by a green dotted line.

From Figure 6.7 it is less obvious which stimuli-frequency conditions generate a higher SNR response in the central-parietal areas (channels CP3, CP1, CPz, CP2, CP4) when compared to the black-white stimulus, since the parietal electrodes across all stimuli and frequencies did not obtain the highest SNR values as indicated by the colour in the SNR topographic maps at these areas which is never yellow. Thus, the z-score analysis was again used to analyse the SSVEP strength in these areas. For the checkerboard and text stimuli, it was noticed that the z-score does not always exceed the threshold of 2, indicating that the SSVEP response is not strong at the parietal region for these stimuli. Furthermore, the z-score magnitudes of these stimuli compared to the black-white stimulus were similar. However, the z-score amplitudes exceeded the threshold of 2 and obtained a value greater than the z-score generated by the black-white stimulus for the 15 Hz and 20 Hz blue-green stimuli, and 7.5 Hz and 10 Hz random dot stimuli. Figure 6.11(b) shows the z-score obtained by the 20 Hz blue-green stimulus and black-white stimulus at the CPz channel. Such result shows that the magnitude of the z-score amplitude of the blue-green stimulus at the first harmonic is twice that of the black-white stimulus, indicating that the SSVEP response is stronger at the blue-green stimulus.

Z-score analysis was also performed on the left and right, temporal and behind the ear areas (channels TP7, CP5, P5, P7, P9, TP8, CP6, P6, P8, P10). Significant z-score results at the fundamental frequencies and harmonics for both left and right areas, that exceed the magnitudes obtained for the black-white stimulus were obtained at: 20 Hz blue-green stimulus, 7.5 Hz, 15 Hz and 20 Hz red-green stimulus, 20 Hz checkerboard stimulus and 7.5 Hz random dot stimulus. Moreover, from these results it could be noted that at 7.5 Hz the random dot stimulus obtains the highest SNR when compared to the red-green stimulus, and the blue-green stimulus obtained the highest SNR at 20 Hz when compared to the red-green and checkerboard stimuli. The z-score at the 20 Hz blue-green stimulus for the P7 channel (left behind the ear channel) and P10 channel (right behind the ear channel) are shown in Figures 6.11(c) and 6.11(d) respectively. Both results show that the z-score magnitude at the fundamental frequency exceeds the threshold of 2 and is larger than the z-score generated by the black-white stimulus. Interestingly, the left temporal areas also obtained a high z-score value that exceeded the black-white stimulus for the 15 Hz random stimulus, which was not observed in the right temporal areas. Conversely, the right temporal areas obtained a higher z-score than

the black-white stimulus for the 10 Hz red-green stimulus which was not observed in the left temporal areas. Apart from these specific stimuli and frequencies, the magnitude of the power of the z-score from both left and right, temporal and behind the ear areas was similar and overall neither side obtained a higher power than the other.

To summarise, from the z-score results it was determined that certain stimuli and frequency parameters do obtain a statistically significant SSVEP response and a higher z-score (which indicates a stronger SSVEP) when compared to the black-white stimulus. Particularly, the blue-green stimulus consistently obtained a higher SSVEP response across the occipital, parietal and temporal regions at the 20 Hz frequency. High SSVEP activations by the blue-green stimulus at the 10 Hz - 24 Hz frequencies were also obtained across the occipital area. The red-green stimulus produces higher SSVEP responses at occipital areas for 10 Hz and 24 Hz and for temporal areas at 7.5 Hz, 15 Hz, 20 Hz. Finally, the random dot stimulus consistently obtained a higher SSVEP response across the occipital, parietal and temporal areas at the 7.5 Hz frequency. The 10 Hz frequency for this stimulus also obtained a high SSVEP response at the occipital and temporal areas.

6.7 Chapter Summary

This chapter describes the main aims of the EEG analysis and gives a description of the hardware and software, and the procedure used to carry out the EEG data recording sessions from six subjects. This was followed by presenting the techniques used to preprocess the raw EEG data and analyse the SSVEP response using the PSD, SNR, z-score and permutation-based statistics techniques.

The permutation pixel-based statistics were performed to find any statistically significant values of the SNR obtained by the different stimuli when compared to the black-white stimulus. Signal-to-noise ratio (SNR) topographic maps showing the average SNR across all subjects at each of the 64 electrodes for every stimulus-frequency condition were also presented. Finally, z-score plots were used to analyse and understand better the results from the SNR topographic maps.

Both the results from the permutation-based statistics and z-score plots show that there is a stronger frontal activation generated by the checkerboard and

random dot stimuli when compared to the black-white stimulus. Both techniques also show that the power on and off symbol and ‘Turn On’ text stimuli do not obtain any significantly higher SSVEP activations when compared to the black-white stimulus. Results from the permutation-based statistics show statistically significantly stronger SNR activations at the occipital (10 Hz - 24 Hz) and left temporal areas (7.5 Hz - 30 Hz) for the blue-green stimulus when compared to the black-white stimulus. These results are confirmed by the SNR and z-score analysis which additionally show stronger magnitudes at the right temporal areas and parietal areas for this stimulus when compared to the black-white stimulus. Results from the permutation-based statistics also show statistically significant higher activations at the left temporal areas for the red-green stimulus, which were also seen when plotting the z-score values. In addition, z-score results show stronger SNR amplitudes than the black-white stimulus at occipital areas and the right temporal areas. Finally, both permutation-based statistics and the z-score analysis confirm that the random dot stimulus SNR is statistically significantly higher at the 7.5 Hz and 10 Hz when compared to the black-white stimulus SNR at the occipital and parietal regions, obtaining the highest SNR values across all the stimuli. Moreover, the z-score analysis shows that the random dot stimulus is also significant at temporal areas.

The next chapter discusses the results obtained from both the fMRI and EEG studies. This chapter examines how the results obtained compare to the existing findings from the literature, discusses any significant and similar findings obtained from both the fMRI and EEG studies and highlights any relevant observations that were concluded from this project.

Chapter 7

Discussion

7.1 Introduction

The outcome of this research has provided insights into the brain response when a subject is presented with repetitive visual stimuli (RVS) with varying characteristics that are typical of SSVEP-based BCIs, using the functional magnetic resonance imaging (fMRI) and electroencephalography (EEG) modalities. This chapter provides a reflection on the research process and discusses the results that were presented in the previous chapters. The limitations and potential consequences of the design are discussed, as well as the implications for the interpretation of the results. The chapter ends with recommendations for future research.

7.2 Project Main Aims

The primary aim of this project was to conduct a separate fMRI and EEG study to analyse the brain's response when presenting the subjects with flickering stimuli of varying parameters. Through this, the cortical brain regions activated during an SSVEP and the location of SSVEPs on the scalp could be analysed. Moreover, any stimuli properties that can increase the SSVEP amplitude at different brain locations could be identified. Brain activity related to SSVEPs that can be robustly captured from non-occipital regions can provide a practical way forward to BCIs.

Seven different stimuli properties were tested in both the fMRI and EEG studies. These were divided into three categories: colour stimuli (black-white, blue-green, red-green stimuli), shape stimuli (symbol and text stimuli) and texture stimuli

(checkerboard and random dot map stimuli). Each stimulus was presented to the subjects via an LCD screen for several trials, flickering at six different frequencies: 7.5 Hz, 10 Hz, 15 Hz, 20 Hz, 24 Hz, 30 Hz. The black-white stimulus was considered as the control stimulus since this stimulus is most commonly used in SSVEP-based BCIs. The brain response to the other colour stimuli, and shape and texture stimuli was compared to that of the control stimulus to study any differences in the SSVEP response. To the best of our knowledge, no fMRI study has been conducted on the brain response to RVS having different properties, and current EEG studies that investigate stimuli properties, use LEDs to render the RVS and present conflicting results. This project also had the objective to design and pioneer a functional MRI setup and experimental protocol to record MRI data from the University of Malta's MRI scanner - it is noteworthy that through this project, the MRI scanner was set up to acquire functional MRI data and this study represents the first functional MRI study carried out locally.

7.3 fMRI Study

After organising and preprocessing the recorded fMRI data from human subjects, the general linear model (GLM) statistical algorithm was applied to obtain z-score values that describe the effect on the blood oxygenation level dependent (BOLD) signal in each voxel during the stimulation period when compared to the rest period. Thus, a higher z-score value indicates a stronger BOLD response, as this signifies that the BOLD signal at that voxel is highly correlated to the predicted hemodynamic response function (HRF) response for the stimulus flickering at a particular frequency during the stimulation period when compared to the rest period. A strong BOLD signal during a stimulation period is related to an increase in neural activity and demand for oxygen supply which signifies that the brain response is responding to the repetitive visual flicker [76]. Voxels whose absolute z-score values are greater than the threshold of 1.5 ($|z| > 1.5$) were considered to be “active” voxels for that component.

In order to identify which areas of the brain had the highest z-score values, and therefore the strongest BOLD response, the most frequent areas where the maximum z-value voxel was located across all subjects and frequencies for every stimulus was analysed. This part of the study provides an in-depth analysis on the most

frequently activated cortical regions in the brain for each subject, which was presented using brain visual maps. The results indicate that the occipital lobe (lateral occipital cortex and lingual gyrus) is the most frequent area exhibiting the maximum z-value voxel across all subjects, stimuli and frequencies. This suggests that voxels in the occipital lobe activate the strongest BOLD response during a stimulation period. Statistically significant activations in the parietal lobe (precuneus cortex and postcentral gyrus) were also observed in four subjects when exposed to the three colour stimuli, the random dot stimulus and the power on and off stimulus. None of the maximum z-value voxels were frequently located in the frontal regions, which suggests that frontal voxels do not evoke a strong BOLD response during a stimulation period when compared to the other lobes. This finding agrees with previous literature by Hillyard et al. [76], Di Russo et al.[78], Sammer et al. [121] and Itthipuripat et al.[51] that used a black-white flickering stimulus to evoke SSVEPs, which also concluded that the most significant and strongest activations were obtained at the occipital lobe that occupies the primary visual cortex.

The z-score values and how they vary with the different areas and frequencies were further analysed in Section 5.3.3. These results also highlight the strong BOLD response in the occipital lobe. The occipital lobe showed the highest z-values for blue-green, symbol, text, checkerboard, and random dot stimuli across a wide frequency range (7.5 Hz - 24 Hz). This contradicts Vij et al.'s [131] findings, which conclude that significant BOLD activations are found in the 1 Hz - 10Hz frequency range only, whilst this study reveals significant BOLD activations at a wider range of frequencies 7.5 Hz - 24 Hz. The power on and off symbol and random dot stimuli particularly had the highest z-scores (> 10) in this frequency range. At 30 Hz, the occipital lobe exhibited the lowest z-score, indicating lower responses at higher frequencies. This contradicts Pan et al.'s [80] claims that there is no statistical difference in the strength of the BOLD response in the visual cortex (occipital lobe) between 7 Hz and 31 Hz stimuli.

The black-white and red-green stimuli differed from the other stimuli. The black-white stimulus led to the frontal lobe achieving the highest z-scores for the 7.5 Hz - 15 Hz range, followed closely by the occipital lobe with slightly lower z-scores. No distinct patterns emerged in the z-scores for the red-green stimuli, as all four areas displayed similar values. Notably, the z-scores for black-white and red-blue stimuli

were consistently low, measuring < 6.3 and < 5.8 , respectively, compared to the other stimuli. This result suggests that these two stimuli have a weaker BOLD response when compared to the other five stimuli.

The z-score value obtained by the different stimuli was compared to the z-score value from the black-white stimulus. It was determined that the ideal frequencies to obtain a strong BOLD response vary between the stimulus and the area in which it is mostly activated. The following list categorises the frequencies into low, mid-range, and high, and assigns the stimuli parameters that obtain a stronger SSVEP response than the black-white stimulus. The 30 Hz frequency was not considered, as no stimulus obtained a stronger SSVEP response at this frequency than the black-white stimulus at the different regions of the brain. Activations in the frontal areas were also discarded in these results since as will be discussed in subsequent paragraphs, the BOLD responses in these areas are most likely not associated with SSVEPs.

- **Low frequencies [7.5 Hz and 10 Hz]:** blue-green (occipital, temporal), symbol (occipital, temporal, parietal), text (occipital, parietal), checkerboard (occipital, parietal), random dot (occipital, temporal, parietal).
- **Mid-range frequencies [15 Hz and 20 Hz]:** blue-green (occipital, temporal), symbol (occipital, temporal, parietal), text (occipital), checkerboard (occipital), random dot (occipital, temporal, parietal).
- **High frequency [24 Hz]:** blue-green (occipital), symbol (occipital), text (occipital), checkerboard (occipital), random dot (occipital, parietal).

When observing the number of activated voxels in the occipital, temporal, parietal and frontal areas, interesting results were observed. This is because, for three out of the six subjects, the parietal and frontal lobes had the highest number of activated voxels for all the stimuli at any frequency. This result suggests that although the strongest activated voxels were obtained in the occipital lobe (as indicated by the z-score values), voxels in the parietal and frontal lobes are still activated whenever RVS are displayed to the subjects. The fMRI studies by Ji et al. [122], Pan et al. [80], and Bayram et al. [79] also found some weaker activations in parietal and frontal cortices which is in line with this study.

It is difficult to give a simple explanation for the activations of the parietal and frontal regions during steady-state visual stimulation, but a number of studies have found that the SSVEP responses in frontal electrodes are responsive to executive function and working memory tasks [213–215]. These tasks have typically been investigated by superimposing the task-related stimuli on a sinusoidally modulated light at a frequency of 13 Hz. Further research is required to determine how these regions interact with the visual regions and whether higher stimulation frequencies can produce oscillations at the stimulation frequency or its sub-harmonics in these areas. Nonetheless, given the findings, a sub-sampling of the visual information in higher areas may be anticipated [216]. The subjects' self-instructed attempts to judge the stimulation rate or a self-instructed working memory condition to anticipate the end of the flicker period, which was constant throughout the entire experiment, may have had an impact on the activation of these areas during the passive visual stimulation condition in the current study.

To better understand if the activations in the parietal and frontal lobes are related to SSVEPs, the results from the EEG study at these areas were analysed. An SSVEP is a periodic response to a visual stimulus flickering at a specific frequency, and it appears in the signal-to-noise ratio (SNR) as a rise in amplitude at the fundamental frequency and its harmonics. Thus, by evaluating the SNR, the presence of any SSVEPs in the EEG data can be detected by observing harmonically related magnitudes at the harmonics of the stimulus frequency. The higher the magnitude of the SNR, the stronger the SSVEP response in the brain is. The average SNR across all subjects at each of the 64 channels when the subjects were presented with the 15 Hz black-white stimulus was visualised on a matrix plot shown in Figure 7.1. Yellow and bright light blue areas show high SNR values, while dark blue areas represent low SNR magnitudes. From this plot, it could be seen that high SNR values at the fundamental frequency (15 Hz) and two harmonics can be observed at occipital electrodes, and some parietal and temporal electrodes. While there is observable activation in the frontal areas and central-frontal areas (which are considered to be part of the parietal region in the fMRI study) associated with light blue regions, there is a lack of clear high SNR values at both the fundamental frequency and its harmonics. This suggests that either frontal and central-frontal electrodes do not exhibit SSVEPs or the presence of SSVEPs in this region is minimal and not distinctly discernible. This observation was seen at all the other

frequencies used in this project (7.5 Hz, 10 Hz, 20, 24 Hz, 30 Hz).

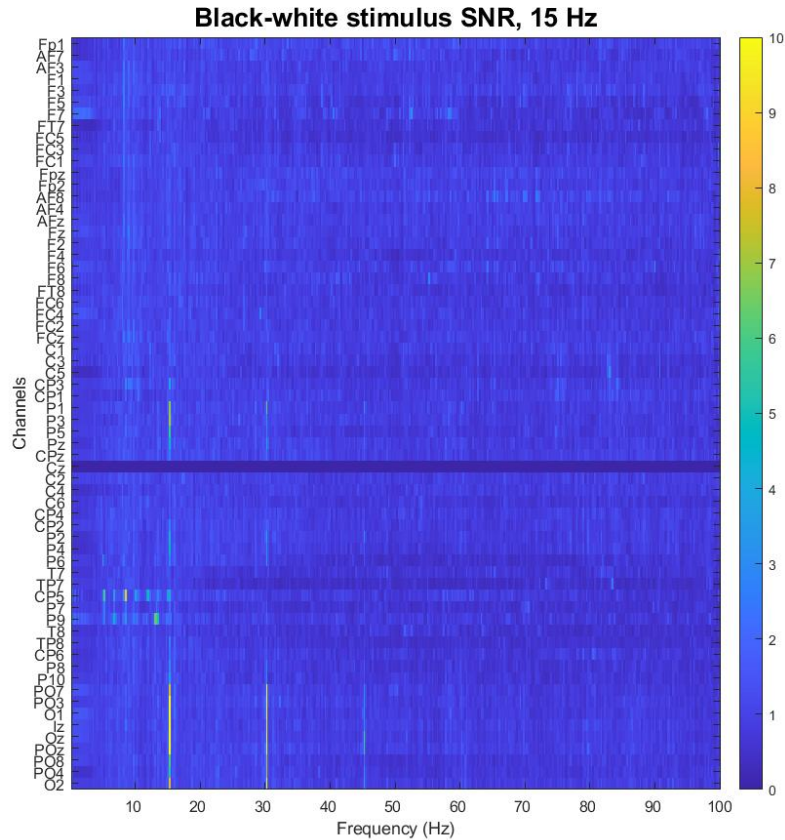


FIGURE 7.1: Average SNR across the six subjects at the 64 channels located across the whole scalp.

To further analyse this observation, the z-score plots for frontal and central-frontal electrodes were analysed to understand if there is any harmonically related content at the fundamental frequency and its harmonics, and if this is statistically significantly stronger in the case SSVEPs are present ($|z| > 2$). Figure 7.2 shows the average z-score across the six subjects for the Fpz, F3, and F4 electrodes during the 10 Hz black-white stimulation period. These electrodes and stimulus-frequency condition were chosen as an example and such result can be extended to other frontal and central-frontal electrodes, and stimulus-frequency conditions. Statistically significant higher activity ($|z| > 2$) was found at the F4 channel at the 8.75 Hz frequency. However, this activity does not correspond to the fundamental frequency or any of its harmonics. This suggests that while significant brain activity was present in this area, SSVEPs were not detected. This outcome may help elucidate why a substantial number of voxels were activated in the parietal and frontal

regions during the fMRI study. Essentially, while statistically significantly stronger data was observed, it may not always be directly related to an SSVEP response during visual stimulation.

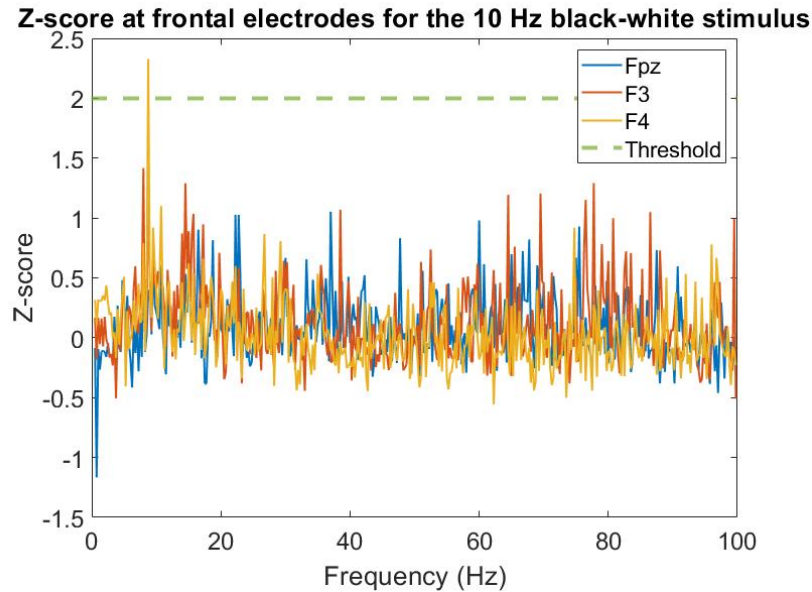


FIGURE 7.2: Average z-score across the six subjects at the Fpz, F3 and F4 electrodes for the 10 Hz black-white stimulus.

While previous fMRI research has focused on black-white stimuli to evoke SSVEPs, this fMRI study has looked at different stimuli properties and their effect on the SSVEP response. Overall, it can be said that the strongest BOLD responses to RVS were found in the occipital lobe. However, from all the tested stimuli, the symbol and random dot stimuli obtained the strongest z-score values in these areas for the 7.5 Hz - 24 Hz frequency range.

7.4 EEG Study

The EEG study provided a way to observe the SSVEP response on the scalp. Permutation-based statistics for multiple comparisons was used to compare statistically significant average SNR values at each fundamental frequency and its harmonics evoked by the six different stimuli parameters with the black-white stimulus. The results obtained show that the SNR evoked by the black-white stimulus at the occipital, temporal and parietal lobe was always greater than the SNR of the power on and off symbol and text stimulus at any frequency. This indicates that

using these proposed stimuli will not evoke a stronger SSVEP response. However, a statistically significant stronger response than the black-white was evoked in the occipital area by the blue-green (10 Hz - 24 Hz) and random dot (7.5 Hz and 10 Hz) stimuli, in the left temporal areas by the blue-green (7.5 Hz - 30 Hz) and red-green (10 Hz - 20 Hz) stimuli, and in frontal areas by the checkerboard and random dot (24 Hz and 30 Hz) stimuli. Although these results indicate that higher frequencies (24 Hz and 30 Hz) for these stimuli can elicit a stronger SNR response than the black-white stimulus at the frontal regions of the brain. One limitation of evaluating the permutation-based statistics at the fundamental frequencies and harmonics is that it does not reveal any information about the nature of the EEG signal and whether the EEG data is harmonically related or not, which would indicate that SSVEPs are present. This was shown in the SNR evaluated in Section 7.3 and was confirmed in the z-score analysis discussed in Chapter 6, that the frontal areas do not contain any SSVEP activity or it is very weak.

The SNR topographic maps offer a clearer depiction of SNR power distribution at each electrode position, aiding in understanding its variations across frequencies for different stimuli. These maps were generated by summing the average SNR values across the six subjects at the fundamental frequency and its two subsequent harmonics. The insights gained from the SNR topographic maps were further assessed using z-scores, which provide an advantage over SNR by indicating whether the response is statistically significant or otherwise.

The SNR topographic maps highlight that the high SNR values were always consistent at the occipital lobe for all frequencies up to the 20 Hz. The z-score plots also show the highest z-score values at the fundamental frequency and its harmonics for the electrodes at the occipital lobe when compared to the other brain regions. This suggests that the occipital lobe, which comprises the visual cortex, locates the highest SSVEP responses. It is also clear that the SNR at the occipital lobe reduces at high frequencies (24 Hz and 30 Hz), suggesting that this frequency range should be avoided in implementing efficient SSVEP-based BCI systems.

Upon examination of the z-score plots, it is evident that the SNR power at the occipital lobe for blue-green (10 Hz - 24 Hz), red-green (10 Hz and 24 Hz), and random dot (7.5 Hz and 10 Hz) stimuli exceeded that of the black-white stimulus.

This aligns with the conclusions drawn from permutation-based statistics, which also confirm the statistical significance of the responses to blue-green and random dot stimuli. These findings contradict the conclusions reached by Bieger et al. [112] and Cao et al. [106], who asserted that the black-white stimulus elicits a superior SSVEP response compared to any coloured RVS in the occipital lobe.

The z-score analysis shows that stronger SSVEP activations than the black-white stimulus were also observed in the temporal areas for the blue-green (20 Hz), red-green (7.5 Hz - 20 Hz), checkerboard (20 Hz) and random dot (7.5 Hz) stimuli. The SNR and z-score results build on the existing evidence of the study by Floriano et al. [110], which concludes that the red-green stimulus elicits the highest SSVEP amplitude for the lower (< 15 Hz) and mid-frequency range (15 Hz - 25 Hz), and the blue-green for the highest frequency range (30 Hz - 40 Hz) in the temporal areas. However, in this study, the red-green stimulus response was superior up to the 20 Hz and not up to 25 Hz as determined by Floriano et al.

The 20 Hz checkerboard stimulus elicited stronger SSVEP responses than the black-white stimulus which supports the evidence by Ming et al. [143] and Waytowich et al. [144] but contradicts Zerafa et al. [111]. This experiment also provides new insights on the random dot stimulus, which, to the best of our knowledge has not been implemented in an EEG SSVEP-based BCI, since its performance at 7.5 Hz and 10 Hz is superior over the black-white stimulus and the other stimuli tested at the occipital, parietal and temporal areas.

The above permutation-based statistics, SNR and z-score findings were combined to analyse the stimuli conditions at the low, mid-range and high frequencies which provide a stronger response than the black-white stimulus:

- **Low frequencies [7.5 Hz and 10 Hz]:** random dot (occipital, parietal, temporal), red-green (temporal).
- **Mid-range frequencies [15 Hz and 20 Hz]:** blue-green (occipital, parietal, temporal), red-green (occipital, temporal), checkerboard (temporal).
- **High frequencies [24 Hz]:** blue-green (occipital), red-green (occipital).

7.5 Combining the fMRI and EEG Results

From both the fMRI and EEG study it is clear that the strongest responses in the brain to any RVS characteristic is located at the occipital lobe. This was observed in five out of the seven stimuli tested in the fMRI study up to the frequency of 24 Hz. This was also observed in the EEG study for all stimuli up to 20 Hz given that the high SNR obtained in the frontal areas for some stimuli was shown not to be related to the SSVEPs after conducting a z-score analysis. Thus, from both studies, it can be concluded that the 30 Hz frequency is not suitable to provide a statistically significantly stronger SSVEP whereas low (7.5 Hz and 10 Hz) and mid-range (15 Hz and 20 Hz) frequencies generate stronger SSVEPs. In particular, mid-range frequencies are preferred since the 15 Hz - 20 Hz stimulation band is less likely to give rise to epileptic seizures [217], false positives due to alpha rhythm (8 Hz – 12 Hz) [148, 218], migraine headaches [219], and visual fatigue [106].

The z-score analysis from the fMRI study indicates that the blue-green, symbol, text, checkerboard and random dot stimuli (five out of the six stimuli properties tested) have a stronger response to visual stimuli in the occipital lobe when compared to the black-white stimulus, whilst the analysis from the EEG study indicates that only the blue-green, red-green and random dot stimuli obtain higher z-score values when compared to the black-white stimulus. Similar evaluations, where different findings are concluded from the fMRI and EEG studies were observed in Pan et al. [80] and Bayram et al. [79]. A potential explanation for this inconsistency could be that the dipoles situated in the visual cortex exhibit varying phase configurations in response to different stimulus frequencies, resulting in distinct amplitudes in the overlaid EEG signals detected on the scalp [80].

Both the fMRI and EEG studies indicate that certain stimuli properties provide a better response than the black-white stimulus at both occipital and non-occipital areas of the brain. The best stimuli for eliciting a statistically significant SSVEP response stronger than the one generated by the black-white stimulus as evidenced by both the fMRI and EEG studies are:

- **Low Frequencies [7.5 Hz and 10 Hz]:** The fMRI study showed that the blue-green, symbol, and random dot stimuli consistently activated the occipital and temporal lobes, suggesting their effectiveness in generating

SSVEP responses. Meanwhile, the EEG study indicated that random dot and red-green stimuli led to activations in the occipital and temporal regions. Furthermore, the activations of the random dot stimulus at this frequency range were higher than the red-green stimulus. Overall, random dot stimuli appear to consistently evoke visual responses across both modalities at this frequency range in the occipital, temporal and parietal areas.

- **Mid-range Frequencies [15 Hz and 20 Hz]:** In the fMRI study, blue-green, symbol, and random dot stimuli activated multiple brain regions, including the occipital, temporal, and parietal lobes. The EEG study also demonstrated robust activations for blue-green, red-green and checkerboard stimuli, particularly in the occipital and temporal regions. These findings suggest that blue-green stimuli consistently evoke SSVEP responses at this frequency range, supported by both brain signal recording modalities at the occipital, parietal and temporal areas.
- **High Frequency [24 Hz]:** The fMRI study indicated that blue-green, shape and texture stimuli activated the occipital lobe at this frequency. The EEG study showed that blue-green and red-green stimuli elicited occipital activations. Blue-green stimuli seem to consistently evoke SSVEP responses across both fMRI and EEG up to the 24 Hz frequency at the occipital lobe.

In conclusion, based on the combined results of the fMRI and EEG studies, the random dot stimuli at the low frequency range (7.5 Hz and 10 Hz) and blue-green stimuli at mid-range and high frequencies (15 Hz, 20 Hz, 24 Hz) appear to be among the most effective for eliciting SSVEP responses. These stimuli consistently engage relevant brain regions, including the occipital, temporal and parietal lobes.

7.6 Overall Conclusions

This work aimed to address the four questions presented in Section 1.2 of the Introduction chapter. The questions and the answers concluded from this work are the following:

- (i) *What is the influence of different colour, shape and texture stimuli on SSVEPs from different areas of the brain?* - Through both the fMRI and EEG studies, it was determined that different colour, shape and texture stimuli parameters

do affect the strength of the BOLD and SSVEP response generated in the brain which was seen to vary with different locations in the brain. Thus, varying these parameters has the potential to improve the efficiency of SSVEP-based BCIs and the electrode locations used to collect the SSVEPs.

- (ii) *Which of the different stimuli parameters brings about the strongest SSVEP response and in which area of the brain is this located?* - Z-score analysis was used in both the fMRI and EEG studies to assess the strength of the brain's response to visual stimuli. Furthermore, permutation-based statistics and the SNR were evaluated in the EEG analysis to determine the magnitude of the SSVEP response. The combined results of the fMRI and EEG studies indicate that the random dot stimulus and blue-green stimulus provide the highest SSVEP responses in the occipital, temporal and parietal regions of the brain.
- (iii) *Is the SSVEP response in non-occipital areas of the brain strong enough to be used to control an SSVEP-based BCI system?* - The SSVEP response in temporal and parietal areas was located, and through the z-score analysis done on the EEG data, this response was determined to be statistically significant. Thus, reliable SSVEPs can be detected from such areas to control BCI systems. Conversely, although brain activity was obtained in frontal areas (as seen by both the fMRI and EEG studies), it was concluded that this activity is not harmonically related to SSVEPs. Thus, electrodes placed in the frontal region are not expected to exhibit SSVEP harmonics as may be use in SSVEP-based BCIs.
- (iv) *How does the SSVEP response evoked by these stimuli vary in different frequency bands?* - In this study, each stimulus was set to flicker at each of the following frequencies: 7.5 Hz, 10 Hz, 15 Hz, 20 Hz, 24 Hz and 30 Hz, to study how the SSVEP response varies at different frequencies. The fMRI study indicated strong BOLD responses up to the 24 Hz frequency and the EEG study conveyed high SNR and z-score values up to the 20 Hz frequency. This suggests that the strength of the SSVEP response decreases with an increase in the flickering stimuli, and high frequencies (> 24 Hz) should be avoided.

7.7 Limitations and Further Improvements

One of the limitations when analyzing SSVEPs using fMRI is that the recorded BOLD signal only provides information about the amount of oxygenated blood present in a particular area of the brain and does not offer any information about the frequency components present. Consequently, the brain activity detected by fMRI cannot definitively be attributed to SSVEPs, unlike EEG, which can detect SSVEPs by examining signal power at the fundamental frequency and its harmonics. However, EEG lacks spatial resolution and does not give any information about the activity in cortical regions of the brain.

The fMRI and EEG experiments were not conducted simultaneously. Thus, any variability in participant state (such as fatigue and alertness) and environmental artefacts (such as background noise) between the two separate sessions could have introduced additional sources of variance in the data. Furthermore, combining and analyzing data from separate fMRI and EEG studies can be complex and challenging. These limitations may be overcome by using a simultaneous fMRI-EEG recording modality which, however, is not available locally. Simultaneous recordings help identify and correct potential artefacts more effectively and improve data quality through artefact correction techniques. Another advantage of simultaneous fMRI - EEG is that it can provide insights into the temporal dynamics of hemodynamic responses. Researchers can examine how the timing of neural activity observed in EEG relates to the onset and duration of hemodynamic responses captured by fMRI.

Results from the fMRI study show that there is inter-subject variability, indicating that individual differences in brain responses to RVS exist. This variability can be influenced by factors such as age, gender, cognitive abilities, and prior experiences. To account for and better understand these variations, larger sample sizes (number of subjects) are needed. A larger and more varied number of participants enhances the study's generalizability to a broader population, making the findings more applicable to various demographic groups. Moreover, increased sample sizes improve the robustness of the results, making them less susceptible to outliers or unusual individual responses that may skew the data. Additionally, larger samples help reduce the impact of chance or random fluctuations in the data.

Finally, to confirm the results obtained by the fMRI and EEG experiments conducted in this study, an online EEG study where a real-time SSVEP-based BCI is controlled using the black-white stimulus and the blue-green, red-green, checkerboard and random dot stimuli, which all obtained stronger responses than the black-white stimuli at certain frequencies and areas, should be implemented. From this real-time experiment, classification and ITR values of the SSVEP-based BCI controlled with the proposed stimuli would then be used to compare the BCI controlled with the standard black-white stimuli. This real-time BCI system can also be tested using dry electrodes to further improve its practicality.

Chapter 8

Conclusions

The goal of this study was to analyse the SSVEP response and how this varies for different stimuli parameters using the functional magnetic resonance imaging (fMRI) and electroencephalography (EEG) brain signal recording modalities. This chapter provides both a summary of the project's findings and conclusions, as well as an overview of the project's contributions.

A comprehensive literature review on SSVEP-based BCIs was presented by focusing mainly on how they have been made more practical throughout the years. It was identified that one possible way to increase the practicality and accessibility of these systems is by using electrodes in non-occipital areas of the brain. Thus, particular attention was given to understanding the location of the generation of the SSVEP by first analysing the visual pathway and then, examining findings from previous fMRI studies that tried to localise the SSVEP in the brain. Through the studies that have worked on improving behind the ear/temporal SSVEP-based BCI, it was identified that varying the stimuli parameters from the standard black-white stimulus may increase the SSVEP response in both the occipital lobe and non-occipital areas. This would lead to more effective and practical BCI systems. Thus, the literature review also focused on different stimuli characteristics analysed using both the fMRI and EEG modalities to discover the brain dynamics of the SSVEP.

The SSVEP was analysed using both the fMRI and EEG modalities in two separate studies. This was done for the primary reasons that fMRI offers an excellent spatial resolution of the brain volume, it can provide detailed anatomical images of the

brain alongside functional data and it can visualize activity in deep brain structures, including cortical regions; on the downside, fMRI has low temporal resolution and records the blood oxygenation level dependent (BOLD) signal, rather than neural responses. On the contrary, EEG excels in temporal resolution and records neural responses. However, EEG suffers from a low spatial resolution since it is measured from sparse electrodes placed on the scalp. The fMRI and EEG studies thus provide complimentary results and were primarily conducted to (i) determine the brain-activated areas in the brain when displaying RVS with different stimuli parameters at different frequencies (ii) identify which stimuli parameters can evoke a stronger SSVEP response than the standard black-white stimulus that has been used in current BCI systems and (iii) and identify potential SSVEP responses in non-occipital areas.

Since fMRI recording was not possible at the start of this investigation, another central aim of this study was to achieve mastery of fMRI recording, preprocessing, and processing, as well as configuring the MRI scanner to permit fMRI recording. Ensuring the precise synchronisation of the experimental task presented to the subjects with the accurate recording of functional data was of great importance for the accuracy and reliability of the fMRI investigation. This endeavour required careful attention to detail and the development of robust protocols to guarantee the seamless integration of cognitive tasks and neuroimaging data acquisition.

Furthermore, this endeavour encompassed a comprehensive understanding of the details of fMRI data acquisition and processing, including artefact correction, data quality assurance, and advanced analytical techniques. This approach facilitated a deeper understanding of the complexities involved in fMRI research, ultimately contributing to the refinement of methodologies in the field.

An in-depth analysis on the most frequently activated brain cortical areas when each subject is exposed to repetitive visual stimuli (RVS) having different stimuli parameters was conducted using fMRI for each subject. The SSVEP response on the scalp was analysed using EEG, which was evaluated using permutation-based statistics, signal-to-noise ratio (SNR), and z-score. The fMRI and EEG results indicate that the SSVEP in the occipital lobe is the strongest compared to the temporal, parietal and frontal lobes. This was concluded from the fMRI study

by observing an increase in the BOLD signal, as evidenced by an increase in the z-statistic value when analysing the stimulation period data using the general linear model (GLM) algorithm. From the EEG study, an increase in the SNR was also noticed at the fundamental frequency and its harmonics at the occipital lobe. This observation was noted for the 7.5 Hz - 24 Hz frequency range for the fMRI study and the 7.5 Hz - 20 Hz frequency range for the EEG study, suggesting that the SSVEP response decreases at the 30 Hz frequency. The EEG study also revealed that the SSVEP response on the scalp at the 30 Hz frequency decreases in the parietal and temporal areas of the brain.

These results suggest that an SSVEP-based BCI using occipital electrodes is expected to be effective. However, this study showed the SSVEP response at temporal and parietal areas is also statistically significant and thus strong enough to be used in an SSVEP-based BCI, specifically when using the blue-green, red-green, checkerboard and random dot stimuli at particular frequencies. In conclusion, considering the combined findings from both fMRI and EEG studies, the random dot stimulus at low frequencies (7.5 Hz and 10 Hz) and blue-green stimulus in the mid to high frequency range (15 Hz, 20 Hz, 24 Hz) brought about the strongest SSVEP responses in the brain. These specific stimuli consistently activate different brain regions, including the occipital, temporal, and parietal lobes.

The data collected from both fMRI and EEG studies was analysed offline. Such conclusions can be verified in future works by developing an online experiment of real-time SSVEP-based BCIs using electrodes from occipital and non-occipital areas of the brain with the proposed stimuli parameters that obtained a high SSVEP response (including the random dot and blue-green stimuli) and with the standard black-white stimulus. Classification accuracies and information transfer rates (ITRs) can be obtained to analyse and compare the performance of a real-time BCI system using the proposed stimuli and the black-white stimulus.

Overall, this project contributed to using fMRI to localise the brain cortical regions that are activated when presenting RVS having different stimuli parameters. Both the fMRI and EEG studies show that the strongest SSVEP response was determined to be evoked at the occipital lobe for all the stimuli parameters tested for the 7.5 Hz - 24 Hz frequency range. However, both studies show that using the random

dot and blue-green stimuli can provide a stronger SSVEP response at occipital, temporal and parietal areas of the brain when compared to the standard black-white stimulus that has been used in current SSVEP-based BCIs. These findings allow the development of more comfortable, accurate, and stable BCIs, possibly with electrodes positioned on the non-occipital areas of the brain, improving the practicality of such systems.

Appendix A

fMRI Data Recording Session Procedures

Once a subject enters the MRI control room after signing the consent form and reading the information sheet, the following procedures are taken by the researcher and radiographer prior to starting an fMRI data recording session:

1. The radiographer asks the subject if he or she has medical implants or metal fragments in their body to ensure that it is safe for the subject to participate in such a study.
2. The subject is asked to remove any metal accessories and remove any clothes that may contain any metal fibres. In this case, the subjects were given a hospital gown to wear while inside the scanner.
3. The experimental protocol is then explained to the subject after which the radiographer directed the subject into the magnet room where the subject is placed on the scanner table in a supine position.
4. The subject is given headphones to wear, and the 64-channel head coil with the mirror is arranged around the head.
5. The push-button audio buzzer is placed in the subject's hands and the subject is instructed to press this whenever they would like to speak to the radiographer in cases where he or she is feeling uncomfortable, to ask a question, to communicate back with the radiographer, and in an emergency.
6. The subject is instructed to remain still during the recording session as any movement would negatively affect the data recorded.
7. After ensuring that the subject is comfortable on the table and that he or she can properly see the visual stimuli presented on the LCD screen via the

mirror, the radiographer exits and closes the magnet room to start the MRI data recording session.

Appendix B

fMRIPrep Processing Workflow

Figure B.1 presents the fMRIPrep workflow comprising two primary components, divided into separate processing streams for both anatomical and functional MRI data. The NIfTI T1-weighted anatomical images are pre-processed using the following steps:

- *INU correction*: The voxel intensity non-uniformity (INU) bias field refers to the gradual, non-anatomical variations in intensity within the same tissue across the image and is generally caused by gradient-driven eddy currents, inhomogeneous reception sensitivity profiles, radiofrequency coil non-uniformity, static field inhomogeneity, and mostly due to the subject's anatomy both inside and outside the field of view [220]. It is crucial to correct for such a field as this can highly impact the performance of further preprocessing steps such as registration and segmentation [220].
- *Fuse and conform*: In this step a single 3D reference image is formed by aligning and averaging all the T1-weighted images to the right, anterior and superior (RAS) orientation and a common voxel size [175, 221].
- *Skull-stripping*: Skull-stripping removes the skull and isolates the brain from extracranial and other non-brain tissue. This step leads to better segmentation of different brain regions and reduces human rater variance [222, 223].
- *Spatial normalisation*: By comparing each subject to a predetermined template, spatial normalisation attempts to build a one-to-one relationship between the brains of various individuals [175]. This is crucial for fMRI data analysis at the between-subject level. fMRIPrep uses a nonrigid method where the tissue is compressed and/or extended to conform to the MNI atlas reference image [224]. Through spatial normalisation, anatomical addresses from atlases that have been mapped to the MNI reference brain space can be used to locate the data in the MRI image. Additionally, a large anatomical

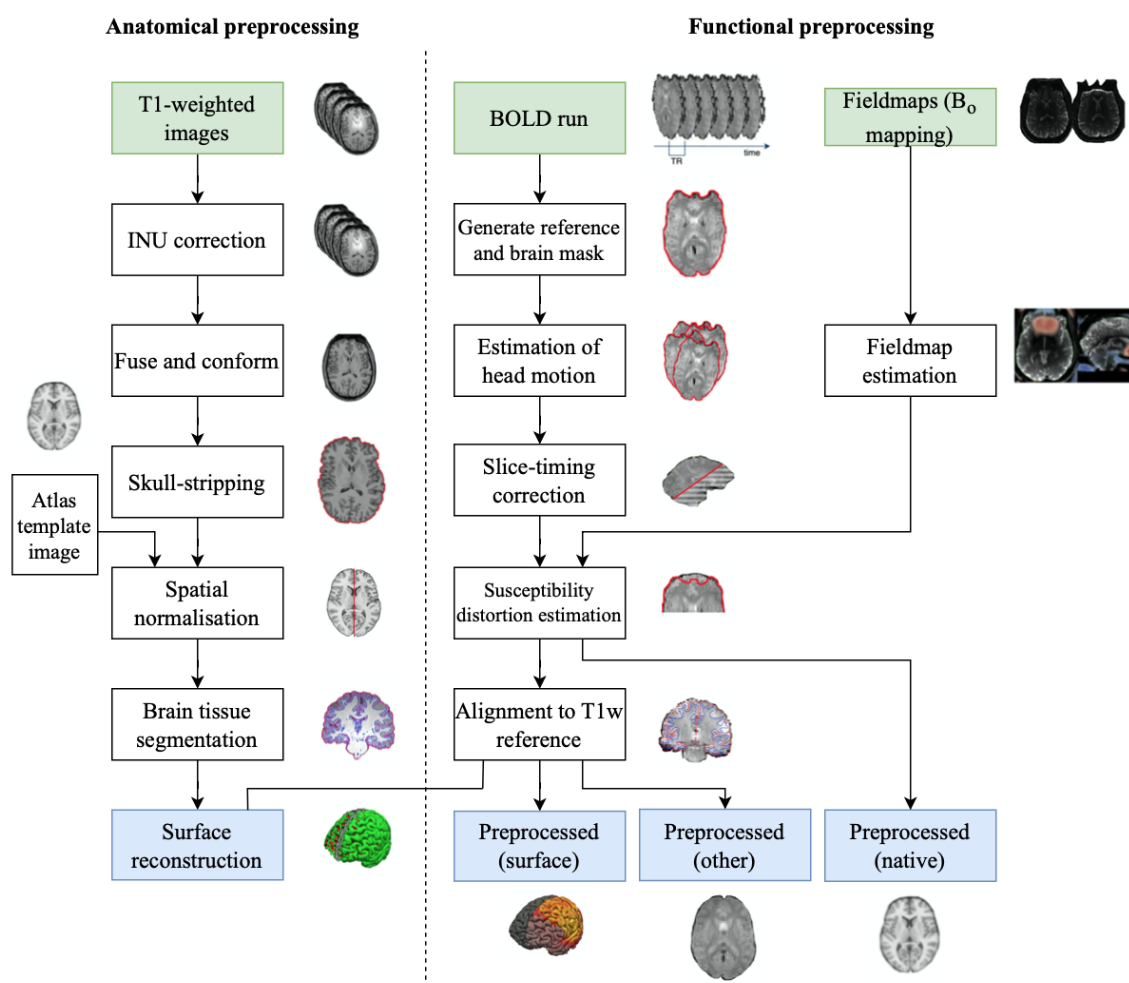
region or volume of interest, such as those defined in the automatic anatomic labelling (AAL) atlas, can be addressed at the voxel level utilising spatial coordinates that Talairach and Tournoux initially created to identify Brodmann regions in image volumes [225].

- *Brain tissue segmentation*: Brain tissue segmentation aims to separate an image into a group of homogenous, nonoverlapping tissues that are semantically significant and share comparable qualities, such as intensity, depth, colour, or texture. Here the three main tissues which are the white matter, grey matter and cerebrospinal fluid are segmented from other parts of the human head such as the skull, marrow, and muscular skin [226–228].
- *Surface reconstruction*: The process of cerebral cortical surface reconstruction uses geometric models of the cortex to identify the inner and outer boundaries of the folded human cerebral cortex from anatomical images. *fMRIprep* uses the FreeSurfer software to accomplish this step [221].

The functional preprocessing consists of the following steps:

- *Reference and brain mask*: The first step of preprocessing the functional MRI images is to perform specialized averaging of the time-series BOLD run into one volume. A brain mask is applied to the data to diminish the size of the dataset which results in speeding up the analysis. This mask eliminates the regions of the skull and neck which are not important for this analysis [229].
- *Estimation of head motion*: When the head moves during scanning, a change in the steady state magnetization is caused since the time between excitations in the tissues that have moved from one slice to the next occurs. This reduces the temporal stability of the signal and eventually increases the false positives and negatives [230–232].
- *Fieldmap estimation*: Echo planar imaging (EPI) which was the MR imaging technique used in this study to record the *fMRI* images, is negatively affected by B^0 field inhomogeneities that cause spatial distortions and signal dropout, particularly near the skull base, commonly affecting the temporal and anterior frontal lobes [233]. Using the recorded fieldmaps, *fMRIprep* computes the B-Spline coefficients to modify the fieldmap to the TOPUP tool [234].
- *Slice-timing correction*: The slices which make up a single *fMRI* volume are not acquired instantaneously, and as a consequence, these are temporally misaligned from one another. These temporal offsets between slices need to be adjusted to obtain an accurate time series analysis of the *fMRI* data by the process known as slice-timing correction. During this step, the time series of each slice is shifted in order to match each slice’s timing with a reference time-point [235, 236].

- *Susceptibility distortion estimation*: In this step, the fieldmaps and an unwarping method are used to reduce the distortion caused by B^0 inhomogeneities. *fMRIprep* uses susceptibility distortion correction (SDC) routines to correct these distortions [221, 232, 237–239].
- *Alignment to T1 reference*: During this step spatial mapping between the BOLD images and the pre-processed T1-weighted images is done. The BOLD series undergoes resampling within its native space, achieved by combining spatial mappings for a one-shot interpolation procedure utilizing a Lanczos kernel [221]. The BOLD images are surface preprocessed by aligning the reference BOLD image of every run and the reconstructed subject via the white and grey matter boundary [221]. Finally, the BOLD series and the T1-weighted based mask are mapped to the standard MNI space. The Lanczos kernel is used to concatenate the transforms and apply them all at once [221].

FIGURE B.1: *fMRIprep* workflow. Adapted from [171].

Appendix C

Brain Activations Visual Maps

The following are MNI atlas images showing the corresponding locations of the most frequently activated z-max voxel for Subjects 2 - 6 for every stimulus.

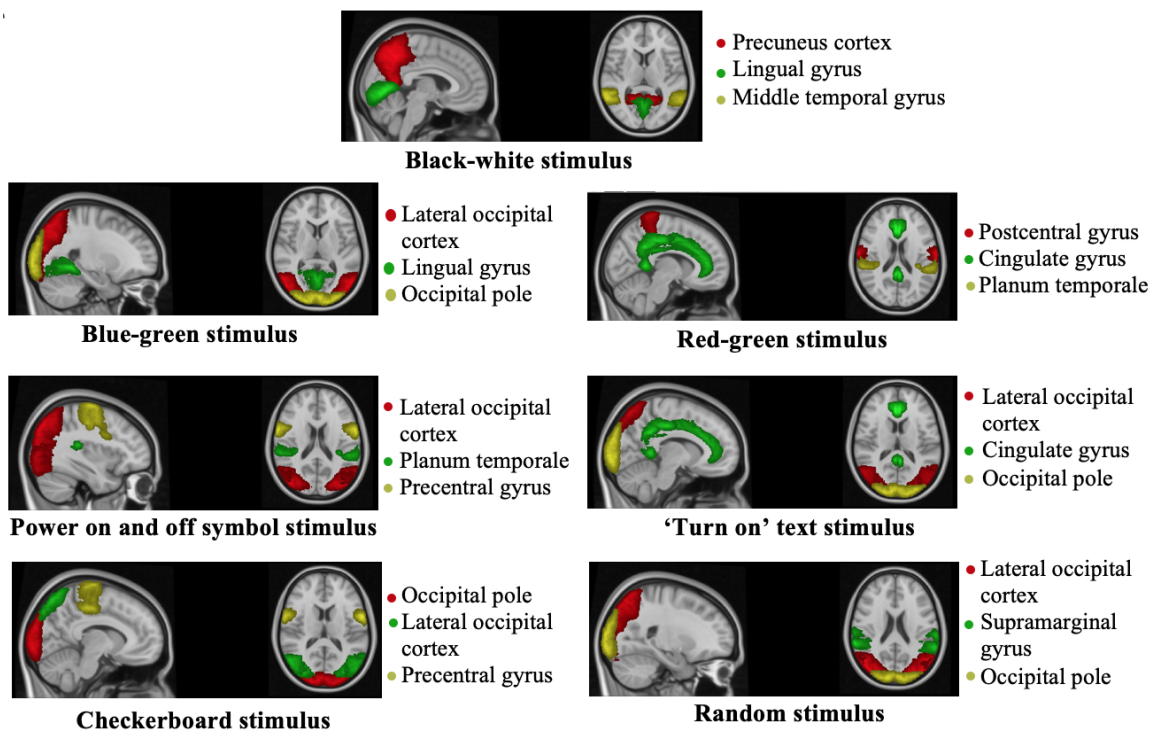


FIGURE C.1: Subject 2.

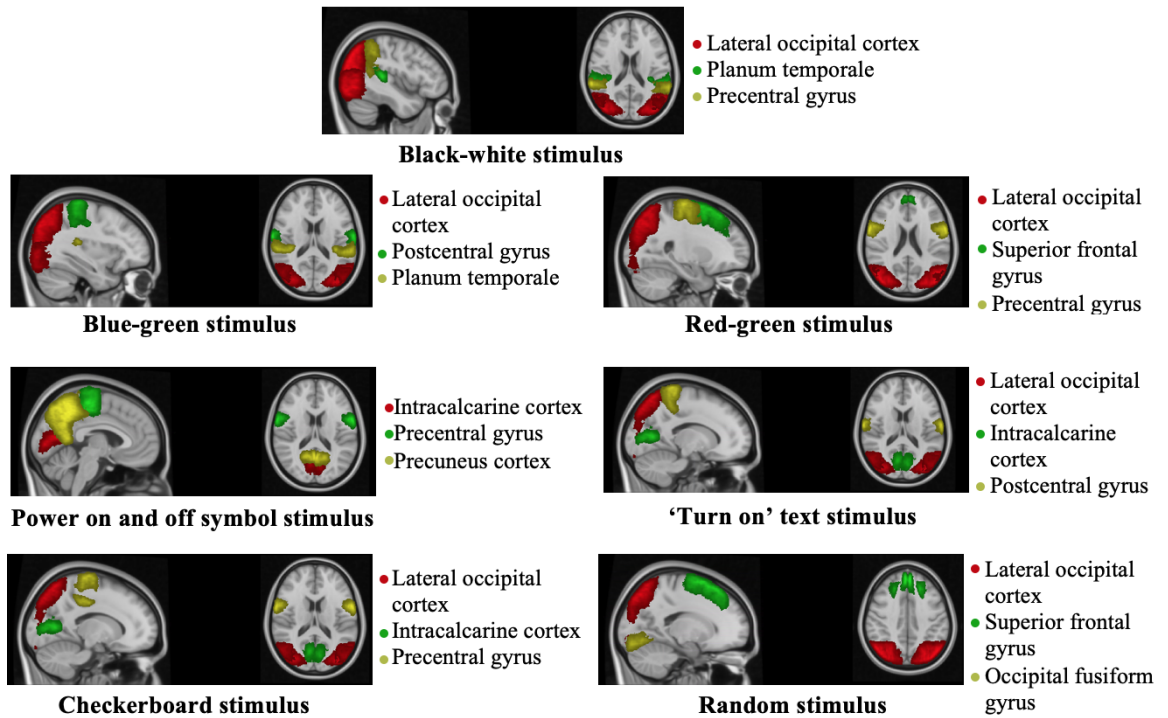


FIGURE C.2: Subject 3.

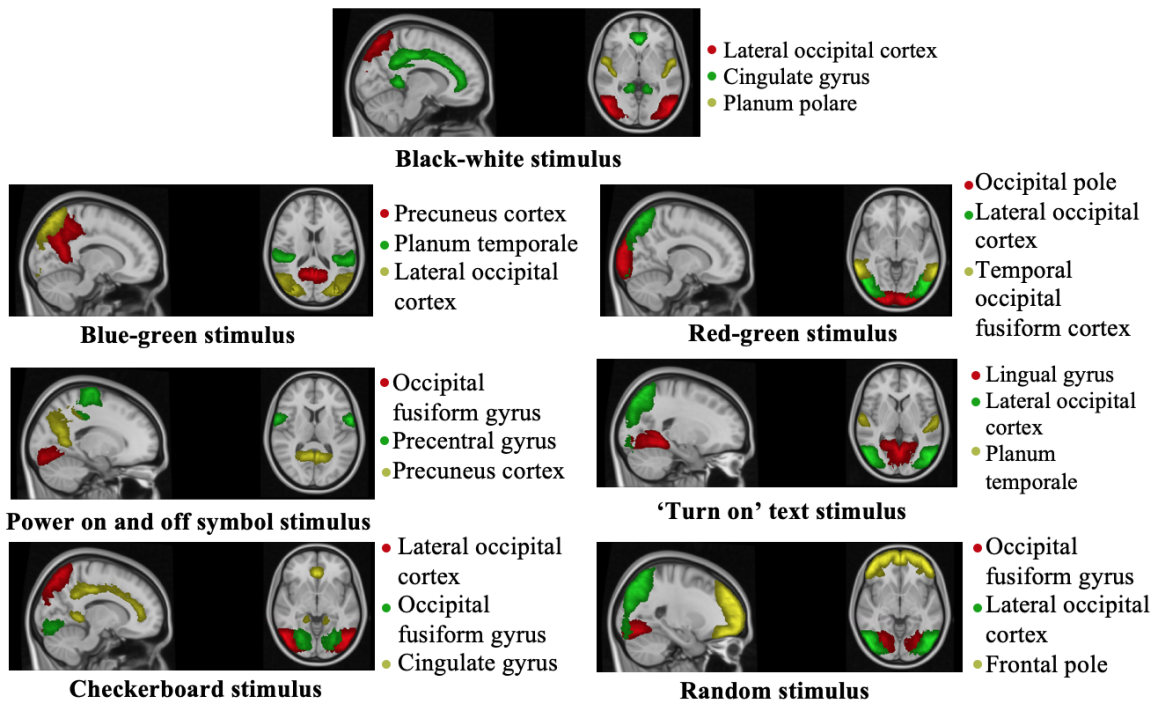


FIGURE C.3: Subject 4.

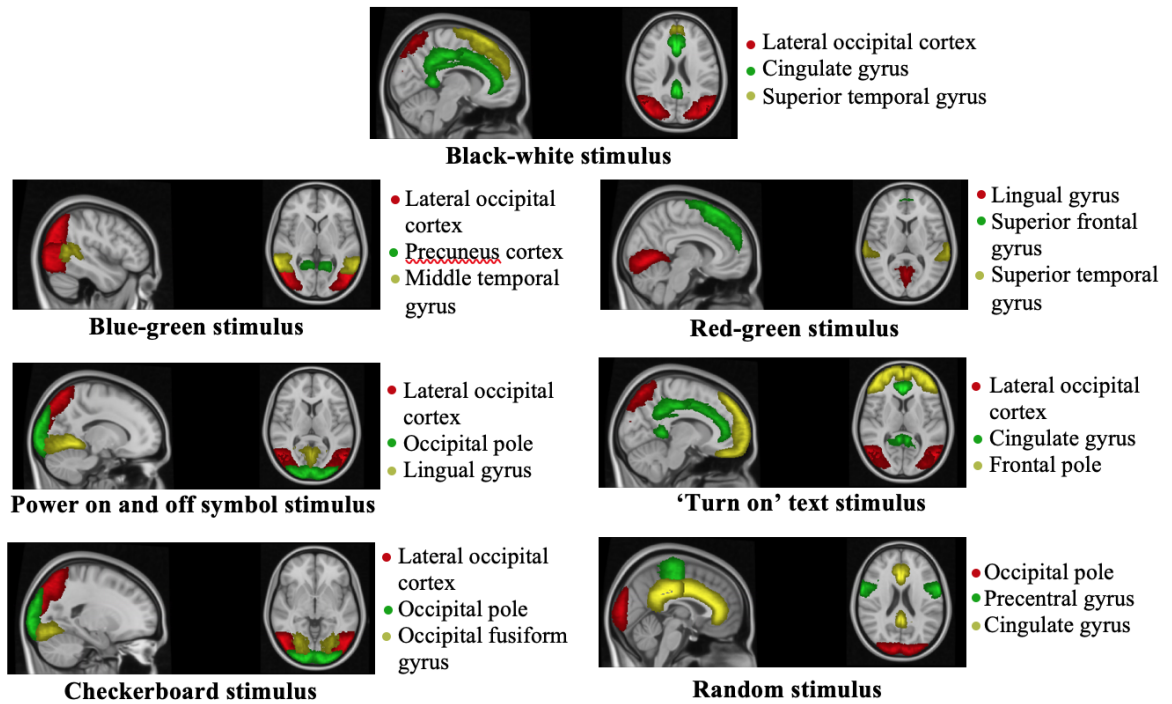


FIGURE C.4: Subject 5.

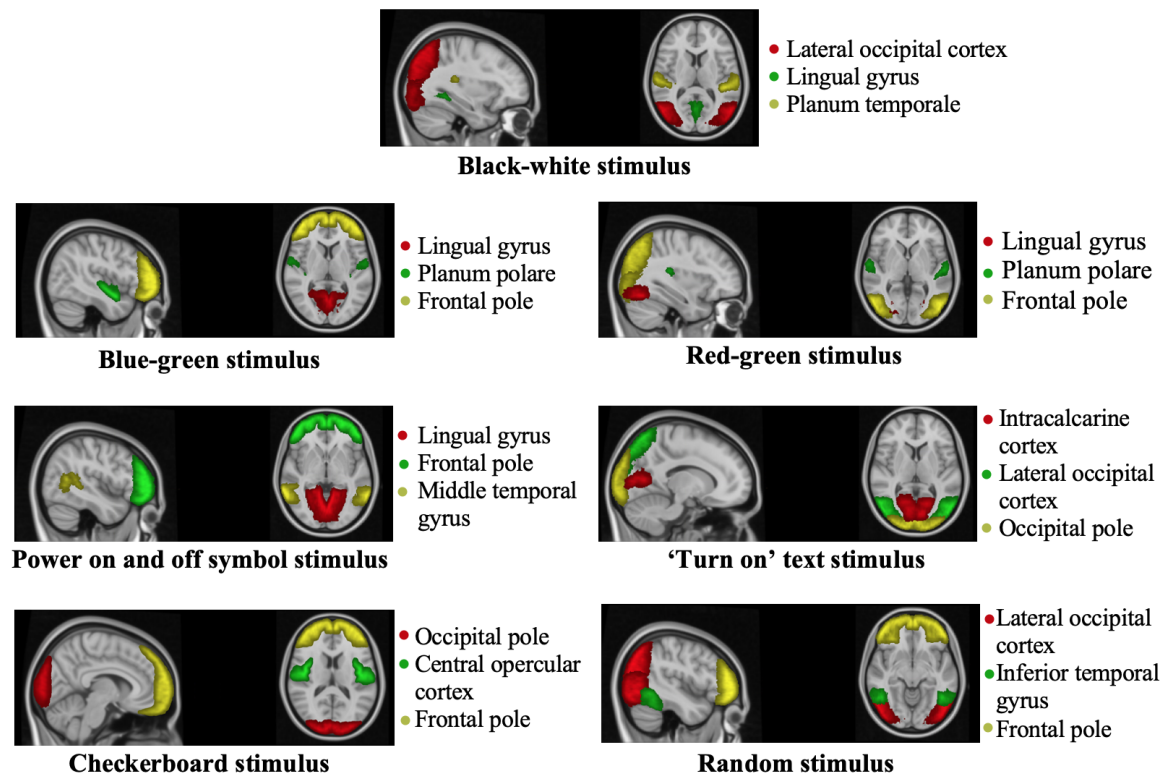


FIGURE C.5: Subject 6.

Bibliography

- [1] Wolpaw, J. R., Birbaumer, N., McFarland, D. J., Pfurtscheller, G., and Vaughan, T. M. Brain-computer interfaces for communication and control. *Clinical Neurophysiology: Official Journal of the International Federation of Clinical Neurophysiology*, 113(6):767–791, June 2002.
- [2] Abdulkader, S. N., Atia, A., and Mostafa, M.-S. M. Brain computer interfacing: Applications and challenges. *Egyptian Informatics Journal*, 16(2): 213–230, July 2015.
- [3] Xu, D., Tang, F., Li, Y., Zhang, Q., and Feng, X. An Analysis of Deep Learning Models in SSVEP-Based BCI: A Survey. *Brain Sciences*, 13(3):483, March 2023.
- [4] Norcia, A. M., Appelbaum, L. G., Ales, J. M., Cottareau, B. R., and Rossion, B. The steady-state visual evoked potential in vision research: A review. *Journal of Vision*, 15(6):4, May 2015.
- [5] Carter, R. *The Human Brain Book*. DK Publishing, New York, 2019.
- [6] Watson, C. *The Brain: An Introduction to Functional Neuroanatomy*. Academic Press, London, 1st edition, 2010.
- [7] Cherry, K. How Neurons Transmit Information Throughout the Body. <https://www.verywellmind.com/what-is-a-neuron-2794890> (accessed June 11, 2023).
- [8] Brown, A. G. *Nerve Cells and Nervous Systems: An Introduction to Neuroscience*. Springer Science & Business Media, December 2012.
- [9] Purves, D. *Neuroscience*. Sinauer Associates, Publishers, Sunderland, Mass, 6th edition, 2017.
- [10] Vandergriendt, C. and Zimlich, R. An Easy Guide to Neuron Diagrams and Types. <https://www.healthline.com/health/neurons> (accessed Feb 5, 2023).

-
- [11] Synapse: Definition, Parts, Types & Function. <https://www.simplypsychology.org/synapse.html> (accessed Feb 6, 2023).
- [12] Teplan, M. Fundamentals of EEG measurement. *Measurement Science Review*, 2, 2002.
- [13] Hero, C. How Neurons Communicate. <https://courses.lumenlearning.com/biology2xmaster/chapter/how-neurons-communicate/> (accessed Jan 28, 2023).
- [14] Lewis, T. and Taylor, A. P. Human brain: Facts, functions & anatomy. <https://www.livescience.com/29365-human-brain.html> (accessed Jan 28, 2023).
- [15] Brain Anatomy and How the Brain Works. <https://www.hopkinsmedicine.org/health/conditions-and-diseases/anatomy-of-the-brain> (accessed Jan 29, 2023).
- [16] Spielman, R. M., Jenkins, W. J., and Lovett, M. D. *Psychology 2e*. OpenStax, 2020.
- [17] Electroencephalography The Complete Pocket Guide. Accessed Feb 4, 2023. Available: <https://imotions.com/blog/learning/best-practice/eeg/>.
- [18] Visual Cortex. https://www.seevidly.com/info/Physiology_of_Vision/The_Brain/Visual_System/Visual_Cortex (accessed Jan 29, 2023).
- [19] Huff, T., Mahabadi, N., and Tadi, P. *Neuroanatomy, Visual Cortex*. StatPearls Publishing, Treasure Island (FL), Jan 2023.
- [20] Rehman, A. and Al Khalili, Y. *Neuroanatomy, Occipital Lobe*. StatPearls Publishing, Treasure Island (FL), 2023.
- [21] Calcarine sulcus. https://en.wikipedia.org/w/index.php?title=Calcarine_sulcus&oldid=1131510178 (accessed Jan 28, 2023).
- [22] Shahid, S. Fusiform gyrus. <https://www.kenhub.com/en/library/anatomy/fusiform-gyrus> (accessed Jan 29, 2023).
- [23] Lateral occipital sulcus. <https://en.wikipedia.org/w/index.php?> (accessed Jan 29, 2023).
- [24] Brain atlas. https://en.wikipedia.org/w/index.php?title=Brain_atlas&oldid=1143966463 (accessed Jan 29, 2023).
- [25] The MNI brain and the Talairach atlas. <https://brainmap.org/training/BrettTransform.html> (accessed Jan 29, 2023).

- [26] Atlases. <https://nist.mni.mcgill.ca/atlasses/> (accessed Jan 29, 2023).
- [27] Warrington, S., Bryant, K. L., Khrapitchev, A. A., Sallet, J., Charquero-Ballester, M., Douaud, G., Jbabdi, S., Mars, R. B., and Sotiropoulos, S. N. XTRACT - Standardised protocols for automated tractography in the human and macaque brain. *NeuroImage*, 217, August 2020.
- [28] B.S., A. F. Brodmann areas. <https://www.kenhub.com/en/library/anatomy/brodmann-areas> (accessed Jan 29, 2023).
- [29] Brodmann area. https://en.wikipedia.org/w/index.php?title=Brodmann_area&oldid=1154768528 (accessed Jan 29, 2023).
- [30] Başar, E. Brain oscillations in neuropsychiatric disease. *Dialogues in Clinical Neuroscience*, 15(3):291–300, September 2013.
- [31] Louis, E. K. S., Frey, L. C., Britton, J. W., Frey, L. C., Hopp, J. L., Korb, P., Koubeissi, M. Z., Lievens, W. E., Pestana-Knight, E. M., and Louis, E. K. S. Electroencephalography (EEG): An introductory text and atlas of normal and abnormal findings in adults, children, and infants. American Epilepsy Society, 2016.
- [32] Brainwaves and Frequency Bands. <https://www.121neurofeedback.com/brainwaves-and-frequency-bands/> (accessed Feb 3, 2023).
- [33] Nicolas-Alonso, L. F. and Gomez-Gil, J. Brain Computer Interfaces, a Review. *Sensors*, 12(2):1211–1279, January 2012.
- [34] Mak, J. N. and Wolpaw, J. R. Clinical Applications of Brain-Computer Interfaces: Current State and Future Prospects. *IEEE reviews in biomedical engineering*, 2:187–199, 2009.
- [35] What is a Brain Computer Interface? <https://cumming.ucalgary.ca/research/pediatric-bci/bci-program/what-bci> (accessed Feb 5, 2023).
- [36] Shih, J. J., Krusienski, D. J., and Wolpaw, J. R. Brain-Computer Interfaces in Medicine. *Mayo Clinic Proceedings*, 87(3):268–279, March 2012.
- [37] Saha, S., Mamun, K. A., Ahmed, K., Mostafa, R., Naik, G. R., Darvishi, S., Khandoker, A. H., and Baumert, M. Progress in Brain Computer Interface: Challenges and Opportunities. *Frontiers in Systems Neuroscience*, 15, 2021.
- [38] Intro to Brain Computer Interface. <http://learn.neurotechedu.com/introtobci/> (accessed Feb 4, 2023).
- [39] Brain-computer interface. https://en.wikipedia.org/w/index.php?title=Brain%E2%80%93computer_interface&oldid=1038129964 (accessed Feb 6, 2023).

- [40] *Functional MRI An Introduction to Methods*. Oxford University Press, New York, 1st edition, 2002.
- [41] Singh, S. P. Magnetoencephalography: Basic principles. *Annals of Indian Academy of Neurology*, 17(Suppl 1):S107–S112, March 2014.
- [42] Chen, W.-L., Wagner, J., Heugel, N., Sugar, J., Lee, Y.-W., Conant, L., Malloy, M., Heffernan, J., Quirk, B., Zinos, A., Beardsley, S. A., Prost, R., and Whelan, H. T. Functional Near-Infrared Spectroscopy and Its Clinical Application in the Field of Neuroscience: Advances and Future Directions. *Frontiers in Neuroscience*, 14, 2020.
- [43] Yuan, H. and He, B. Brain-Computer Interfaces Using Sensorimotor Rhythms: Current State and Future Perspectives. *IEEE transactions on bio-medical engineering*, 61(5):1425–1435, May 2014.
- [44] Picton, T. W. The P300 wave of the human event-related potential. *Journal of Clinical Neurophysiology: Official Publication of the American Electroencephalographic Society*, 9(4):456–479, October 1992.
- [45] Amiri, S., Rabbi, A., Azinfar, L., Fazel-Rezai, R., Amiri, S., Rabbi, A., Azinfar, L., and Fazel-Rezai, R. *A Review of P300, SSVEP, and Hybrid P300/SSVEP Brain- Computer Interface Systems*. IntechOpen, June 2013.
- [46] Tsoneva, T., Garcia-Molina, G., and Desain, P. SSVEP phase synchronies and propagation during repetitive visual stimulation at high frequencies. *Scientific Reports*, 11(1), March 2021.
- [47] Wan, B., Xiong, B., Huang, J., and Yang, P. A Novel SSVEP-based Word Speller Based on Sliding Multi-Window Strategy. In *2021 9th International Winter Conference on Brain-Computer Interface (BCI)*, pages 1–5, Gangwon, Korea (South), February 2021.
- [48] Lin, K., Gao, S., and Gao, X. Boosting the information transfer rate of an SSVEP-BCI system using maximal-phase-locking value and minimal-distance spatial filter banks. *Tsinghua Science and Technology*, 24(3):262–270, June 2019.
- [49] Chen, X., Liu, B., Wang, Y., and Gao, X. A Spectrally-Dense Encoding Method for Designing a High-Speed SSVEP-BCI With 120 Stimuli. *IEEE Transactions on Neural Systems and Rehabilitation Engineering*, 30:2764–2772, 2022.
- [50] West, K. L., Zuppichini, M. D., Turner, M. P., Sivakolundu, D. K., Zhao, Y., Abdelkarim, D., Spence, J. S., and Rypma, B. BOLD Hemodynamic

- Response Function Changes Significantly with Healthy Aging. *NeuroImage*, 188:198–207, March 2019.
- [51] Itthipuripat, S., Sprague, T. C., and Serences, J. T. Functional MRI and EEG Index Complementary Attentional Modulations. *The Journal of Neuroscience*, 39(31):6162–6179, July 2019.
- [52] Farnsworth, B. What is EEG (Electroencephalography) and How Does it Work? <https://imotions.com/blog/learning/research-fundamentals/what-is-eeg/> (accessed Feb 8, 2023).
- [53] Quoc, L. M. Why use EEG for research? <https://www.emotiv.com/blog/why-use-eeg-for-research/> (accessed Feb 4, 2023).
- [54] Mathewson, K. E., Harrison, T. J. L., and Kizuk, S. A. D. High and dry? Comparing active dry EEG electrodes to active and passive wet electrodes. *Psychophysiology*, 54(1):74–82, January 2017.
- [55] Granados, E. Wet, dry, active and passive electrodes. What are they, and what to choose? <https://www.brainlatam.com/blog/wet-dry-active-and-passive-electrodes-what-are-they-and-what-to-choose-413> (accessed Feb 10, 2023).
- [56] Ortiz, A. Main features of EEG sensor layer. <https://www.bitbrain.com/blog/ee-g-sensor-layer> (accessed Feb 5, 2023).
- [57] Types of EEG Electrodes: Gel, Water, and Dry. <https://info.tmsi.com/blog/types-of-ee-g-electrodes> (accessed Feb 15, 2023).
- [58] Lopez-Gordo, M. A., Sanchez-Morillo, D., and Valle, F. P. Dry EEG Electrodes. *Sensors (Basel, Switzerland)*, 14(7):12847–12870, July 2014.
- [59] What Are Active and Passive Electrodes? | EEG Electrodes. <https://zeto-inc.com/blog/active-and-passive-electrodes-what-are-they-pros-cons/> (accessed Feb 11, 2023).
- [60] Laszlo, S., Ruiz-Blondet, M., Khalifian, N., Chu, F., and Jin, Z. A direct comparison of active and passive amplification electrodes in the same amplifier system. *Journal of Neuroscience Methods*, 235:298–307, September 2014.
- [61] 10–20 system (EEG). [https://en.wikipedia.org/w/index.php?title=10%E2%80%9320_system_\(EEG\)&oldid=1040419178](https://en.wikipedia.org/w/index.php?title=10%E2%80%9320_system_(EEG)&oldid=1040419178) (accessed July 6, 2023).
- [62] Huang, J. Overview of Cerebral Function. <https://www.merckmanuals.com/professional/neurologic-disorders/>

- function-and-dysfunction-of-the-cerebral-lobes/
overview-of-cerebral-function (accessed Feb 9, 2023).
- [63] Kim, B., Kim, H., Kim, S., and ran Hwang, Y. A brief review of non-invasive brain imaging technologies and the near-infrared optical bioimaging. *Applied Microscopy*, 51(1):9, June 2021.
- [64] Castellano, G. The Benefits of MRI Imaging. <https://www.ainpc.com/2022/12/09/benefits-of-mri-imaging/> (accessed Feb 6, 2023).
- [65] MRI Basics. https://my-ms.org/mri_basics.htm (accessed Dec 11, 2022).
- [66] Preston, D. C. MRI Basics. <https://case.edu/med/neurology/NR/MRI%20Basics.htm> (accessed Jan 4, 2023).
- [67] Hird, R. 2 - The Basics of MRI Interpretation | Radiology | Geeky Medics. <https://geekymedics.com/the-basics-of-mri-interpretation/> (accessed Dec 12, 2022).
- [68] Magnetic Resonance Imaging (MRI). <https://www.nibib.nih.gov/science-education/science-topics/magnetic-resonance-imaging-mri> (accessed Jan 4, 2023).
- [69] Lloyd-Jones, G. MRI interpretation. https://www.radiologymasterclass.co.uk/tutorials/mri/mri_scanner (accessed Dec 15, 2022).
- [70] Kawahara, D. and Nagata, Y. T1-weighted and T2-weighted MRI image synthesis with convolutional generative adversarial networks. *Reports of Practical Oncology and Radiotherapy*, 26:35–42, February 2021.
- [71] Jenkinson Mark, C. M. *Introduction to Neuroimaging analysis*. Oxford University Press, New York, 1st edition, 2018.
- [72] Peelle, J. Preliminaries — Introduction to MRI. <http://jpeelle.net/mri/general/preliminaries.html> (accessed Jan 3, 2023).
- [73] Gaillard, F. BOLD imaging. <https://radiopaedia.org/articles/bold-imaging> (accessed Jan 4, 2023).
- [74] Elster, A. D. <http://mriquestions.com/does-boldbrain-activity.html> (accessed Feb 11, 2023), .
- [75] Jahn, A. Chapter 3: The Hemodynamic Response Function (HRF). https://andysbrainbook.readthedocs.io/en/latest/SPM/SPM_Short_Course/SPM_Statistics/SPM_03_Stats_HRF_Overview.html (accessed Jan 8, 2023), .

- [76] Hillyard, S. A., Hinrichs, H., Tempelmann, C., Morgan, S. T., Hansen, J. C., Scheich, H., and Heinze, H.-J. Combining steady-state visual evoked potentials and fMRI to localize brain activity during selective attention. *Human Brain Mapping*, 5:287–292, 1997.
- [77] Samara, M., Farmaki, C., Zacharioudakis, N., Pediaditis, M., Krana, M., and Sakkalis, V. Comparison between dry and wet EEG electrodes in an SSVEP-based BCI for robot navigation. In *2022 IEEE 22nd International Conference on Bioinformatics and Bioengineering (BIBE)*, pages 333–338, Taichung, Taiwan, November 2022.
- [78] Russo, F. D., Pitzalis, S., Aprile, T., Spitoni, G., Patria, F., Stella, A., Spinelli, D., and Hillyard, S. A. Spatiotemporal analysis of the cortical sources of the steady-state visual evoked potential. *Human Brain Mapping*, 28:323–334, April 2007.
- [79] Bayram, A., Bayraktaroglu, Z., Karahan, E., Erdogan, B., Bilgic, B., Özker, M., Kasikci, I., Duru, A. D., Ademoglu, A., Öztürk, C., Arıkan, K., Tarhan, N., and Demiralp, T. Simultaneous EEG/fMRI Analysis of the Resonance Phenomena in Steady-State Visual Evoked Responses. *Clinical EEG and Neuroscience*, 42:98–106, April 2011.
- [80] Pan, J., Gao, X., and Gao, S. An fMRI Study on the Spectral and Spatial Properties of Steady-State Visual Evoked Response. In *2009 2nd International Conference on Biomedical Engineering and Informatics*, pages 1–5, Tianjin, China, 2009.
- [81] Zafar, R., Malik, A. S., Kamel, N., and Dass, S. C. fMRI based brain state analysis of visual activities. In *2015 IEEE Student Symposium in Biomedical Engineering & Sciences (ISSBES)*, pages 46–49, UiTM, Shah Alam, Malaysia, November 2015.
- [82] Lin, J.-S. and Shieh, C.-H. An SSVEP-Based BCI System and its Applications. *International Journal of Advanced Computer Science and Applications*, 5(10), 2014.
- [83] Guger, C., Allison, B., Grosswindhager, B., Prückl, R., Hintermüller, C., Kapeller, C., Bruckner, M., Krausz, G., and GuenterEdlinger, . How Many People Could Use an SSVEP BCI? *Frontiers in Neuroscience*, 6, 2012.
- [84] Lin, B.-S., Wang, H.-A., Huang, Y.-K., Wang, Y.-L., and Lin, B.-S. Design of SSVEP Enhancement-Based Brain Computer Interface. *IEEE Sensors Journal*, 21:14330–14338, July 2021.

- [85] Tang, J., Xu, M., Han, J., Liu, M., Dai, T., Chen, S., and Ming, D. Optimizing SSVEP-Based BCI System towards Practical High-Speed Spelling. *Sensors*, 20(15):4186, July 2020.
- [86] Wai, A. A. P., Lee, M.-H., Lee, S.-W., and Guan, C. Improving the Performance of SSVEP BCI with Short Response Time by Temporal Alignments Enhanced CCA. In *2019 9th International IEEE/EMBS Conference on Neural Engineering (NER)*, pages 155–158, San Francisco, CA, USA, March 2019.
- [87] Li, Y., Xiang, J., and Kesavadas, T. Convolutional Correlation Analysis for Enhancing the Performance of SSVEP-Based Brain-Computer Interface. *IEEE Transactions on Neural Systems and Rehabilitation Engineering*, 28: 2681–2690, December 2020.
- [88] Wang, L., Xu, M., Mei, J., Han, J., Wang, Y., Jung, T.-P., and Ming, D. Enhancing performance of SSVEP-based BCI by unsupervised learning information from test trials. In *2020 42nd Annual International Conference of the IEEE Engineering in Medicine & Biology Society (EMBC)*, pages 3359–3362, Montreal, QC, Canada, July 2020.
- [89] Xiaogang Chen,, Yijun Wang,, Nakanishi, M., Tzyy-Ping Jung,, and Xiaorong Gao,. Hybrid frequency and phase coding for a high-speed SSVEP-based BCI speller. In *2014 36th Annual International Conference of the IEEE Engineering in Medicine and Biology Society*, pages 3993–3996, Chicago, IL, August 2014.
- [90] Ko, L.-W., Lin, S.-C., Liang, W.-G., Komarov, O., and Song, M.-S. Development of SSVEP-based BCI using common frequency pattern to enhance system performance. In *2014 IEEE Symposium on Computational Intelligence in Brain Computer Interfaces (CIBCI)*, pages 30–35, Orlando, FL, USA, December 2014.
- [91] Won, D.-O., Zhang, H. H., Guan, C., and Lee, S.-W. A BCI speller based on SSVEP using high frequency stimuli design. In *2014 IEEE International Conference on Systems, Man, and Cybernetics (SMC)*, pages 1068–1071, San Diego, CA, USA, October 2014.
- [92] Nakanishi, M., Wang, Y., Chen, X., Wang, Y.-T., Gao, X., and Jung, T.-P. Enhancing Detection of SSVEPs for a High-Speed Brain Speller Using Task-Related Component Analysis. *IEEE transactions on bio-medical engineering*, 65:104–112, January 2018.
- [93] Saravanakumar, D. and Reddy, M. R. A high performance hybrid SSVEP based BCI speller system. *Advanced Engineering Informatics*, 42, October 2019.

- [94] Rezeika, A., Benda, M., Stawicki, P., Gembler, F., Saboor, A., and Volosyak, I. 30-Targets Hybrid BNCI Speller Based on SSVEP and EMG. In *2018 IEEE International Conference on Systems, Man, and Cybernetics (SMC)*, pages 153–158, Miyazaki, Japan, October 2018.
- [95] Liu, S., Zhang, D., Qiao, M., Wang, K., Zhao, S., Yang, Y., and Yan, T. Mind Controlled Vehicle Based on Lidar SLAM Navigation and SSVEP Technology. In *2021 9th International Winter Conference on Brain-Computer Interface (BCI)*, pages 1–4, Gangwon, Korea (South), February 2021.
- [96] Punsawad, Y. and Wongsawat, Y. Hybrid SSVEP-motion visual stimulus based BCI system for intelligent wheelchair. In *2013 35th Annual International Conference of the IEEE Engineering in Medicine and Biology Society (EMBC)*, pages 7416–7419, Osaka, July 2013.
- [97] Mangion, J. Exploitation of EEG-Extracted Eye Movement for a Hybrid SSVEP Home Automation System. Master’s thesis, University of Malta, Msida, Malta, 2020.
- [98] Lin, K., Cinetto, A., Wang, Y., Chen, X., Gao, S., and Gao, X. An online hybrid BCI system based on SSVEP and EMG. *Journal of Neural Engineering*, 13, April 2016.
- [99] Zhou, Y., He, S., Huang, Q., and Li, Y. A Hybrid Asynchronous Brain-Computer Interface Combining SSVEP and EOG Signals. *IEEE Transactions on Biomedical Engineering*, 67:2881–2892, October 2020.
- [100] Xing, X., Wang, Y., Pei, W., Guo, X., Liu, Z., Wang, F., Ming, G., Zhao, H., Gui, Q., and Chen, H. A High-Speed SSVEP-Based BCI Using Dry EEG Electrodes. *Scientific Reports*, 8:14708, October 2018.
- [101] Hasan, M. K., Mondal, C., Mahmud, N. A., and Ahmad, M. Performance analysis of SSVEP based wireless Brain computer Interface for wet and dry electrode. In *2015 International Conference on Advances in Electrical Engineering (ICAEE)*, pages 64–67, Dhaka, December 2015.
- [102] Silva, A. D. D., da Cruz Junior, G., and Junior, C. G. P. A Fast and Accurate SSVEP Brain Machine Interface Using Dry Electrodes and High Frequency Stimuli by Employing Ensemble Learning. *IEEE Latin America Transactions*, 18(06):1000–1007, June 2020.
- [103] Edlinger, G., Krausz, G., and Guger, C. A dry electrode concept for SMR, P300 and SSVEP based BCIs. In *2012 ICME International Conference on Complex Medical Engineering (CME)*, pages 186–190, Kobe, Japan, July 2012.

- [104] Guermandi, M., Benatti, S., Morinigo, V. J. K., and Bertini, L. A Wearable Device for Minimally-Invasive Behind-the-Ear EEG and Evoked Potentials. In *2018 IEEE Biomedical Circuits and Systems Conference (BioCAS)*, pages 1–4, Cleveland, OH, October 2018.
- [105] Hsu, H.-T., Lee, I.-H., Tsai, H.-T., Chang, H.-C., Shyu, K.-K., Hsu, C.-C., Chang, H.-H., Yeh, T.-K., Chang, C.-Y., and Lee, P.-L. Evaluate the Feasibility of Using Frontal SSVEP to Implement an SSVEP-Based BCI in Young, Elderly and ALS Groups. *IEEE Transactions on Neural Systems and Rehabilitation Engineering*, 24:603–615, May 2016.
- [106] Cao, T., Wan, F., Wong, C. M., da Cruz, J. N., and Hu, Y. Objective evaluation of fatigue by EEG spectral analysis in steady-state visual evoked potential-based brain-computer interfaces. *BioMedical Engineering OnLine*, 13:28, December 2014.
- [107] Duart, X., Quiles, E., Suay, F., Chio, N., García, E., and Morant, F. Evaluating the Effect of Stimuli Color and Frequency on SSVEP. *Sensors*, 21:117, December 2020.
- [108] Tello, R. J. M. G., Müller, S. M. T., Ferreira, A., and Bastos, T. F. Comparison of the influence of stimuli color on Steady-State Visual Evoked Potentials. *Research on Biomedical Engineering*, 31:218–231, September 2015.
- [109] Po-Lei Lee,, Chia-Lung Yeh,, Cheng, J. Y.-S., Chia-Yen Yang,, and Gong-Yau Lan,. An SSVEP-Based BCI Using High Duty-Cycle Visual Flicker. *IEEE Transactions on Biomedical Engineering*, 58:3350–3359, December 2011.
- [110] Floriano, A., Diez, P. F., and Bastos-Filho, T. F. Evaluating the Influence of Chromatic and Luminance Stimuli on SSVEPs from Behind-the-Ears and Occipital Areas. *Sensors*, 18:615, February 2018.
- [111] Zerafa, R., Camilleri, T., Falzon, O., and Camilleri, K. P. Comparison of plain and checkerboard stimuli for brain computer interfaces based on steady state visual evoked potentials. In *2013 6th International IEEE/EMBS Conference on Neural Engineering (NER)*, pages 33–36, San Diego, CA, USA, November 2013.
- [112] Bieger, J., Molina, G. N. G., and Zhu, D. Effects of Stimulation Properties in Steady-State Visual Evoked Potential Based Brain-Computer Interfaces. In *Engineering in Medicine and Biology Society (EMBC), 2010 Annual International Conference of the IEEE*, 2010.
- [113] Szalowski, A. and Picovici, D. Investigating stimuli graphics’ size and resolution performance in Steady State Visual Evoked Potential. In *2017*

- 28th Irish Signals and Systems Conference (ISSC)*, pages 1–6, Killarney, Co Kerry, Ireland, June 2017.
- [114] Gilford, C. Controlling External Devices Using an SSVEP-based BCI. Bachelor’s thesis, University of Malta, Msida, Malta, 2022.
- [115] Wang, Y.-T., Nakanishi, M., Wang, Y., Wei, C.-S., Cheng, C.-K., and Jung, T.-P. An Online Brain-Computer Interface Based on SSVEPs Measured From Non-Hair-Bearing Areas. *IEEE Transactions on Neural Systems and Rehabilitation Engineering*, 25(1):14–21, January 2017.
- [116] Fong, D. H. C., Cohen, A., Boughton, P., Raftos, P., Herrera, J. E., Simon, N. G., and Putrino, D. Steady-State Visual-Evoked Potentials as a Biomarker for Concussion: A Pilot Study. *Frontiers in Neuroscience*, 14:171, March 2020.
- [117] Visual cortex. https://en.wikipedia.org/w/index.php?title=Visual_cortex&oldid=1142436905 (accessed Feb 6, 2023).
- [118] Cotrina, A. *Toward Brain-Computer Interaction in Paralysis*. Springer International Publishing, 1st edition, 2017.
- [119] Vialatte, F.-B., Maurice, M., Dauwels, J., and Cichocki, A. Steady-state visually evoked potentials: Focus on essential paradigms and future perspectives. *Progress in Neurobiology*, 90:418–438, April 2010.
- [120] Two-streams hypothesis. https://en.wikipedia.org/w/index.php?title=Two-streams_hypothesis&oldid=1146682488 (accessed March 9, 2023).
- [121] Sammer, G., Blecker, C., Gebhardt, H., Kirsch, P., Stark, R., and Vaitl, D. Acquisition of typical EEG waveforms during fMRI: SSVEP, LRP, and frontal theta. *NeuroImage*, 24:1012–1024, February 2005.
- [122] Ji, H., Chen, B., Petro, N. M., Yuan, Z., Zheng, N., and Keil, A. Functional Source Separation for EEG-fMRI Fusion: Application to Steady-State Visual Evoked Potentials. *Frontiers in Neurorobotics*, 13, May 2019.
- [123] Chen, X., Wang, Y., Nakanishi, M., Gao, X., Jung, T.-P., and Gao, S. High-speed spelling with a noninvasive brain-computer interface. *Proceedings of the National Academy of Sciences*, 112(44), November 2015.
- [124] Chan, W.-H., Chiang, K.-J., Nakanishi, M., Wang, Y.-T., and Jung, T.-P. Evaluating the Performance of Non-Hair SSVEP-Based BCIs Featuring Template-Based Decoding Methods. In *2018 40th Annual International Conference of the IEEE Engineering in Medicine and Biology Society (EMBC)*, pages 1972–1975, Honolulu, HI, July 2018.

- [125] Lan, W., Yang, H., He, J., Leng, Y., Wang, R., Iramina, K., and Ge, S. Effect of Channel and Reference Selection on a Non-occipital Steady-State Visual Evoked Potential-Based Brain-Computer Interface. In *2021 IEEE 5th Information Technology, Networking, Electronic and Automation Control Conference (ITNEC)*, pages 1274–1280, Xi'an, China, October 2021.
- [126] Yu-Te Wang,, Nakanishi, M., Kappel, S. L., Kidmose, P., Mandic, D. P., Yijun Wang,, Chung-Kuan Cheng,, and Tzyy-Ping Jung,. Developing an online steady-state visual evoked potential-based brain-computer interface system using EarEEG. In *2015 37th Annual International Conference of the IEEE Engineering in Medicine and Biology Society (EMBC)*, pages 2271–2274, Milan, August 2015.
- [127] Fang-Cheng Lin,, Zao, J. K., Kuan-Chung Tu,, Yijun Wang,, Yi-Pai Huang,, Che-Wei Chuang,, Hen-Yuan Kuo,, Yu-Yi Chien,, Ching-Chi Chou,, and Tzyy-Ping Jung,. SNR analysis of high-frequency steady-state visual evoked potentials from the foveal and extrafoveal regions of Human Retina. In *2012 Annual International Conference of the IEEE Engineering in Medicine and Biology Society*, pages 1810–1814, San Diego, CA, August 2012.
- [128] Diez, P. F., Mut, V. A., Avila Perona, E. M., and Lacia Leber, E. Asynchronous BCI control using high-frequency SSVEP. *Journal of NeuroEngineering and Rehabilitation*, 8:39, 2011.
- [129] Liang, L., Yang, C., Wang, Y., and Gao, X. High-Frequency SSVEP Stimulation Paradigm Based On Dual Frequency Modulation *. In *2019 41st Annual International Conference of the IEEE Engineering in Medicine and Biology Society (EMBC)*, pages 6184–6187, Berlin, Germany, July 2019.
- [130] Sakurada, T., Kawase, T., Komatsu, T., and Kansaku, K. Use of high-frequency visual stimuli above the critical flicker frequency in a SSVEP-based BMI. *Clinical Neurophysiology*, 126:1972–1978, October 2015.
- [131] Vij, N., Zuobin, W., Bjornsdotter, M., Dauwels, J., and Vialatte, F. B. A multimodal approach to analysis of steady state visually evoked potentials. In *2013 IEEE Symposium on Computational Intelligence in Bioinformatics and Computational Biology (CIBCB)*, pages 183–188, Singapore, Singapore, April 2013.
- [132] Pastor, M. A., Artieda, J., Arbizu, J., Valencia, M., and Masdeu, J. C. Human Cerebral Activation during Steady-State Visual-Evoked Responses. *The Journal of Neuroscience*, 23(37):11621–11627, December 2003.
- [133] Li, X., Wang, X., Wong, C. M., Wen, R., Wan, F., and Hu, Y. Influence of Stimuli Color Combination on Online SSVEP-based BCI Performance. In

- 2019 IEEE International Conference on Computational Intelligence and Virtual Environments for Measurement Systems and Applications (CIVEMSA)*, pages 1–5, Tianjin, China, June 2019.
- [134] Bramão, I., Faísca, L., Forkstam, C., Reis, A., and Petersson, K. M. Cortical Brain Regions Associated with Color Processing: An fMRI Study. *The Open Neuroimaging Journal*, 4:164–173, November 2010.
- [135] Cavina-Pratesi, C., Kentridge, R., Heywood, C., and Milner, A. Separate Channels for Processing Form, Texture, and Color: Evidence from fMRI Adaptation and Visual Object Agnosia. *Cerebral Cortex*, 20:2319–2332, October 2010.
- [136] Mullen, K. T., Chang, D. H. F., and Hess, R. F. The selectivity of responses to red-green colour and achromatic contrast in the human visual cortex: an fMRI adaptation study. *European Journal of Neuroscience*, 42:2923–2933, December 2015.
- [137] Teng Cao,, Feng Wan,, Peng Un Mak,, Pui-In Mak,, Mang I Vai,, and Yong Hu,. Flashing color on the performance of SSVEP-based brain-computer interfaces. In *2012 Annual International Conference of the IEEE Engineering in Medicine and Biology Society*, pages 1819–1822, San Diego, CA, August 2012.
- [138] Embrandiri, S. S., Teja, S. S. S., Ramasubba Reddy M., and Chandrachoodan, N. Effect of stimulation shapes on the Steady-State Visual-Evoked response. In *2015 41st Annual Northeast Biomedical Engineering Conference (NEBEC)*, pages 1–2, Troy, NY, USA, April 2015.
- [139] Stylianou-Korsnes, M., Reiner, M., Magnussen, S. J., and Feldman, M. W. Visual recognition of shapes and textures: an fMRi study. *Brain Structure and Function*, 214:355–359, May 2010.
- [140] Freud, E., Culham, J. C., Plaut, D. C., and Behrmann, M. The large-scale organization of shape processing in the ventral and dorsal pathways. *eLife*, 6, October 2017.
- [141] Denys, K. The Processing of Visual Shape in the Cerebral Cortex of Human and Nonhuman Primates: A Functional Magnetic Resonance Imaging Study. *Journal of Neuroscience*, 24:2551–2565, March 2004.
- [142] Kraut, M., Hart, J., Soher, B. J., and Gordon, B. Object shape processing in the visual system evaluated using functional MRI. *Neurology*, 48:1416–1420, May 1997.

- [143] Ming, G., Wang, Y., Pei, W., and Chen, H. Optimizing Spatial Contrast of a New Checkerboard Stimulus for Eliciting Robust SSVEPs. In *2019 9th International IEEE/EMBS Conference on Neural Engineering (NER)*, pages 175–178, San Francisco, CA, USA, March 2019.
- [144] Waytowich, N. R., Yamani, Y., and Krusienski, D. J. Optimization of Checkerboard Spatial Frequencies for Steady-State Visual Evoked Potential Brain–Computer Interfaces. *IEEE Transactions on Neural Systems and Rehabilitation Engineering*, 25:557–565, June 2017.
- [145] Srinivasan, R., Fornari, E., Knyazeva, M. G., Meuli, R., and Maeder, P. fMRI responses in medial frontal cortex that depend on the temporal frequency of visual input. *Experimental Brain Research*, 180(4):677–691, June 2007.
- [146] Beason-Held, L. L., Purpura, K. P., Krasuski, J. S., Maisog, J. M., Daly, E. M., Mangot, D. J., Desmond, R. E., Optican, L. M., Schapiro, M. B., and VanMeter, J. W. Cortical regions involved in visual texture perception: a fMRI study. *Cognitive Brain Research*, 7:111–118, October 1998.
- [147] Wu, Z., Lai, Y., Xia, Y., Wu, D., and Yao, D. Stimulator selection in SSVEP-based BCI. *Medical Engineering & Physics*, 30:1079–1088, October 2008.
- [148] Zhu, D., Bieger, J., Garcia Molina, G., and Aarts, R. M. A Survey of Stimulation Methods Used in SSVEP-Based BCIs. *Computational Intelligence and Neuroscience*, 2010:1–12, 2010.
- [149] Zhenghua Wu,. The difference of SSVEP resulted by different pulse duty-cycle. In *2009 International Conference on Communications, Circuits and Systems*, pages 605–607, Milpitas, CA, USA, July 2009.
- [150] Oralhan, Z. and Tokmakçi, M. The Effect of Duty Cycle and Brightness Variation of Visual Stimuli on SSVEP in Brain Computer Interface Systems. *IETE Journal of Research*, 62:795–803, November 2016.
- [151] Nakanishi, M., Wang, Y., Wang, Y.-T., Mitsukura, Y., and Jung, T.-P. Generating Visual Flickers for Eliciting Robust Steady-State Visual Evoked Potentials at Flexible Frequencies Using Monitor Refresh Rate. *PLoS ONE*, 9, June 2014.
- [152] Lemée, J.-M., Berro, D. H., Bernard, F., Chinier, E., Leiber, L.-M., Menei, P., and Ter Minassian, A. Resting-state functional magnetic resonance imaging versus task-based activity for language mapping and correlation with perioperative cortical mapping. *Brain and Behavior*, 9, 2019.

- [153] Al-Arfaj, H. K., Al-Sharydah, A. M., AlSuhaybani, S. S., Alaqeel, S., and Yousry, T. Task-Based and Resting-State Functional MRI in Observing Eloquent Cerebral Areas Personalized for Epilepsy and Surgical Oncology Patients: A Review of the Current Evidence. *Journal of Personalized Medicine*, 13(2):370, February 2023.
- [154] Wang, Y., Wang, Y.-T., and Jung, T.-P. Visual stimulus design for high-rate SSVEP BCI. *Electronics Letters*, 46(15):1057, 2010.
- [155] PsychoPy. <https://www.psychopy.org/index.html> (accessed Nov 11, 2022).
- [156] University of Malta Magnetic Resonance Imaging Platform. <https://www.um.edu.mt/platforms/umri/> (accessed June 12, 2023).
- [157] Elster, A. D. <http://mriquestions.com/mr-system-layout.html> (accessed Jan 7, 2023), .
- [158] Head/Neck 64. <https://www.siemens-healthineers.com/en-us/magnetic-resonance-imaging/options-and-upgrades/coils/64-channel-head-neck-coil> (accessed Jan 12, 2023).
- [159] Smiddy, C. Siemens Audio Systems Guide. <https://wiki.library.ucsf.edu/display/Neuro/Siemens+Audio+Systems+Guide> (accessed Jan 6, 2023).
- [160] InroomViewingDevice. <https://www.nordicneurolab.com/product/inroomviewing-device> (accessed Jan 7, 2023).
- [161] Mirror head matrix coil. https://shop.siemens-healthineers.com/en-au/product/A_07580280 (accessed Jan 7, 2023).
- [162] 32-Channel Head Coil. <https://www.siemens-healthineers.com/magnetic-resonance-imaging/options-and-upgrades/coils/32-channel-head-coil> (accessed Jan 6, 2023).
- [163] LiveTrack AV for fMRI. <https://www.crslltd.com/tools-for-functional-imaging/mr-safe-eye-tracking-for-fmri/livetrack-fmri/> (accessed Jan 12, 2023).
- [164] Solution for functional MRI. <https://www.nordicneurolab.com/product/fmri-acquisition> (accessed March 11, 2023).
- [165] Presenting Stimuli — PsychoPy. <https://psychopy.org/coder/codeStimuli.html> (accessed Dec 4, 2022).

- [166] Acquiring and using field maps. <https://lcni.uoregon.edu/wiki/acquiring-and-using-field-maps/> (accessed March 23, 2023).
- [167] Model 9855, 40-4000 Lux Digital light meter for LED. <https://www.sefram.com/en/products/environmental-testers/9855-40-4000-lux-digital-light-meter-for-led.html> (accessed Dec 28, 2022).
- [168] Current Edition. <https://www.dicomstandard.org/current> (accessed Feb 5, 2023).
- [169] BIDSKIT. <https://github.com/jmtyszka/bidskit> (accessed March 3, 2023).
- [170] Welcome to MRIQCEPTION! <https://github.com/elizabethbeard/mriqception> (accessed March 18, 2023).
- [171] fMRIPrep: A Robust Preprocessing Pipeline for fMRI Data — fmriprep version documentation. <https://fmriprep.org/en/stable/> (accessed Feb 27, 2023).
- [172] Esteban, O., Ciric, R., Finc, K., Blair, R. W., Markiewicz, C. J., Moodie, C. A., Kent, J. D., Goncalves, M., DuPre, E., Gomez, D. E. P., Ye, Z., Salo, T., Valabregue, R., Amlien, I. K., Liem, F., Jacoby, N., Stojić, H., Cieslak, M., Urchs, S., Halchenko, Y. O., Ghosh, S. S., De La Vega, A., Yarkoni, T., Wright, J., Thompson, W. H., Poldrack, R. A., and Gorgolewski, K. J. Analysis of task-based functional MRI data preprocessed with fMRIPrep. *Nature Protocols*, 15:2186–2202, July 2020.
- [173] BIDS-Validator. <https://github.com/bids-standard/bids-validator> (accessed March 18, 2023).
- [174] Image Quality Metrics (IQMs). <https://mriqc.readthedocs.io/en/latest/measures.html> (accessed April 2, 2023).
- [175] Esteban, O., Markiewicz, C. J., Blair, R. W., Moodie, C. A., Isik, A. I., Erramuzpe, A., Kent, J. D., Goncalves, M., DuPre, E., Snyder, M., Oya, H., Ghosh, S. S., Wright, J., Durnez, J., Poldrack, R. A., and Gorgolewski, K. J. fMRIPrep: a robust preprocessing pipeline for functional MRI. *Nature Methods*, 16:111–116, January 2019.
- [176] Zhang, S., Li, X., Lv, J., Jiang, X., Guo, L., and Liu, T. Characterizing and Differentiating Task-based and Resting State FMRI Signals via Two-stage Sparse Representations. *Brain imaging and behavior*, 10:21–32, March 2016.
- [177] Monti, M. Statistical Analysis of fMRI Time-Series: A Critical Review of the GLM Approach. *Frontiers in Human Neuroscience*, 5, 2011.

- [178] Elster, A. D. General Linear Model (GLM). <http://mriquestions.com/general-linear-model.html> (accessed Feb 29, 2023), .
- [179] Goebel, R. The General Linear Model (GLM). <https://download.brainvoyager.com/bv/doc/UsersGuide/StatisticalAnalysis/TheGeneralLinearModel.html> (accessed March 18, 2023), .
- [180] Snoek, L. The GLM, part 1: estimation. https://lukas-snoek.com/NI-edu/fMRI-introduction/week_2/glm_part1_estimation.html (accessed March 8, 2023).
- [181] Jahn, A. https://andysbrainbook.readthedocs.io/en/latest/fMRI_Short_Course/Statistics/03_Stats_HRF_Overview.html (accessed Dec 15, 2023), .
- [182] Glen, S. T-Score vs. Z-Score: What's the Difference? <https://www.statisticshowto.com/probability-and-statistics/hypothesis-testing/t-score-vs-z-score/> (accessed July 21, 2023).
- [183] FSL. <https://fsl.fmrib.ox.ac.uk/fsl/fslwiki> (accessed Jan 17, 2023).
- [184] FEAT/GuideStats. [https://web.mit.edu/fsl_v5.0.10/fsl/doc/wiki/FEAT\(2f\)GuideStats.html](https://web.mit.edu/fsl_v5.0.10/fsl/doc/wiki/FEAT(2f)GuideStats.html) (accessed March 1, 2023).
- [185] Triana, A. M., Glerean, E., Saramäki, J., and Korhonen, O. Effects of spatial smoothing on group-level differences in functional brain networks. *Network Neuroscience*, 4:556–574, July 2020.
- [186] Spatial Smoothing. <https://support.brainvoyager.com/brainvoyager/functional-analysis-preparation/29-pre-processing/86-spatial-smoothing> (accessed Jan 23, 2023).
- [187] Smith, S. FILM - Voxelwise Timeseries Analysis. <https://www.fmrib.ox.ac.uk/datasets/techrep/tr04ss2/tr04ss2/node3.html> (accessed Jan 2, 2023).
- [188] MCFLIRT. <https://fsl.fmrib.ox.ac.uk/fsl/fslwiki/MCFLIRT> (accessed Jan 15, 2023).
- [189] Products. <https://www.biosemi.com/products.htm> (accessed March 2, 2023).
- [190] Labview. https://www.biosemi.com/software_biosemi_acquisition.htm (accessed March 2, 2023).
- [191] MATLAB. <https://www.mathworks.com/products/matlab.html> (accessed on Dec 14, 2022).

- [192] Active electrodes. https://www.biosemi.com/active_electrode.htm (accessed March 3, 2023).
- [193] ActiveTwo AD-Box. https://www.biosemi.com/ad-box_activetwo.htm (accessed March 3, 2023).
- [194] USB receiver. <https://www.biosemi.com/receiver.htm> (accessed March 7, 2023).
- [195] Thirakul, A. and Smith, L. *ActiveTwo System: Operating Guidelines*, 2015.
- [196] Biosemi: What is the .bdf file format? https://www.biosemi.com/faq/file_format.htm (accessed March 9, 2023).
- [197] BioSemi: What is the function of the CMS and DRL electrodes. <https://www.biosemi.com/faq/cms&drl.htm> (accessed March 9, 2023).
- [198] Mitch, W. Bipolar And Monopolar Recordings - Mind and Brain. <https://www.mitchmedical.us/mind-brain/bipolar-and-monopolar-recordings.html> (accessed March 8, 2023).
- [199] Repovš, G. Dealing with Noise in EEG Recording and Data Analysis. In *Informatica Medica Slovenica*, volume 15, pages 18–25, 2010.
- [200] Wang, D., Liu, A., Xue, B., Wu, L., and Chen, X. Improving the performance of SSVEP-BCI contaminated by physiological noise via adversarial training. *Medicine in Novel Technology and Devices*, 18, June 2023.
- [201] Han, Y., Park, S., Ha, J., and Kim, L. Hybrid approach of SSVEP and EEG-based eye-gaze tracking for enhancing BCI performance. In *2023 11th International Winter Conference on Brain-Computer Interface (BCI)*, pages 1–4, February 2023.
- [202] John G. Proakis, D. G. M. *Digital Signal Processing: Principles, Algorithms and Applications*. Prentice-Hall, New Jersey, U.S.A, 4th edition, 2007.
- [203] Alan V. Oppenheim, R. W. *Discrete-Time Signal Processing*. Pearson, New Jersey, U.S.A, 3rd edition, 2021.
- [204] Rangayyan, R. M. *Biomedical Signal Analysis: A Case Study Approach*. John Wiley Sons, Inc., Hoboken, New Jersey, 2nd edition, 2021.
- [205] Tsoneva, T., Garcia-Molina, G., Van De Sant, J., and Farquhar, J. Eliciting steady state visual evoked potentials near the visual perception threshold. In *2013 6th International IEEE/EMBS Conference on Neural Engineering (NER)*, pages 93–96, San Diego, CA, USA, November 2013.

- [206] Berumen-Salazar, J. G. Steady state visual evoked potentials and the visual perception curve. Master's thesis, University of Twente, Enschede, the Netherlands, September 2016.
- [207] Cohen, M. X. *Analyzing Neural Time Series Data*. The MIT Press, Cambridge MA, 1st edition, 2014.
- [208] Maris, E. and Oostenveld, R. Nonparametric statistical testing of EEG- and MEG-data. *Journal of Neuroscience Methods*, 164:177–90, September 2007.
- [209] Lillo, E., Mora, M., and Lucero, B. Automated diagnosis of schizophrenia using EEG microstates and Deep Convolutional Neural Network. *Expert Systems with Applications*, 209:118236, December 2022.
- [210] Zhang, J., Zhao, S., Huang, W., and Hu, S. Brain Effective Connectivity Analysis from EEG for Positive and Negative Emotion. In *Neural Information Processing*, Lecture Notes in Computer Science, pages 851–857. Springer International Publishing, October 2017.
- [211] Kumar, V. Statistical Tests to Check Stationarity in Time Series. <https://www.analyticsvidhya.com/blog/2021/06/statistical-tests-to-check-stationarity-in-time-series-part-1/> (accessed on June 12, 2023).
- [212] Patterson, K. *Unit Root Tests in Time Series Volume 1*. Palgrave Macmillan, Basingstoke, February 2011.
- [213] Christodoulou, C., DeLuca, J., Ricker, J., Madigan, N., Bly, B., Lange, G., Kalnin, A., Liu, W., Steffener, J., Diamond, B., and Ni, A. Functional magnetic resonance imaging of working memory impairment after traumatic brain injury. *Journal of Neurology, Neurosurgery, and Psychiatry*, 71:161–168, August 2001.
- [214] Nie, J., Zhang, Z., Wang, B., Li, H., Xu, J., Wu, S., Zhu, C., Yang, X., Liu, B., Wu, Y., Tan, S., Wen, Z., Zheng, J., Shu, S., and Ma, L. Different memory patterns of digits: a functional MRI study. *Journal of Biomedical Science*, 26(1), March 2019.
- [215] Borst, J. P. and Anderson, J. R. Using model-based functional MRI to locate working memory updates and declarative memory retrievals in the fronto-parietal network. *Proceedings of the National Academy of Sciences*, 110:1628–1633, January 2013.
- [216] Demiralp, T., Bayraktaroglu, Z., Lenz, D., Junge, S., Busch, N. A., Maess, B., Ergen, M., and Herrmann, C. S. Gamma amplitudes are coupled to theta phase in human EEG during visual perception. *International Journal*

- of Psychophysiology: Official Journal of the International Organization of Psychophysiology*, 64:24–30, April 2007.
- [217] Fisher, R. S., Harding, G., Erba, G., Barkley, G. L., Wilkins, A., and Epilepsy Foundation of America Working Group,. Photic- and pattern-induced seizures: a review for the Epilepsy Foundation of America Working Group. *Epilepsia*, 46:1426–1441, September .
- [218] Yijun, W., Ruiping, W., Xiaorong, G., and Shang kai, G. Brain-computer interface based on the high-frequency steady-state visual evoked potential. In *Proceedings. 2005 First International Conference on Neural Interface and Control, 2005.*, pages 37–39, May 2005.
- [219] Xie, J., Xu, G., Wang, J., Li, M., Han, C., and Jia, Y. Effects of Mental Load and Fatigue on Steady-State Evoked Potential Based Brain Computer Interface Tasks: A Comparison of Periodic Flickering and Motion-Reversal Based Visual Attention. *PLoS ONE*, 11, September 2016.
- [220] Dai, X., Lei, Y., Liu, Y., Wang, T., Ren, L., Curran, W. J., Patel, P., Liu, T., and Yang, X. Intensity non-uniformity correction in MR imaging using residual cycle generative adversarial network. *Physics in medicine and biology*, 65, November 2020.
- [221] Processing pipeline details. <https://fmripiprep.org/en/stable/workflows.html> (accessed March 2, 2023).
- [222] Kalavathi, P. and Prasath, V. B. S. Methods on Skull Stripping of MRI Head Scan Images—a Review. *Journal of Digital Imaging*, 29:365–379, June 2016.
- [223] Pei, L., Ak, M., Tahon, N. H. M., Zenkin, S., Alkarawi, S., Kamal, A., Yilmaz, M., Chen, L., Er, M., Ak, N., and Colen, R. A general skull stripping of multiparametric brain MRIs using 3D convolutional neural network. *Scientific Reports*, 12, June 2022.
- [224] Brett, M. The MNI brain and the Talairach atlas. <https://brainmap.org/training/BrettTransform.html> (accessed Jan 6, 2023).
- [225] Talairach Coordinate Space. <http://www.talairach.org/about.html> (accessed April 8, 2023).
- [226] Rao, V. M., Wan, Z., Arabshahi, S., Ma, D. J., Lee, P.-Y., Tian, Y., Zhang, X., Laine, A. F., and Guo, J. Improving across-dataset brain tissue segmentation for MRI imaging using transformer. *Frontiers in Neuroimaging*, 1, 2022.
- [227] Roy, S. and Bandyopadhyay, S. K. A New Method of Brain Tissues Segmentation from MRI with Accuracy Estimation. *Procedia Computer Science*, 85: 362–369, 2016.

- [228] Despotović, I., Goossens, B., and Philips, W. MRI Segmentation of the Human Brain: Challenges, Methods, and Applications. *Computational and Mathematical Methods in Medicine*, 2015:1–23, 2015.
- [229] Jahn, A. Chapter 6: Masking and Scaling. https://andysbrainbook.readthedocs.io/en/latest/AFNI/AFNI_Short_Course/AFNI_Preprocessing/06_AFNI_Masking_Scaling.html (accessed June 17, 2023), .
- [230] Goto, M., Abe, O., Miyati, T., Yamasue, H., Gomi, T., and Takeda, T. Head Motion and Correction Methods in Resting-state Functional MRI. *Magnetic Resonance in Medical Sciences*, 15:178–186, 2016.
- [231] Maziero, D., Rondinoni, C., Marins, T., Stenger, V. A., and Ernst, T. Prospective motion correction of fMRI: Improving the quality of resting state data affected by large head motion. *NeuroImage*, 212, May 2020.
- [232] Elster, A. D. fMRI Data Preprocessing. <http://mriquestions.com/data-pre-processing.html> (accessed on March 23, 2023), .
- [233] Funai, A. K., Fessler, J. A., Yeo, D. T., Olafsson, V. T., and Noll, D. C. Regularized field map estimation in MRI. *IEEE transactions on medical imaging*, 27:1484–1494, October 2008.
- [234] Moodie, C. A. Fieldmap estimation. <https://fmriprep.org/en/0.6.0/sdc/estimation.html> (accessed July 13, 2023).
- [235] Parker, D. B. and Razlighi, Q. R. The Benefit of Slice Timing Correction in Common fMRI Preprocessing Pipelines. *Frontiers in Neuroscience*, 13, 2019.
- [236] Goebel, R. <https://www.brainvoyager.com/bv/doc/UsersGuide/Preprocessing/SliceScanTimeCorrection.html> (accessed Jan 14, 2023), .
- [237] Begnoche, J. P., Schilling, K. G., Boyd, B. D., Cai, L. Y., Taylor, W. D., and Landman, B. A. EPI susceptibility correction introduces significant differences far from local areas of high distortion. *Magnetic resonance imaging*, 92:1–9, October 2022.
- [238] Clark, I. A., Callaghan, M. F., Weiskopf, N., Maguire, E. A., and Mohammadi, S. Reducing Susceptibility Distortion Related Image Blurring in Diffusion MRI EPI Data. *Frontiers in Neuroscience*, 15, 2021.
- [239] SDCFlows. <https://www.nipreps.org/sdcflows/master/index.html> (accessed July 15, 2023).